JIMMA UNIVERSITY

SCHOOL OF GRADUATE STUDIES

JIMMA INSTITUTE OF TECHNOLOGY

FACULTY OF CIVIL AND ENVIRONMENTAL ENGINEERING

BEHAVIOUR OF CONCRETE FILLED STEEL TUBULAR COLUMN SUBJECTED TO AXIAL AND CYCLIC LATERAL LOADS

A thesis submitted to the School of Graduate Studies of Jimma University in partial fulfillment of Master of Science in Structural Engineering.

By

Debisa Getachew

May, 2019

Jimma, Ethiopia

JIMMA UNIVERSITY

SCHOOL OF GRADUATE STUDIES

JIMMA INSTITUTE OF TECHNOLOGY

FACULTY OF CIVIL AND ENVIRONMENTAL ENGINEERING

BEHAVIOUR OF CONCRETE FILLED STEEL TUBULAR COLUMN SUBJECTED TO AXIAL AND CYCLIC LATERAL LOADS

A thesis submitted to the School of Graduate Studies of Jimma University in partial fulfillment of Master of Science in Structural Engineering.

By

Debisa Getachew

Advisor: Engr. Elmer C.Agon

Co-Advisr: Engr. S.Sasivaradhan

May, 2019

Jimma, Ethiopia

DECLARATION

I, the undersigned, hereby certify that the work which is being presented in this thesis entitled "Behaviour of Concrete Filled Steel Tubular Column Subjected to Axial and Cyclic Lateral Loads" by me in partial fulfilment of the requirements for the award of degree of **Master of Science** in **Structural Engineering** from **Jimma University** is my authentic record of own work and has not been presented for a degree in any other university and that all sources of material used for the thesis have been duly acknowledged.

Name of Candidate: Debisa Getachew

Signature: _____

Date of submission: _____

This research is submitted for examination in approval of my advisor.

Engr. Elmer C. Agon _____ _____

Advisor Signature Date

This research is submitted for examination in approval of my Co-advisor.

Engr. S.Sasivaradhan _____ _____

Co-advisor Signature Date

APPROVED BY BOARD OF EXAMINERS

_____ _____ _____

External Examiner Signature Date

_____ _____ _____

Internal Examiner Signature Date

_____ _____ _____

Chairman Signature Date

ACKNOWLEDGEMENT

First and most of all, I would like to thank almighty God for his unended blessings and being with me in my every activity.

Secondly, I would like to express my most sincere gratitude and appreciation to my advisor Engr. Elmer C. Agon and Co-advisor Engr. S.Sasivaradhan for their immense guidance all through this research study.

Thirdly, my great appreciation extends to all my friends who have contributed directly or indirectly for preparation of this report.

At last, but not least, I have no words to express my warm feeling of appreciation and thanks to my families for their lovely encouragement.

ABSTRACT

Concrete filled steel tube (CFST) columns are widely used in the construction of modern buildings and bridges due to its abundant structural benefits like excellent seismic behavior, ultimate load bearing capacity, excellent ductility and energy absorption capacity, particularly in zones of high seismic area. These composite constructions combine the advantages of both steel tube and concrete, namely the speed of construction and high strength. The aim of this research was to conduct numerical study on behavior of CFST columns under axial and cyclic lateral loads using finite element software. The lateral load carrying capacity under cyclic load was investigated due to change in different parameters such as diameter to thickness (D/t) ratio, concrete compressive strength, steel grade and slenderness ratio.

Proper material constitutive models for concrete and steel were used while modeling of concrete-filled steel tube and verified by the nonlinear finite element program ABAQUS against experimental data from reviewed literatures. The cross sections of the concrete filled steel tube in the numerical analysis were categorized into three groups, i.e., circular cross-section, square cross-section and steel reinforced circular section.

Through the numerical analyses, it has been shown that for circular concrete filled steel tubular column, the steel tube provides good confining effect to concrete especially when the diameter-to-tube thickness ratio is small. For square concrete filled steel tubular column, the tubes do not provide too much confining effect to concrete when the width to thickness ratio is large. Axial load capacity of steel reinforced-concrete filled-steel tubular column (SRCFST) has been enhanced due to introduction of reinforcing steel to undertake higher loads. Effect different parameters such as steel contribution ratio, yield strength of steel section, concrete compressive strength on lateral load capacity were carried out. Result showed that the lateral load capacity circular concrete filled steel column significantly increased by D/t ratio, increase in steel grade, decrease in slenderness ratio and slightly increase due to increase of concrete grade. From finite element analysis, SRCFST columns have higher peak lateral load and deformability than common concrete filled steel tubular (CFST) columns due to the presence of the section steel. Moreover, the result showed that circular concrete filled steel tubular columns have lighter weight, higher bending stiffness, and better cyclic performance than square concrete filled steel tubular columns.

Table of Contents

LIST of FIGURES

LIST of TABLES

ACRONYMS

ACI	American Institute of Concrete
CFT	Concrete filled tube
CCFT	Circular Concrete Filled Tube
CFST	Concrete Filled Steel Tube
EBCS	Ethiopian Building Code Standard
FE	Finite Element
FECC	Fully Encased Composite
HSC	High Strength Concrete
PECC	Partially Encased Composite Column
SCFT	Square Concrete Filled Tube
SRCFT	Steel Reinforced Concrete Filled Tube

CHAPTER ONE

1 INTRODUCTION

1.1 General

Composite construction system first appeared in the united states of America in 1894. However, the design guidelines were established in 1930 (Gajanan and Sabnis 1939; Eggmann 2003). Composite column is a structural member that uses a combination of structural steel shapes, pipes or tubes with or without reinforcing steel bars and concrete to provide adequate load carrying capacity to sustain either axial compressive loads alone or a combination of axial loads and bending moments. In composite column both steel and concrete sections resist the external loading by interacting together by bond and friction. This column type is being used worldwide for the construction of high-rise buildings since it can reduce the size of the column in the building and increase the usable space of the floor plan. In addition, composite column enhances the overall rigidity of the building and provides significant shear resistance to strong earthquakes and other lateral loads (Md. Soebur Rahman, 2016).

In recent times, steel-concrete composite construction is being widely used to meet performance and functional requirements of mid to high-rise structures as well as large span structures. Composite columns, which consist of the reinforced concrete and encased steel sections, make advantages of these two materials, so that the strength of the concrete and the steel sections can be fully utilized. Steel sections, usually with high yield strength and good ductility, contribute to the bearing capacity and ductility of the column. By using the composite action between the concrete and the steel sections, the bearing capacity of the composite column is larger than the summation of the bearing capacities of the concrete and the steel sections.

The interactive and integral behavior of concrete and the structural steel elements makes the composite column a very cost effective and structural efficient member among the wide range of structural elements in building and bridge constructions. There are three types of composite columns commonly used in building construction.

a. Fully encased composite column (FECC), column in which structural steel section is completely covered by concrete.
b. Partially encased composite column (PECC), the steel section is partially covered by concrete
c. Concrete filled steel tube (CFST), concrete is confined by surrounding steel section.

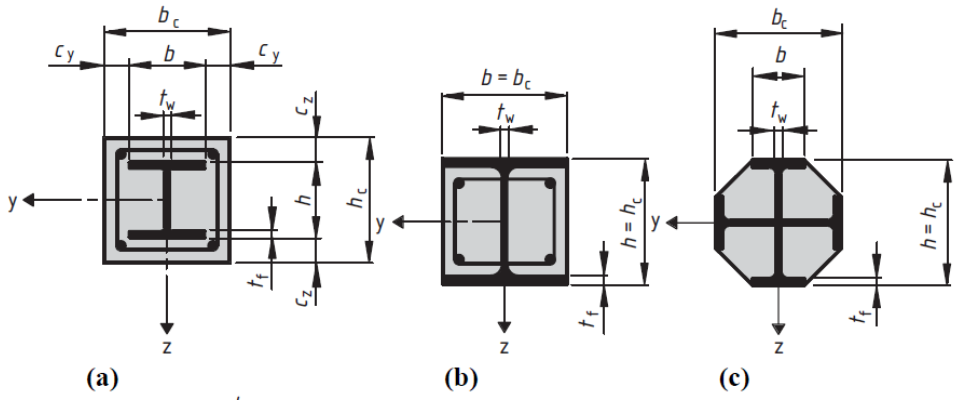

(*Source: Euro code 4, 2004)*

Figure 1.1: Typical Cross-Section of Composite Columns with Fully and Partially Concrete-Encased H-Section

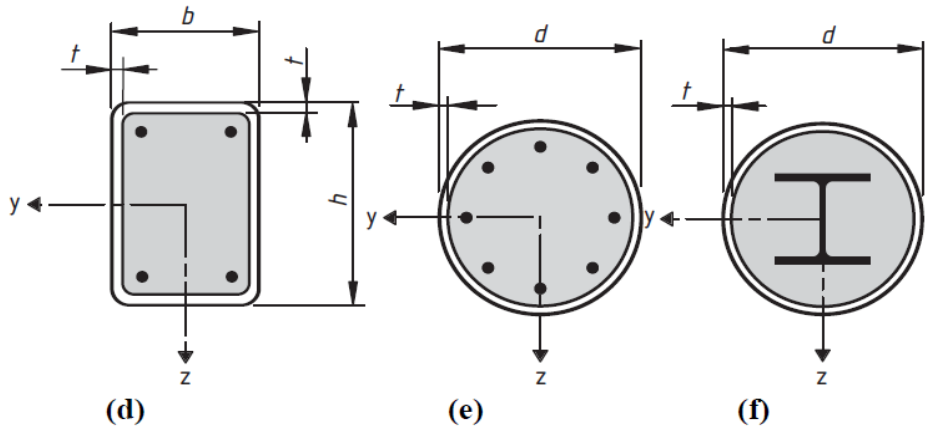

(*Source: Euro code 4, 2004)*

Figure 1.2: Typical Cross-Sections of concrete filled steel tube

1.2 Concrete filled steel tubular columns

A Concrete filled steel tube (CFST) is simply constructed by filling a hollow rectangular or circular structural steel tube with concrete. The interactive and integral behavior of the concrete and the steel tube makes the CFST column a very cost effective and efficient member in structural applications.

Due to high load carrying capacity and convenience of designing column-beam connections, square concrete-filled steel tubular (SCFST) columns have been increasingly employed in the structural engineering.

The enhanced structural properties come from the composite action of constituent elements. The confinement effect created by steel casing enhances the material properties of concrete by putting the concrete under a tri axial state of stresses thereby increasing the strength and ductility of concrete. Additionally, the inward buckling of the steel tube is prevented by the concrete, thus increasing the stability and strength of the column as a system. Among other advantages of CFST columns are the speed of construction, saving on formwork for the concrete core, provides large tensile and compressive capacities and possible use of simple standardized connections.

CFST columns are the composite structures in which steel tube is filled with concrete as shown in Figure 1.2. Uses of CFST in Civil Engineering structures has been increasing due to its abundant structural benefits. The steel tube serves as formwork for casting of concrete which reduces the overall construction cost of the structure. The steel tube provides confinement to the to the core's strength and ductility while the concrete core delays bending and buckling of the steel tube. CFST columns are suitable for tall buildings, bridges with very tall piers in high seismic regions since concrete delays the local buckling of steel hollow sections and increases the ductility of the section significantly. The use of CFST columns has much advantages over hollow tube structures as it reduces the cost by increasing the floor area by a reduction in the required size of column.

1.2.1 Behavior of Concrete filled steel tube at loading stage

The structural behavior of the concrete filled steel tube is affected by the poission's ratio of both steel and concrete. At the initial stage of loading, Poisson's ratio of the concrete is lower than that of steel. Hence the steel tube does not contribute confining effect to the concrete. when the longitudinal strain increases, lateral expansion of the concrete gradually becomes biaxially stressed and concrete core becomes triaxially stressed. So due to the biaxial stress in the steel tube, the steel tube cannot sustain normal yield stress and hence transfer the load from tube to core. The load transfer mechanism is same for both circular and square concrete filled stel tubes.

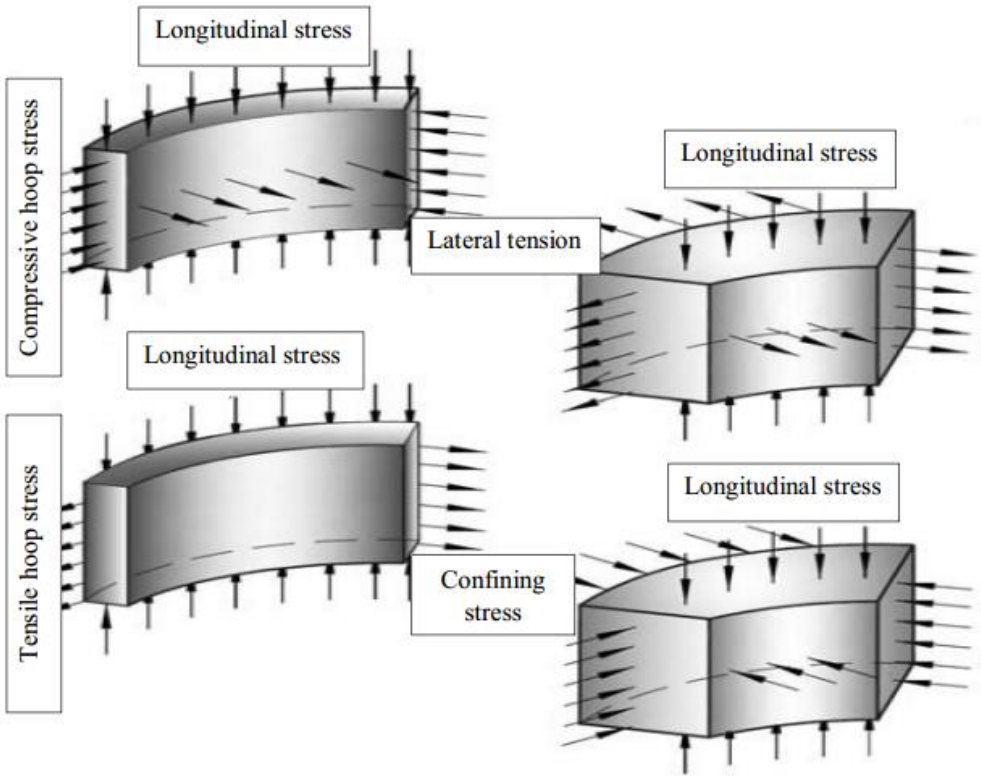

(Source: Kuranovas, Kvedaras , 2007)

Figure 1.3: Stress condition in steel tube and concrete core at different loading stage

Previous researches have shown that square concrete filled steel tubes is not as good compared to circular concrete filled steel tubes due to the confining pressure acts in concrete core by square tube is less and that's why local buckling is more likely to occur.

1.3 Statement of the Problem

Steel-concrete composite construction has gained wide acceptance worldwide as an alternative to pure steel and reinforced concrete construction. Despite the excellent engineering properties of CFSTs they are not as widely used as traditional structural steel and reinforced concrete members for construction in our country. Now a day's reinforced concrete buildings constructed in seismic zone four are suffered from earth quake forces and hence composite structures shall be incorporated for building construction to alleviate the occurrence of the damage.

Although much research has been performed on the topic, the amount of finite element analysis regarding CFSTs and SRCFSTs is significantly less than that available for traditional steel or reinforced concrete members. In our Current code, design methods for CFST under cyclic

loading are limited. Extensive experimental researches have been conducted to investigate the behavior of concrete filled steel tubular column and the experiment results provide insight into the flexural behavior of CFST, however the experimental programs by their very nature are limited and therefore it is hard to investigate the full range of important design parameters. Numerical modeling can complement and extend these results because they can simulate geometries, sizes, and demands that are difficult or even impossible to be simulated experimentally.

1.4 Research Objectives

1.4.1 General Objective

The general objective of this research is to develop a reliable finite element model in order to study the non-linear response of CFST columns under static axial and cyclic lateral loadings.

1.4.2 Specific Objectives

The specific objective of this research are:

- To investigate the various types of reinforcing steel section which improve the strength and hysteresis behavior of CFST columns under axial and lateral cyclic loading.
- To compare CFST column types based on their lateral load resistance
- To perform parametric study with a view to explore effect of several geometric and material variables on strength.
- Develop a finite element model using ABAQUS that can predict the behavior of CFST and SRCFST columns subjected to constant axial load and various cyclic loading.

1.5 Significance of the Study

The philosophy of modern seismic codes is based on the energy dissipation capacity of structures. This is mainly achieved through the ductility behavior, i.e. the ability of an element or a structural system to dissipate large amount of energy through inelastic cyclic deformations without substantial reduction of its resistance.

The study on the behavior of CFST under lateral cyclic loading has the following importance.

- It assists to practice the use of concrete filled steel tubular columns in seismic prone regions.
- It enables designers to identify the type of CFST columns which has high resistance to lateral load in high seismic zone.

- Lighter CFST and SRCFST columns can replace traditional steel or reinforced columns with equivalent resistance.

1.6 Scope of the Study

In the present study, CFST columns under axial and cyclic lateral loading has been analyzed using ABAQUS 6.14 software and the results obtained have been validated with available experimental results from different literatures like [Schneider,1998], and [Qin,2013].

Concrete filled steel tubular columns are analyzed using ABAQUS software up to the failure and the load deformation curves are plotted. The comparisons among CFST columns are made by the load deflection curves. The scope of this study covers the following:

- ✓ Only numerical approach was carried out using nonlinear finite element analysis software.
- ✓ Partially encased composite and fully encased columns were not considered in the analysis.
- ✓ Isolated CFST columns with varying parameters were investigated under combination of axial and lateral load.
- ✓ The study did not cover the effect of high strength concrete
- ✓ No experimental test on concrete filled steel tubular column has been conducted.

CHAPTER TWO

2 LITERATURE REVIEW

2.1 General

Now a day, the concrete filled steel tube columns are widely used in construction. CFST columns are extensively used in structures involving very large applied moments, particularly in zones of high seismic risk. CFST have been used in frame structures as girder, beam and column. The steel tube serves as formwork for casting while the concrete reduces the construction cost. The use of CFST columns provide large saving in cost by increasing the floor area by a reduction in the required size of column.

In the following sections the previous research works on concrete filled tube columns including experimental and analytical studies are discussed.

2.2 Review of the available experimental investigation on CFT

This section reviews some of the previous research that focused on the experimental tests of CFT elements. Innovations, principal contributions and main conclusions of selected previous research studies relevant to this work are briefly discussed.

Huang et al. (2002) tested CFT columns having circular and square cross sections to investigate the effect of the steel tube wall thickness and the diameter-to-thickness ratio (D/t) on the column strength. Nevertheless, the structural behavior of CFST columns is still not well defined. In particular, the composite action between the concrete core and the steel tube makes it difficult to precisely evaluate the mechanical behavior of the structure. In addition, the different Poisson's ratios of the constituent materials of steel and concrete may cause a smaller confinement effect than expected, and the occurrence of slip along the interface between the concrete core and the steel tube leads to a decrease of the strength of CFT columns.

Varma et al. (2004) developed a fiber-based model for modeling the plastic hinge region of a CFT member in combined bending and axial load, where finite element-based effective stress‑strain curves were used for the concrete and steel fibers. The formulation for this model is a two-step process. First, the behavior of the plastic hinge region of the CFT member under axial load is determined using a three-dimensional finite element model, and effective stress‑ strain curves are derived for steel and concrete from the results of the finite element analysis. Second, using

these stress‑strain curves, a fiber model of the CFT is constructed, which is then used to simulate the behavior of the column when subjected to combined axial load, shear, and bending moment. Simple finite element models based on beam theory cannot directly take into account the cyclic load buckling behavior of a steel tube, the interface action between steel tube and in-filled concrete, and the confinement of concrete infill. These features can be taken into account in a direct manner only by using a refined finite-element model. According to the testing procedures conducted by Varma et al. 2004, a CFT square column of length L = 1.5 m and fixed at its base is subjected to a constant axial compressive load P and a cyclically varying lateral loading H at its top as shown in Fig. 2a. The axial load P is applied with the aid of a rigid plate at the top surface of the column and a pre-stressed cable so as to point always to the base of the column and in the direction of the chord of its displaced shape.

Gupta et al., (2007) presented experimental and computational study on the behaviour of circular concentrically loaded concrete filled steel tube columns till failure. Eighty-one specimens were tested to investigate the effect of diameter and D/t ratio of a steel tube on the load carrying capacity of the concrete filled tubular columns. The effect of the grade of concrete and volume of fly ash in concrete was also investigated. The effect of these parameters on the confinement of the concrete core was also studied. Diameter to wall thickness ratio between $25 < D/t < 39$, and the length to tube diameter ratio of $3 < L / D < 8$ was investigated. Strength results of Concrete Filled Tubular columns were compared with the corresponding findings of the available literature. Also a nonlinear finite element model was developed to study the load carrying mechanism of CFTs using the Finite Element code ANSYS. This model was validated by comparison of the experimental and computational results of load–deformation curves and their corresponding modes of collapse. From the experimental and computational study it was found that for both modes of collapse of concrete filled tubular columns at a given deflection the load carrying capacity decreases with the increase in % volume of fly ash up to 20% but it again increases at 25% fly ash volume in concrete.

Tort and Hajjar (2010) presented a beam finite element formulation to analyze composite square CFT beam-column members with interlayer slip subjected to monotonic, cyclic, and transient dynamic loads and derived by the mixed finite-element principles within a distributed plasticity approach. A computational study was conducted to investigate the nonlinear response

of composite frames consisting of rectangular concrete-filled steel tube RCFT beam-columns and steel framing subjected to static and dynamic loads. Following mixed finite-element principles, a three-dimensional fiber-based beam finite-element model was developed, allowing slip deformation between steel tube and the concrete core. Comprehensive material constitutive relations were developed for the steel tube and the concrete core through examining the experimental results in the literature. The uniaxial stress-based steel and concrete constitutive relations include modeling of the effects of confinement, steel tube local buckling, cycling concrete into both tension and compression, cyclic softening, and other key cyclic phenomena observed for steel and concrete in RCFT members. The finite-element model was verified against a wide range of experimental tests under monotonic, quasi-static cyclic, and pseudo-dynamic loading conditions. The mixed finite-element model produced strong correlations with experimental results to simulate the nonlinear response of RCFT members with excellent computational efficiency.

Dundu (2012) conducted experimental study to investigate the behaviour of twenty four concrete-filled steel tube (CFST) columns, loaded concentrically in compression to failure. Parameters in the tests include length, diameter, strength of the steel tubes and the strength of the concrete. These tests were classified into two series i.e., series-1 and series-2. Concrete mix was designed for compressive cube strength (f_{cu}) at 28 th day of approximately 40 MPa for series-1 and 30 MPa for series-2. The large slenderness ratio caused all composite columns in Series 1 to fail by overall flexural buckling. Although overall flexural buckling was also experienced in the composite columns of series 2 tests, the stockier columns failed by crushing of the concrete and yielding of the steel tube. Confinement effects are significant for circular short columns subjected to concentric loading. In slender column s, confinement effects are negligible since the lateral deflection prior to failure increases the bending moment and reduce the mean compressive strain in the concrete.

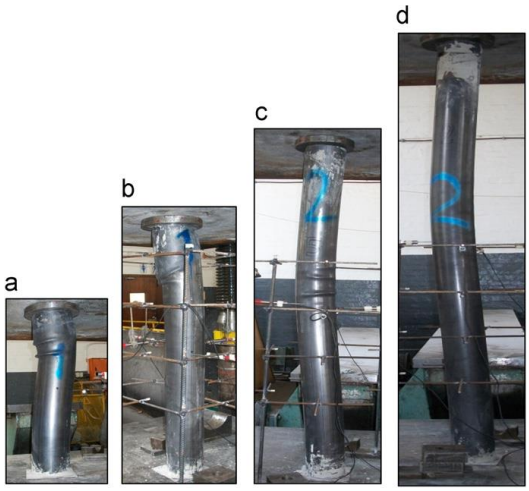

Source : (Dundu, 2012)

Figure 2.1 Typical failure modes of Series 2 columns. (a) 1.0m, (b) 1.5m, (c) 2.0m and (d) 2.5m.

Qin and Xiao (2013) conducted on eight concrete-filled steel tubular (CFT) columns were tested subjected to cyclic loading under constant axial load. Experimental parameters included axial compression ratio, loading sequences, and strength of concrete and steel. The failure mode of steel and core concrete were analyzed. The test results showed that different axial compression ratios and loading sequences have effects on the load carrying capacity, ductility and energy dissipation capacity of CFT columns, and the failure modes of the CFT columns, which can be categorized into two types, local buckling failure of steel tube in compression zone, and low cycle fatigue tearing rupture failure of steel tube. The paper also evaluated the seismic behavior through the energy index obtained from each cycle.

Burak Evirgen (2014) studied Sixteen hollow cold formed steel tubes and 48 concrete filled steel tube. The effects of width/thickness ratio (b/t), the compressive strength of concrete and geometrical shape of cross section parameters on ultimate loads, axial stress, ductility and buckling behavior were investigated for axial compression tests. Circular, hexagonal, rectangular and square sections, 18.75, 30.00, 50.00, 100 b/t ratio values and 13, 26, 35 MPa concrete compressive strength values were chosen for the experimental procedure. Analytical models of specimens were developed using a finite element program (ABAQUS) and the results are compared. Circular specimens are the most effective samples according to both axial stress and ductility values.

2.3 Previous analytical research studies

In addition to experimental investigation, many analytical models have been presented so far to predict the cyclic behavior of CFT columns, which have been mostly based on beam theory in conjunction with concentrated or distributed plasticity modeling. Some of numerical analysis on CFST are presented as follows.

Hu et al., (2005) investigated finite element analysis of CFST columns subjected to an axial compressive force and bending moment in combination. Proper material constitutive models for concrete-filled tube (CFT) columns subjected to an axial compressive force and bending moment in combination were proposed and verified using the non-linear finite element program ABAQUS compared against experimental data. In the numerical analysis, the cross sections of the CFT columns are categorized into three groups, i.e., ones with circular sections, ones with square sections, and ones with square sections stiffened with reinforcing ties. Constitutive models of steel reinforcing ties, steel tubes and concrete were proposed. In the analysis, the poisson's ratio μ_s and the elastic modulus E_s of the steel tube were assumed to be 0.3 and 200GPa, respectively. The uni-axial behavior of the steel tube is similar to that of the reinforcing tie and thus can be simulated by an elastic–perfectly plastic model. In this study, it was shown that the lateral confining pressure generally increases with the increasing of the axial load ratio F/Fu and the lateral confining pressure f_l for a CFT with the SS section is much higher than that for a CFT with the SU section and is of about the same order as that for a CFT with the CU section. The use of reinforcing ties enhances the lateral confining pressure of the tubes. For a CFT with the SS section, the lateral confining pressure f_l generally increases with the decreasing of the tie spacing.

Singh, H. and Gupta, P, K. (2013) presented a numerical investigation into the behavior of rectangular concrete filled steel tubular (CFST) short columns loaded in axial compression. Nonlinear finite-element analysis was performed for the compression process using commercial software ABAQUS 6.9. A total of sixteen specimens of different steel tube sizes, wall thickness, length and filled with normal as well as high strength concrete were chosen for modeling from the available literature. In the proposed model, the steel tube was modeled as an elastic-perfectly plastic material. The poisson's ratio for steel was taken as 0.3. Von-Mises yield criterion was used to define the yield surface for steel. The compressive strength of concrete

was enhanced by the confinement provided by the steel casing. The confined concrete model adopted by **Hu et al., 2005** was used to define the stress-strain behaviour for concrete in the modeling procedure. The proposed model was validated by comparing its results with those of the corresponding experimental specimens. It was observed that the computational model is able to map the deformed shapes and the load deformation pattern of the CFST columns across different column sizes and filled with different grades of concrete.

Raghabendra Yadav et al., (2017) presented numerical study on seismic behavior of CFST bridge piers were carried out by using OpenSEES. The aim of this study was to simulate CFST bridge piers with varying different parameters to clarify the effect of such increase on lateral load carrying capacity and on the post-yield behavior of CFST piers. In this paper, five different models were created and lateral load carrying capacity under cyclic loading was investigated due to change different parameters like diameter to thickness ratio, steel grade, concrete grade and slenderness ratio. In order to simulate actual behaviour of CFST columns, concrete properties like Young's modulus (E_{cc}), compressive strength (f_{ck}), Poisson's ratio (μ) and tensile strength (f_{tk}) of confined concrete are taken from GB50010-2010 and different properties of steel as, Young's modulus (E_s), yield stress (f_y), Poisson's ratio (μ) and ultimate stress (f_u) are taken from GB50017-2003. Results shows that the lateral load capacity significantly increased by D/t ratio, increase in steel grade and decrease in slenderness ratio and slightly increase due to increase of concrete grade.

Even though there have been numerous experimental test series for concrete filled columns in the past, most of the documentation in the specialized literature is limited to columns with certain characteristics (i.e. small cross-sections, short elements and small D/t ratios). Specimens with these characteristics are the only viable option when the capabilities of the laboratory equipment are limited, making the testing of full-scale specimens impractical. The results from specimens with lower slenderness but a wide range of cross-section sizes have been useful for the quantification of the cross-section strength and behavior of short elements, where the length effects do not have a critical impact.

Farajpourbonab et al., (2018) studied steel reinforced concrete filled tube (SRCFT) columns are formed by inserting a steel section into a concrete-filled steel tube. The aim of study was investigating the various types of reinforcing steel section to improve the strength and hysteresis

behavior of SRCFT columns under axial and lateral cyclic loading. The researcher conducted numerical study on a series of composite columns. First, FEM procedure has been verified by the use of available experimental studies. Next, eight composite columns having different types of cross sections were analyzed using ANSYS software. For comparison purpose, the base model was a CFT column used as a benchmark specimen. Nevertheless, the other specimens were SRCFT types. The results showed that reinforcement of a CFT column through this method leads to enhancement in load-carrying capacity, enhancement in lateral drift ratio, ductility, preventing of local buckling in steel shell, and enhancement in energy absorption capacity. Under cyclic displacement history, it was observed that the use of cross-shaped reinforcing steel section causes a higher level of energy dissipation and the moment of inertia of the reinforcing steel sections was found to be the most significant parameter affecting the hysteresis behavior of SRCFT columns.

From the detailed literature mentioned above it should be noted that there is necessity to direct an effort towards for gaining a better understanding of the cyclic behavior of concrete filled steel tubular columns to be able represent the behavior by analytical models. Hence it has been decided to use ABAQUS software for analytical modeling.

CHAPTER THREE

3 FINITE ELEMENT MODELING

3.1 General

Finite element modeling is generally more complex and time consuming, but permits more accurate investigation of composite action, concrete damage, as well as local and global instabilities (**Moon et al., 2013**). There are two major reasons for application of finite element models to composite structures specially CFST columns. First, although experiments have played significant role in research on CFST columns, they are expensive and time consuming. Extensive data are needed to understand the behavior of CFT columns. Tests covering various aspect ratios, different type of loadings and various cross-sectional shapes are needed for a detailed study on CFT columns. A parametric study using finite element models is affordable and allows the study of virtually limitless combinations of the parameters of interest. In addition, tests cannot provide as much insight into the complicated pattern of stress distribution revealed by numerical simulations. Therefore, a detail analysis of CFST column using finite element analysis is a useful approach as long as the analytical model is calibrated with experimental results.

In order to study the non-linear response of concrete filled steel tubular (CFST) columns a three-dimensional finite element software, "ABAQUS 6.14-1" was used. ABAQUS was founded by David Habbitt Bengt Karlsson and Paul Sorensen in1978. It is a set of advanced general purpose finite element system, which is also one of the strongest function finite element software. It can also control the very large, complex and highly nonlinear simulation. Because of the strong analysis ability and the reliability of complex system simulation, ABAQUS 6.14-1, has been widely used in the study and industry by all over the world, and it plays a tremendous role in the large number of high-tech product development.

ABAQUS has four main analysis modules: ABAQUS/Standard provides general analysis ability, such as stress and deformation, heat transfer, mass transfer, etc.; ABAQUS/Explicit is used to the explicit integral and solve dynamic equation for time, and it provides the powerful tool for dealing with the complex contact problem. It is mainly used to solve the high speed dynamics problems, such as collision, drop, explosion, etc. (**Wang, 2012**).

3.2 Parts

In this research, three different models were analyzed; namely, circular concrete filled steel tube, steel reinforced concrete filled steel tube and square concrete filled steel tube. Parts of each model are shown in figure 3.1.

Parts used in circular concrete filled steel tubular column

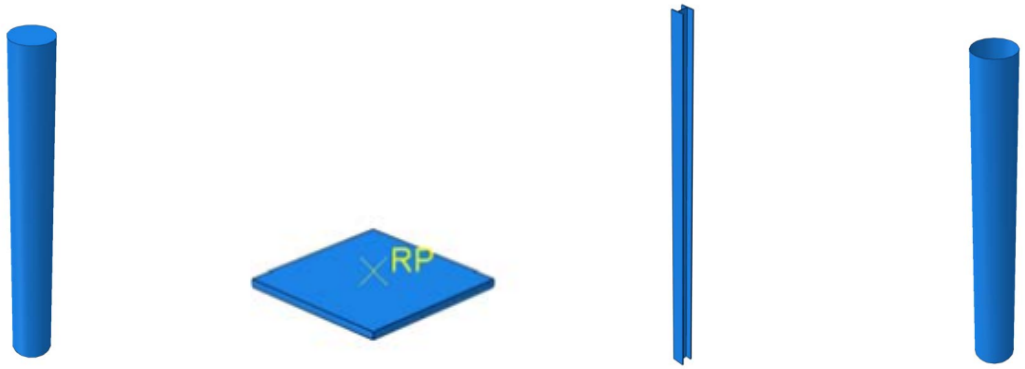

a) Concrete core b) loading plate c) I- section steel d) steel tube

Parts used in square concrete filled steel tubular column

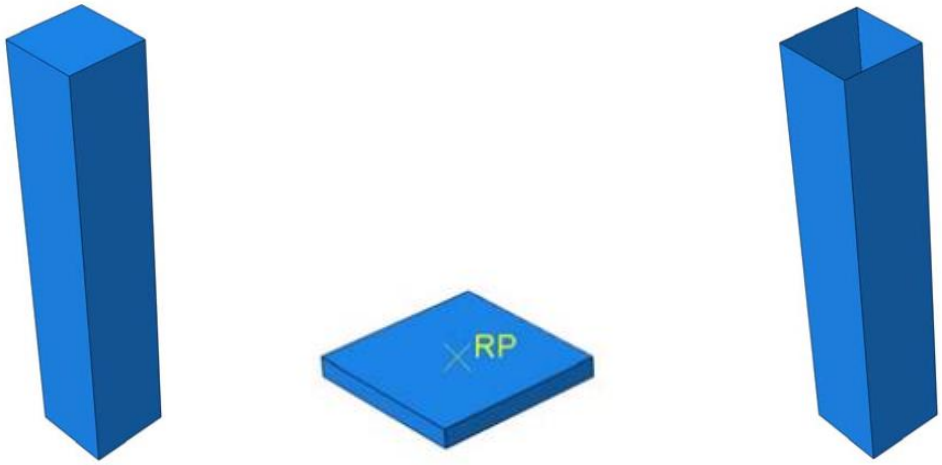

a) concrete core b) loading plate c) square steel tube

Figure 3.1: Parts used in finite element modelling

3.3 Element Type

Element types and mesh size are very important in finite element modeling as they strongly affect the accuracy of results and the simulation speed. To choose an appropriate element type, several types were selected for analysis in the sensibility study: (i) the 4-noded doubly-curved with reduced integration shell element (S4R) (ii) 8-node solid- reduced integration element (C3D8R).

ABAQUS has several element types suitable for numerical analysis: solid two and three dimensional elements, membrane and truss elements, beam elements, and shell elements. The major aim of the analysis is to predict the formation of inelastic local instabilities in a cross-section and the corresponding rotation capacity. Beam, membrane and truss elements are not appropriate for the buckling problem. Solid three dimensional elements ("brick" elements) may be suitable, but the solid elements have only translation degrees of freedom at each node, and require a fine mesh to model regions of high curvature. A finer mesh does not necessarily imply more total degrees of freedom, as one must consider the number of elements and the degrees of freedom of each element. Element types in each part of ABAQUS models are solid element and shell element and their descriptions are depicted as follows.

A. Solid element

In the ABAQUS 6.14, element library there are different types of elements, for example hexahedron (brick), shell, triangular prism. etc. The most commonly used element for concrete studies is the three-dimensional brick elements, is shown in Figure 3.1.

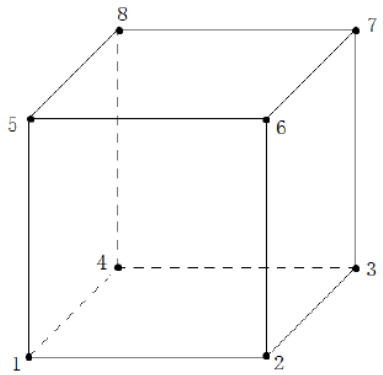

Figure 3.2: The three-dimensional brick elements

C3D8R: is an eight-node reduced-integration brick element, which has one Gauss point at the center. Due to insufficient stiffness, spurious singularity may occur. It is possible for the elements to be distorted, so that the strains calculated at the integration point are all zero, which leads to uncontrolled distortion of the mesh. In modelling of concrete core part, **C3D8R** has been used as solid element type.

B. Shell element: steel tube

To analyze the local buckling behaviour, the geometrically nonlinear 4-node thick shell element, **S4R** was used to model the thin-walled steel tubes. The accuracy of S4R element with the 3-surface cyclic plasticity model to compute the hysteretic behaviour of stiffened rectangular hollow steel columns was confirmed by **Goto et al. (2007)**. In this study, S4R element with six degrees of freedom at each node has been used to model the outer steel shell. Steel tube is modeled with iso-parametric shell elements. The formulation of shell elements allows large displacement analysis, which is used to investigate the possibility of local buckling.

C. Modeling of steel plate

Steel plates were used to distribute the load over the column section. The loading plates attached to both ends of the column were modeled as 3-dimensional brick elements, type C3D8 (8 noded linear brick) with six degrees of freedom at each node. Steel plates at the ends of the columns were defined as rigid elements in the numerical model. The rigid plate was assumed in order to eliminate any concern that the top and bottom edges of the columns could be being damaged through the analysis, and to apply axial compressive load uniformly to the column ends. The rigid plates were meshed using four-node three dimensional bilinear rigid quadrilateral elements (R3D4), with an element size of 20 mm. The surfaces of these elements were also defined to connect with the edge of the column. The load was applied as a static uniform displacement through the top of the rigid plate's reference point.

3.4 Material Properties

In this study two types of material were defined in the finite element modeling: a nonlinear concrete damage plasticity model and elasto-plastic confining steel tube.

3.4.1 Concrete Modeling

The appropriate modeling of composite structures and reinforced concrete structures is a major challenge, in particular due to the material properties of concrete. Unlike steel, concrete is a material that in compression behaves in a non-linear way from the very beginning. Modeling of composite and reinforced concrete structures requires very precise determination of material parameters and constitutive relations between strain and stress.

In ABAQUS, the nonlinear characteristics of concrete is achieved by defining concrete constitutive model. In the elastic stage, we enter elastic modulus and poisson's ratio. However, there are three different models which can be chosen to model plastic stage of concrete: Concrete smeared cracking, concrete damaged plasticity model and cracking model for concrete. The plasticity model of concrete damaged plasticity model had been chosen in this model since it has good convergence for structures subjected to cyclic loading.

3.4.1.1 Concrete Damaged Plasticity Model

The concrete damaged plasticity (CDP) model is capable of capturing the behavior of concrete and quasi-brittle materials. The inelastic behavior of concrete can be incorporated using isotropic damage elasticity with the isotropic tension and the compression plasticity. The model considers the degradation of the elastic stiffness due to tensile and compressive plastic straining.

The material property input in ABAQUS is grouped into two, uni-axial stress strain curves and plasticity parameters. These are shown in the following sections:

I. Concrete under uniaxial compression

Figure shows the response of concrete under uniaxial compressive loading. The concrete will behave linearly until its stress reaches initial yield (σ_{c0}). Beyond σ_{c0} hardening is developed in the concrete and then, after reaching the ultimate stress (σ_{cu}), strain softening is observed.

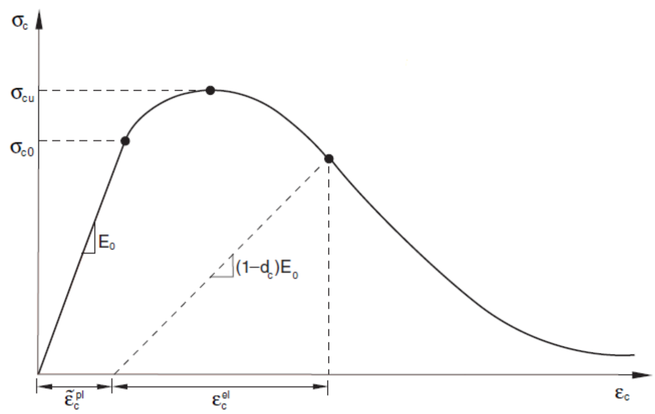

Figure 3.3: Stress-strain curve for plain unconfined concrete under uniaxial loading in compression (ABAQUS 6.14, 2014)

To interpret the concrete damaged plasticity (CDP) model accurately, the compressive behavior, tensile behavior and plasticity, need to be considered.

Compressive Behavior of CDP

Compressive behavior is defined as: the uniaxial compressive response of plain material beyond its elastic range. The inelastic strain is shown in ABAQUS 6.14 documentation and is calculated as equation (3.1):

$$\tilde{\varepsilon}_c^{in} = \varepsilon_c - \varepsilon_{0c}^{el} \quad \ldots\ldots\ldots\ldots\ldots\ldots\ldots\ldots\ldots\ldots\ldots\ldots\ldots\ldots\ldots\ldots\ldots\ldots\ldots\ldots\ldots\ldots\ldots\ldots\ldots\ldots\ldots\ldots\ldots\ldots\ldots\ldots\ldots (3.1)$$

Where $\tilde{\varepsilon}_c^{in}$ Inelastic compressive strain of concrete

ε_{0c}^{el} Elastic compressive strain of concrete at yield, ${}^{\sigma_c}/_{E_0}$

Concrete behavior can also be determined without uniaxial compression testing, knowing only the average compressive strength of concrete, f_{cm} and the modulus of longitudinal elasticity of concrete, E_{cm}.

II. Concrete under uniaxial tension

The stress-strain for concrete under uniaxial tension is shown in figure 3.3. In the first stage of loading concrete will experience linear elastic behavior until the failure stress (σ_{t0}) is reached. The failure stress corresponding to micro-cracking that occurs in the concrete. Beyond

σ_{t0}(second stage), the micro cracks continue to increase and this can be denoted as the softening the response of stress-strain relationship.

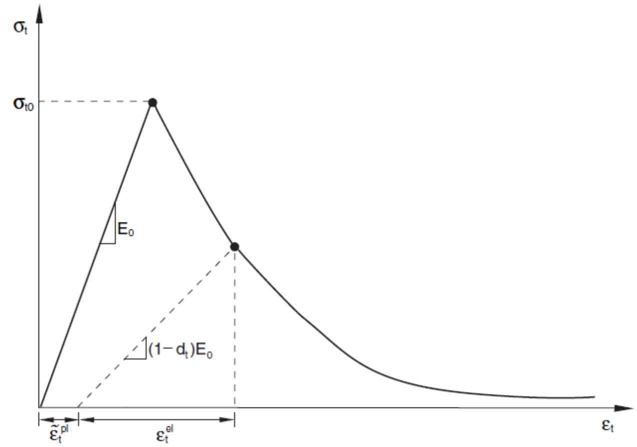

Figure 3.4: Stress-strain curve for plain unconfined concrete under uniaxial loading in tension (ABAQUS 6.14)

Tensile behavior for CDP

The tensile behavior of concrete is defined as the uniaxial tensile response of the material in its post-failure range. The cracking strain is calculated shown in eq. 3-2.

$$\tilde{\varepsilon}_t^{ck} = \varepsilon_t - \varepsilon_{0t}^{el} \quad \ldots\ldots\ldots\ldots\ldots\ldots\ldots\ldots\ldots\ldots\ldots\ldots\ldots\ldots\ldots\ldots\ldots\ldots\ldots\ldots\ldots.. (3.2)$$

Where $\tilde{\varepsilon}_t^{ck}$ $Cracking\ strain\ of\ concrete$

ε_{0t}^{el} $Elastic\ tensile\ strain\ of\ concrete\ at\ yield, {}^{\sigma_t}/_{E_0}$

III. Plasticity Parameters for CDP model

There are five parameters used in ABAQUS for defining the plasticity of CDP model, namely, i) dialation angle (ψ), ii) eccentricity (ϵ), iii) ${}^{\sigma_{b0}}/_{\sigma_{c0}}$, iv) K_c and v) viscosity parameter.

Dialation angle: The dialtion angle mesures the inclination of the plastic strain at a high confining pressure. A material with a low value of this angle experiences brittle behavior, where as high values indicate that the material has a high ductile behavior. Most researchers adopted a value of 20° or 30° for confined concrete.

Eccentricity: It is a parameter, that defines the rate at which the function approaches the asymptote (the flow potential tends to a straight line as the eccentricity tends to zero). The default value is ϵ = 0.1.

$\boldsymbol{\sigma_{b0}}/\boldsymbol{\sigma_{c0}}$: It is the ratio of iniatial equi-biaxial compressive yield stress to initial uniaxial compression yield stress is required as an input to ABAQUS. The default input value of 1.16 was chosen. Papankolaou and Kappos (2007) poposed the following equation to predict the ratio of yield stresses.

$$f_{bo}/f'_c = 1.5(f'_c)^{-0.075} \ldots\ldots\ldots\ldots\ldots\ldots\ldots\ldots (3.3)$$

$\boldsymbol{K_c}$: The ratio of the second stress invariant on the tensile meridian, q (TM), to the compressive meridian, q (CM), adopted for different evolutions of strength under tension and compression. The default value 0.667 was used.

According to Yu et al. (2010) the following equation has been developed for k_c:

$$K_c = \frac{5.5}{5 + 2(f')^{0.075}} \ldots\ldots\ldots\ldots\ldots\ldots\ldots\ldots (3.4)$$

Viscosity Parmeter:

The viscosity parameter (μ) is defined in ABAQUS to represent the relaxation time of the visco-plastic system. By changing this value softening behavior and stiffness degradation behavior of the material models may be influenced. By defining a small number μ in ABAQUS, convergence difficulties were overcomed. In this study, default value has been taken, i.e. zero.

Table 3.1: **Plasticity Parameters for CDP model**

Material	Dialation angle	Eccentricity	$\frac{\sigma_{b0}}{\sigma_{c0}}$	K_c	Viscosity Parameter (μ)
Concrete	36	0.1	1.167	0.667	0

3.4.1.2 Confined Concrete

In concrete filled steel tubular column, concrete is confined by steel tube. In order to define concrete behavior in FE model, stress-strain diagram was established for confined concrete. based on empirical formula as shown in figure below. The equivalent stress-strain diagram for confined concrete under compressive loading was used in FE model.

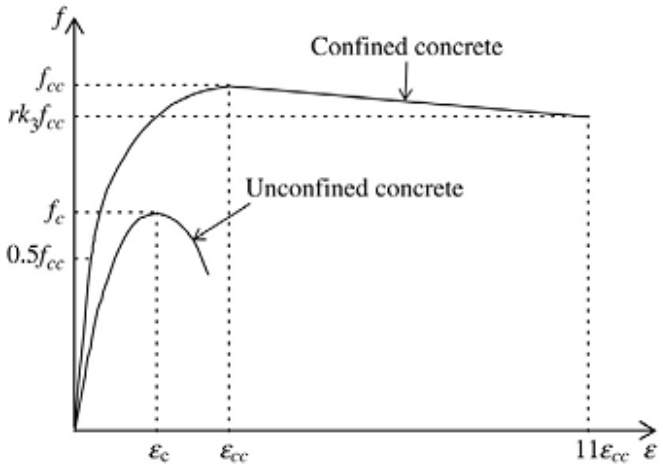

Figure 3.5: Equivalent stress-strain diagram for unconfined and confined concrete uniaxially loaded

Circular concrete filled steel tubular column

The confinement of concrete is influenced by the diameter-to-thickness ratio (D/t) of the tubes. The material parameters shown in figure 3.4 and used in defining the nonlinear compressive behavior of the concrete filled steel tube are defined as follows according to **Mander.et al. (1988)**:

- f'_{cc} = the confined concrete compressive strength

  $f'_{cc} = f'_c + k_1 f_l$ ……(3.5)
- f'_c = the unconfined concrete cylinder compressive strength
- $f_l = the\ lateral\ confining\ pressure\ from\ steel\ tube$

  $f_l = \frac{2\sigma_\theta t}{D}$ ……(3.6)

  $\sigma_\theta = 0.1 f_y$ ……(3.7)
- $\varepsilon_{cc} = the\ corresponding\ confined\ strain\ to\ f'_{cc}$

$$\varepsilon_{cc} = \varepsilon_c \left(1 + k_2 \frac{f_l}{f'_c}\right) \ldots \ldots \ldots \ldots \ldots \ldots \ldots \ldots \ldots \ldots \ldots \ldots \ldots \ldots \ldots \ldots \ldots \ldots \ldots \ldots \ldots . (3.8)$$

- ❖ $\varepsilon_c = 0.003$ $\quad$ *as recommended by ACI specification*
- ❖ $k_1 = 4.1$ *and* $k_2 = 20.5$ $\quad$ *as proposed by Richard. et al.*, 2000
- ❖ $k_3 = \begin{Bmatrix} 1 & 21.7 \le \frac{D}{t} \le 40 \\ 0.00003391\left(\frac{D}{t}\right)^2 - 0.010085\left(\frac{D}{t}\right) + 1.3491, & 40 \le \frac{D}{t} \le 150 \end{Bmatrix}$

, as proposed by Hu.et.al., 2003, ...(3.9)

$$r = \begin{Bmatrix} 1 \;, & f'_c \le 30\; Mpa \\ \frac{(f'_c - 30)(0.5 - 1)}{(100 - 30)} + 1, & 30 < f'_c < 100\; MPa \\ 0.5 & 100 \le f'_c\; MPa \end{Bmatrix} \ldots \ldots \ldots . (3.10)$$

, as proposed by Ellobody and Young , (2006)

Square concrete filled steel tubular column

According to **Hu et al., 2003**, the lateral confining pressure for square concrete filled steel tube is determined as:

$$\frac{f_l}{\sigma_y} = \begin{Bmatrix} 0.055048 - 0.001885 * \left({}^{b}/_{t}\right) & (17 \le b/t \le 29.2) \\ 0 & (29.2 \le b/t \le 150) \end{Bmatrix} \ldots \ldots \ldots \ldots (3.11)$$

The strength degradation parameter corresponding to $11\varepsilon_{cc}$ for concrete filled steel square column is calculated as follows:

$$k_3 = \begin{Bmatrix} 0.000178 * (b/t)^2 - 0.02492 * (b/t) + 1.2722 & (17 \le b/t \le 70 \\ 0.4 & (70 \le b/t \le 150) \end{Bmatrix} \ldots \ldots (3.12)$$

As shown in figure 3.4, the confined concrete goes through three phases when axially loaded such that:

- ➢ First stage: $\left(0 \le \varepsilon \le 0.5 \frac{f'_{cc}}{\varepsilon_{cc}}\right)$

  In this stage, the confined concrete is assumed to behave linearly untill it reaches the proportionality limit which is $0.5f'_{cc}$ as given by Hu, et.al, 2003. Actually, the Young's

modulus of confined concrete (E_{cc}) can be calculated using the ACI code, 2011,

equation: $E_{cc} = 4700\sqrt{f'_{cc}}\, MPa.$ ... ... (3.13)

$The\ confined\ concrete's\ poisson's\ ratio\ \nu = 0.2$, [$Ellobody, et\ al.$ 2006]

- Second stage: $(0.5\frac{f'_{cc}}{E_{cc}} \le \varepsilon \le \varepsilon_{cc})$

  This is the nonlinear phase of the curve that starts from the proportionality limit ($0.5f'_{cc}$) till the confined concrete strength f'_{cc}. This portion of the curve can be described by equation (3.14) proposed by (Desayi and Krishnan , 1964), where the uniaxial stress (f) and the corresponding strain (ε) are the knowns of this equation.

$$f = \frac{E_{cc}\varepsilon}{1 + \left[(R + R_E - 2)\left(\frac{\varepsilon}{\varepsilon_{CC}}\right)\right] - \left[(2R - 1)\left(\frac{\varepsilon}{\varepsilon_{CC}}\right)^2\right] + \left[R\left(\frac{\varepsilon}{\varepsilon_{CC}}\right)^3\right]} \quad \ldots\ldots\ldots (3.14)$$

where $R_E = \frac{\varepsilon_{CC}E_{CC}}{f'_{cc}}$

$R = \frac{R_E(R_\sigma - 1)}{(R_\varepsilon - 1)^2} - \frac{1}{R_\varepsilon}$

$R_\varepsilon = R_\sigma = 4 \quad as\ proposed\ by$ (Ellobody et al., 2006).

- Third stage: $(\varepsilon_{cc} \le \varepsilon \le 11\varepsilon_{cc})$

  This is the descending phase of the curve that starts from the confined concrete strength f'_{cc} untill the lower stress value $rk_3f'_{cc}$.

The tensile behavior of the confined concrete was assumed to be linear throughout its increasing and decreasing stages as given by stress strain diagram shown in figure 43.

Montoya et al., 2006, proposed an equation to calculate f_{ct} for uncofined concrete that can be used for confined concrete.

$$f_{ct} = 0.65\left(f'_c\right)^{0.33} \quad \ldots\ldots\ldots (3.15)$$

After developing the uniaxial stress-strain diagram for confined concrete is determined in both compression and tension, the concrete material behavior can then be defined in ABAQUS by defining the following three main sections:

- ✓ General: In ABAQUS /Explicit model density is required to be defined. Concrete density varies from 2400 kg/m^3. However, In this analysis this section is not needed since the analysis type is ABAQUS/ Standard.

- ✓ Elastic: The linear segment of the confined concrete's stress-strain was defined using Young's modulus of confined concrete$E_{cc} = 4700\sqrt{f'_{cc}}$ and concrete's Poisson's ratio (ν = 0.2)
- ✓ Plastic: concrete damaged plasticity is utilized is section. The parameters defined in this section are shown in table 3

3.4.2 Steel Tube modelling

The idealized stress-strain curve for steel was developed as propsed by Tao et al (2013). Tao et al. (2013) proposed stress-strain diagram for structural steel with validity range of f_y from 200 MPa to 800 MPa. The stress-strain model used in CFST was expressed as follows.

$$\sigma = \begin{cases} E_s * \varepsilon & 0 \le \varepsilon < \varepsilon_y \\ f_y & \varepsilon_y \le \varepsilon < \varepsilon_p \\ f_u - (f_u - f_y) * \left(\frac{\varepsilon_u - \varepsilon}{\varepsilon_u - \varepsilon_p}\right)^p & \varepsilon_p \le \varepsilon < \varepsilon_u \\ f_u & \varepsilon \ge \varepsilon_u \end{cases} \quad \ldots\ldots\ldots\ldots\ldots\ldots\ldots\ldots\ldots\ldots\ldots\ldots (3.16)$$

where, $\varepsilon_y = \frac{f_y}{E_S}$, $p = E_p * \left(\frac{\varepsilon_u - \varepsilon_p}{f_u - f_y}\right)$ *and* $E_p = 0.02E_s$

ε_p and ε_u are determined using the following equation

$$\varepsilon_p = \begin{cases} 15\varepsilon_y & f_y \le 300MPa \\ [15 - 0.018(f_y - 300)]\varepsilon_y & 300MPa < f_y \le 800MPa \end{cases} \quad \ldots\ldots\ldots\ldots (3.17)$$

$$\varepsilon_u = \begin{cases} 100\varepsilon_y & f_y \le 300MPa \\ [100 - 0.15(f_y - 300)\varepsilon_y & 300MPa < f_y \le 800MPa \end{cases} \quad \ldots\ldots\ldots (3.18)$$

For simplicity , stress-strain curve of steel is idealized as trilinear curve. The curve is divided into three parts with three linear curves. First part of the curve is elastic up to yield point withe the slope equal to the elastic modulus of steel. The second part is constant at yield stress f_y which is plastic in nature. The third part of the curve shows strain hardening starting from ε_t up to ultimate stress $f_{ult}$and ultimate strain ε_u of steel. ($\varepsilon_p = 15\varepsilon_y$)

The material properties obtained from the standard coupon test were input to the ABAQUS model as a set of points on the stress - strain curve. (ABAQUS 6.14) uses true stress and true

strain, and hence the values of engineering stress and engineering strain from the standard coupon test were modified before being inserted into the model using the following equations:

$$\sigma = \sigma(1 + e) \ldots \ldots \ldots \ldots \ldots \ldots \ldots (3.19)$$

$$e = ln(1 + e) - \frac{\sigma}{E} \ldots \ldots \ldots \ldots \ldots \ldots \ldots (3.20)$$

where σ - True stress

e - Engineering stress

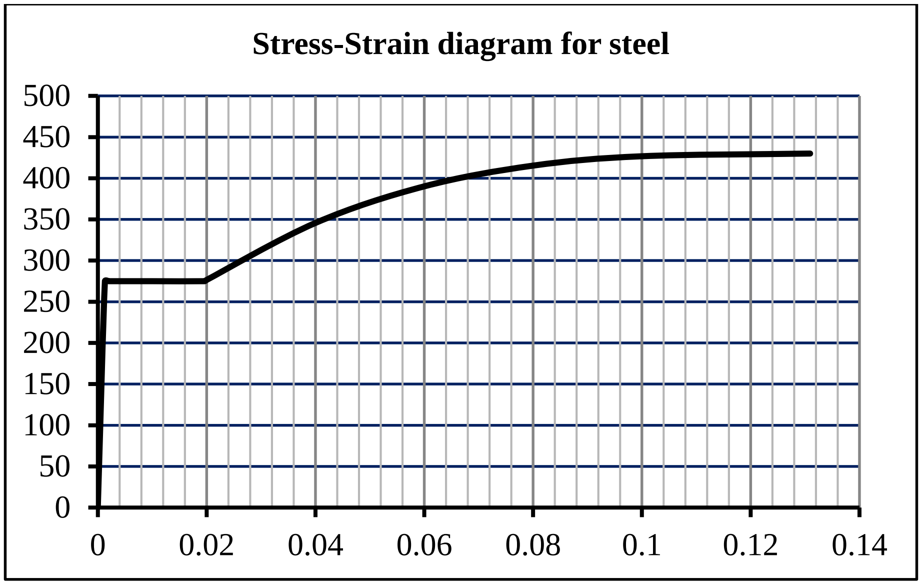

Figure 3.6: The constitutive stress – strain model for steel used in the analysis for S-275

There are three main parts to define steel behavior in ABAQUS:

- Density: Steel average density is $7.85 \times 10^{-6}\ kg/mm^3$. Since the model in this section is standard analysis defining density is not required.
- Elastic: The linear segment of the steel's stress-strain curve is defined in this section. The young's modulus of steel ($E = 210GPa$) and its poisson's ratio (ν = 0.3)
- Plastic: The nonlinear part of the stress-strain curve was defined.

3.5 Constraints

When considering composite materials to ensure physical contact, different linking methods are available. Two types of constraint were selected in these models; the embedded region constraint and the "Tie" constraint.

I. Embedded Region

The concrete behavior is independent of the steel behavior, so the interaction between concrete and steel, the embedded bond (perfect bond) was defined in this study to simulate load transfer between concrete and steel in steel reinforced concrete filled tube (SRCFT). During modelling in ABAQUS concrete core was considered as embedded region whereas steel tube was considered as host region.

II. Tie Constraint

In concrete filled tube,the constraint between steel and concrete was chosen to be a "Tie" constraint in ABAQUS. In using this constraint, some basic rules must be followed. In principle, the master surface should be applied to the stronger material compared with the material using the slave surface. Hence concrete surface was defined as master surface where as steel surface chosen as slave surface during simulation.

3.6 Boundary condition and load application.

Each models were considered fixed at base and free at its top end to allow lateral movement.

For this case, the specimen is subjected to constant gravity load and incremental cyclic lateral top displacements. Moment-curvature response reflects the change between cycles and load cases, so the degradation in both strength and stiffness was tracked throughout the load protocol.

Cyclic loading studies on concrete filled tube columns were focused on standard loading protocols with varying drift amplitude to obtain the cyclic behaviour, without considering the effects of amplitude and number of cycles on damage accumulation. The overall buckling of in-filled columns is relatively simple, but the complexity increases with failure modes under the combination of axial load and lateral cyclic load.

3.6.1 Drift ratio

The drift ratio is taken as the lateral displacement normalized by height measured from the top of the bottom plate to the point of lateral load application. The loading procedure was continued until the failure of the specimen.

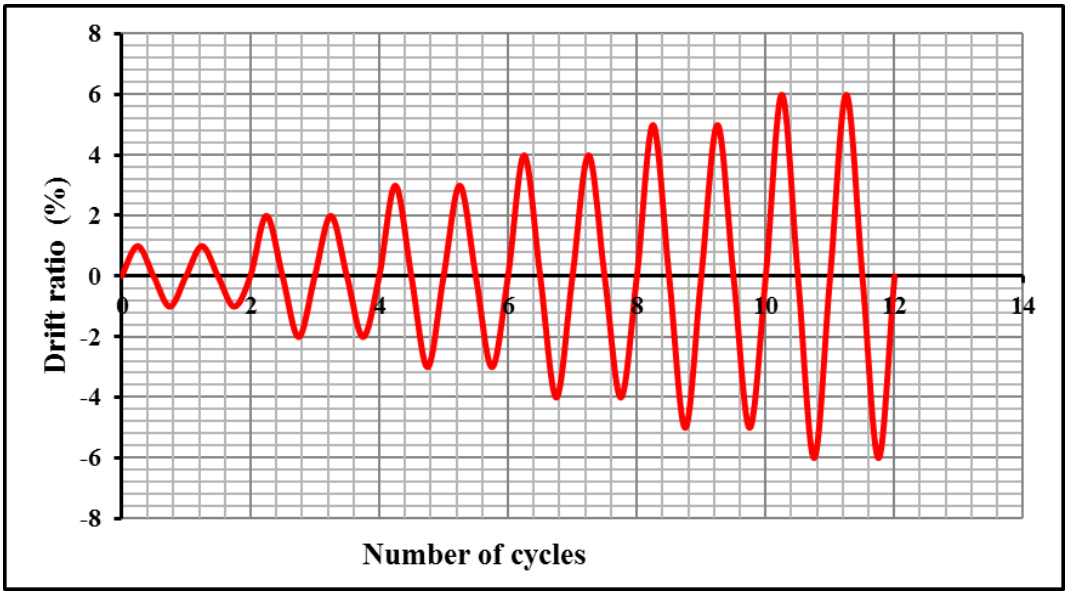

Figure 3.7: Loading protocol

3.7 Mesh Size

The mesh size of FE model has a big influence on the computed softening behaviour of concrete. It is desirable to minimize the number of elements within a model, provided the results of the analysis are not unduly affected by removing the elements. In this analysis an aspect ratio of 20 was used for mesh refinement of circular concrete filled tube and aspect ratio of 50 was used for square concrete steel tubular column.

A mesh size sensitivity study was conducted to determine the most suitable finite element mesh size. The mesh size should be fine enough to achieve the desired accuracy. However, mesh refinement leads to an increase in the simulation time and requires more computational resource.

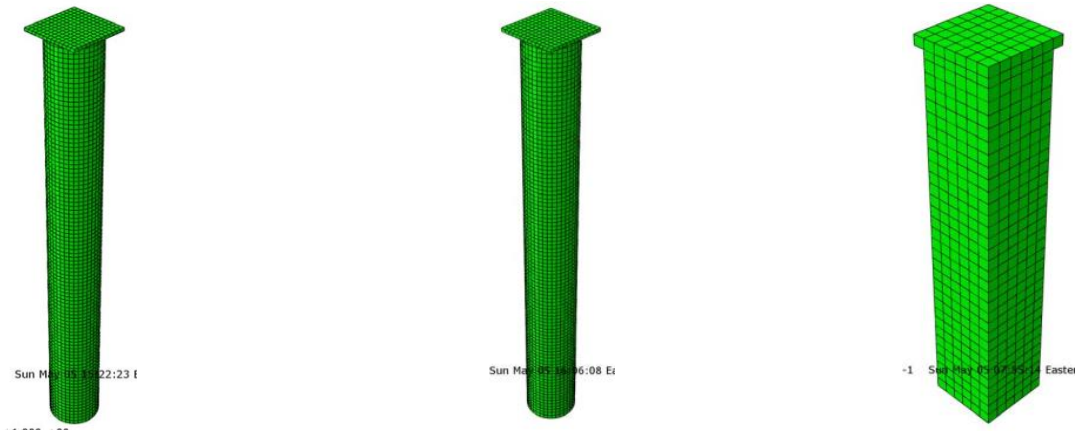

Figure 3.8: Circular and square concrete filled steel tubular meshed models.

3.8 Validation of finite element method with experiment from literature review

To verify the validity of the finite element models of the concrete filled steel tubular columns, the simulation results were compared with the existing experimental results.

Experimental test from (**Schneider,1998**) was used to verify the finite element model of this study. Two main aspects of the model results are considered in the comparisons with the experimental results: the failure mode, axial load-shortening results.

Similar to the failure modes observed in the tested specimens, the dominant failure mode in the FE analysis of the concrete filled steel tube column is local buckling of the structural steel accompanied with crushing of concrete infill. Steel tube bulged outwards locally near loading ends and in the mid-height of the sample.

Schneider (1998) presented experimetal and analytical study on behavior of axially loaded concrete filled steel tubes. Fourteen specimens were tested: namely, three circular, five square and six rectangular. Among them one of square concrete filled steel tubular column with following properties has been taken for validation.

Table 3.2: Schneider's work on square concrete filled steel tubular columns.

Sample	Length (mm)	Size (B x t) (mm)	E_s (MPa)	Ec (MPa)	f_c (MPa)	f_y (MPa)	Peak Load (kN)
S4	635	127 x5.67	203944	23528	23.8	312	1179

The axial load versus axial shortening predicted by the proposed FE model is compared with the experimental results for the same CFST specimen as shown in fgure 3.9. The sample stiffness and its ultimate capacity predicted by the FE model relatively close to the actual tested specimen.

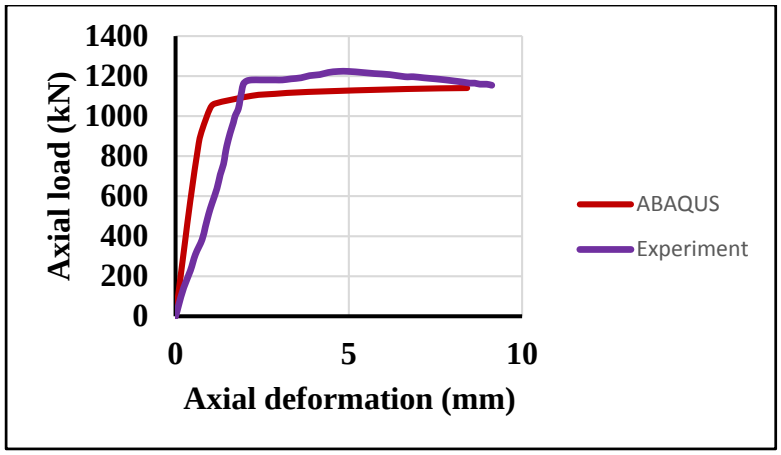

Figure 3.9: Comparison of axial load vs axial shortening of square concrete filled steel tubular column (from finite element model)

The deformation in Schneider's study was 2.05 mm for peak load of 1179 kN. From finite element model, deformation was 0.996 mm for peak load of 1036.92 kN. Similar trend is observed in both graphs. Once peak load is achieved, load step gradually decreases with further increase in deformation. Hence steps are taken up to certain points where peak load is achieved.

Based on the above comparisons it can be concluded that the FE model is relatively validated for monotonic loading and can be further used to conduct comprehensive parametric studies to investigate other different parameters.

Material properties from Qin,2013 was taken to validate model for cyclic loading.

Specimen	Diameter	thickness	D/t	Height	Fc	Fy	Fu	P
	mm	mm		mm	Mpa	Mpa	Mpa	kN
CN-56-20-A	336	6	56	1500	35	339	439	1300

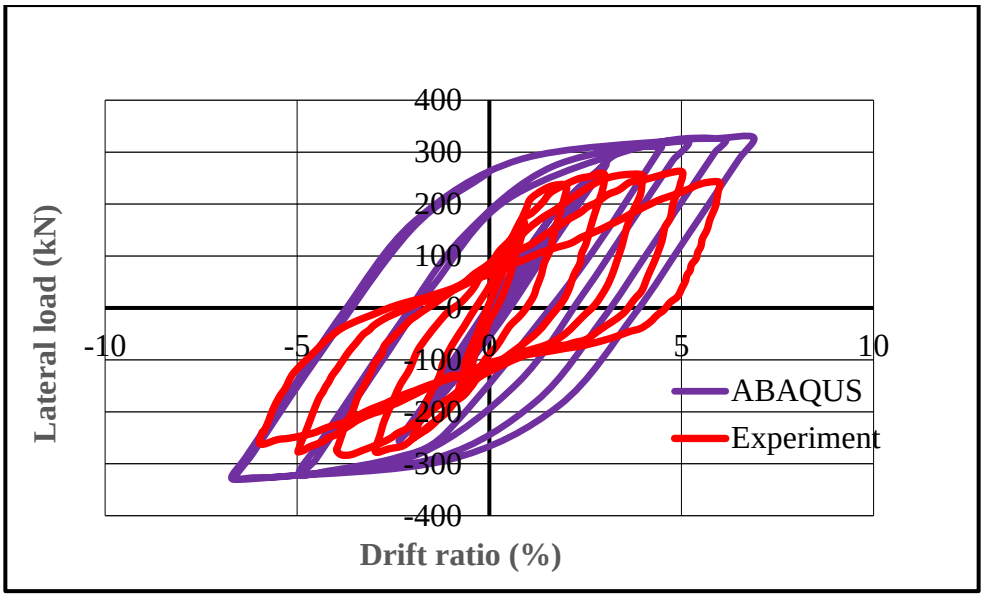

Figure 3.10: Hysteretic curve from ABAQUS based on [Qin P. and Xiao Y., 2013) model

Figure 3.11 shows that hysteretic curve from finite element model and hysteretic curve from experimental result by [Qin P. and Xiao Y., 2013]. Hysteretic curve from finite element model yields peak lateral load of 328.66 kN and peak drift ratio of 6.88 % whereas experimental result from Qin P. and Xiao Y., 2013, yields peak lateral load of 250 kN and drift ratio of 6.7 %. Percentage of difference between the two peak values gives 23.78% which is in the acceptable range.

CHAPTER FOUR

4 PARAMETRIC STUDIES

4.1 Circular Concrete Filled Steel Tube

Concrete filled tube with outer diameter of 368 mm was studied to incorporate effect of several geometric and material parameters those can significantly affect its behavior.

A comprehensive parametric study was performed using non-linear three-dimensional finite element analysis which includes a wide range of aspect ratios, concrete with different compressive strengths and slenderness ratios.

For parametric study on concrete filled tube circular and square section were analyzed.

Study parameters for concrete filled tube are:

- Steel contribution ratio
- Column slenderness ratio
- Steel yield strength
- Compressive strength of concrete

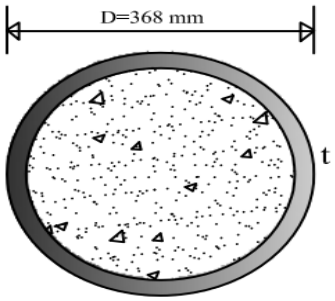

Figure 4.1: Cross section of Circular concrete filled steel tube

Table 4.1: Investigating effect of thickness on CFT columns

Column specimen	Diameter (mm)	Thickness (mm)	d/t	Length (mm)	Area of Section (mm^2)	Concrete strength (fcu) MPa	Steel yield Strength(fs) MPa
CFT-1	368	10	36.8	3000	11200	30	275
CFT-2	368	12	30.67	3000	13400	30	275
CFT-3	368	14	26.28	3000	15600	30	275
CFT-4	368	16	23	3000	17700	30	275
CFT-5	368	20	18.4	3000	21900	30	275

Table 4.2: Investigating effect of Compressive Strength on CFT columns

Column specimen	Diameter (mm)	Thickness (mm)	d/t	Length (mm)	Area of Section (mm^2)	Concrete strength (fcu) MPa	Steel yield Strength(fs) MPa
CFT-6	368	14	26.28	3000	15600	25	275
CFT-7	368	14	26.28	3000	15600	30	275
CFT-8	368	14	26.28	3000	15600	37	275
CFT-9	368	14	26.28	3000	15600	50	275

Table 4.3: Investigating effect of height on CFT columns

Column specimen	Diameter (mm)	Thickness (mm)	d/t	Length (mm)	Area of Section (mm^2)	Concrete strength (fcu) MPa	Steel yield Strength(fs) MPa
CFT-10	368	14	26.28	2500	15600	30	275
CFT-11	368	14	26.28	3000	15600	30	275
CFT-12	368	14	26.28	3500	15600	30	275
CFT-13	368	14	26.28	4000	15600	30	275

Table 4.4: Investigating effect of yield strength of steel on CFT columns

Column specimen	Diameter (mm)	Thickness (mm)	d/t	Length (mm)	Area of Section (mm^2)	Concrete strength (fcu) MPa	Steel yield Strength(fs) MPa
CFT-14	368	14	26.28	3000	15600	30	235
CFT-15	368	14	26.28	3000	15600	30	275
CFT-16	368	14	26.28	3000	15600	30	355

4.2 Steel reinforcing concrete filled steel tube

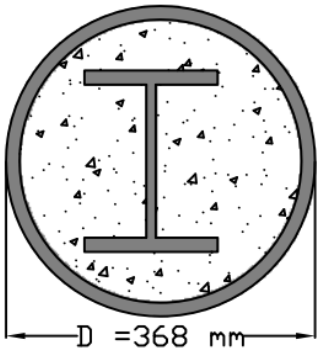

Figure 4.2: Steel reinforced concrete filled steel tube cross section

Table 4.5: Investigating effect of reinforcing steel thickness on S-RCFST

Column specimen	Steel tube properties					A_a I-section (cm^2)	Concrete strength (fcu) MPa	Steel yield Strength (fs) MPa
	D (mm)	T (mm)	d/t	H (mm)	Aa (cm^2)			
SRCFT-1	368	14	26.3	3000	156	**21.2**	C-30	S-275
SRCFT-2	368	14	26.3	3000	156	**25.3**	C-30	S-275
SRCFT-3	368	14	26.3	3000	156	**31.4**	C-30	S-275
SRCFT-4	368	14	26.3	3000	156	**45.3**	C-30	S-275

Table 4.6: Investigating effect of Compressive strength SRCFT

Column specimen	Steel tube properties					A_a I-section (cm^2)	Concrete strength (fcu) MPa	Steel yield Strength (fs) MPa
	D (mm)	T (mm)	d/t	H (mm)	Aa (cm^2)			
SRCFT-5	368	14	26.3	3000	156	31.4	C-25	S-275
SRCFT-6	368	14	26.3	3000	156	31.4	C-30	S-275
SRCFT-7	368	14	26.3	3000	156	31.4	C-37	S-275
SRCFT-8	368	14	26.3	3000	156	31.4	C-50	S-275

Table 4.7: Investigating effect of slenderness ratio on S-RCFT

Column specimen	Steel tube properties					A_a I-section (cm^2)	Concrete strength (fcu) MPa	Steel yield Strength (fs) MPa
	D (mm)	T (mm)	d/t	H (mm)	Aa (cm^2)			
SRCFT-9	368	14	26.3	2500	156	31.4	C-30	S-275
SRCFT-10	368	14	26.3	3000	156	31.4	C-30	S-275
SRCFT-11	368	14	26.3	3500	156	31.4	C-30	S-275
SRCFT-12	368	14	26.3	4000	156	31.4	C-30	S-275

Table 4.8: Investigating effect of Steel yield strength on S-RCFT

Column specimen	Steel tube properties					A_a I-section (cm^2)	Concrete strength (fcu) MPa	Steel yield Strength (fs) MPa
	D (mm)	T (mm)	d/t	H (mm)	Aa (cm^2)			
SRCFT-13	368	14	26.3	3000	156	31.4	C-25	S-235
SRCFT-14	368	14	26.3	3000	156	31.4	C-30	S-275
SRCFT-15	368	14	26.3	3000	156	31.4	C-37	S-355

4.3 Square concrete filled steel tube

The square CFST column is still increasingly used in construction of structures for the reasons of being easier in beam-to-column connection design, high cross sectional bending stiffness and good aesthetic effects. Moreover, with increasing span of bridges and height of buildings, the cross section area of a square CFST column is often designed large enough to provide required high load carrying capacity.

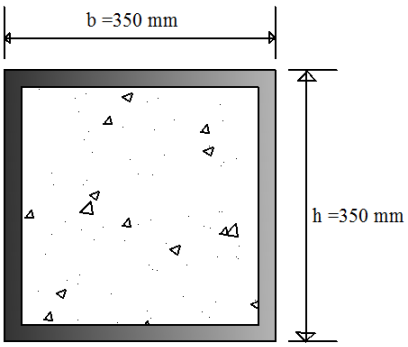

Figure 4.3: Cross section for square concrete filled steel tube

For square concrete filled tube varying parameters are shown below.

Table 4.9: Investigating effect of thickness on CFT columns

Column specimen	Steel section (mm x mm)	Thickness (mm)	Length (mm)	Area of steel(mm^2)	Concrete Strength (fcu) MPa	Steel yield Strength (fyk) MPa
S-CFT-1	350 X350	10	3000	13600	C-30	S-275
S-CFT-2	350 X350	12.5	3000	16800	C-30	S-275
S-CFT-3	350 X350	16	3000	21300	C-30	S-275

Table 4.10: Investigating effect of concrete compressive strength on S-CFT columns

Column specimen	Steel section (mm x mm)	Thickness (mm)	Length (mm)	Area of steel (mm^2)	Concrete Strength (fcu) MPa	Steel yield Strength (fyk) MPa
S-CFT-4	350 X350	12.5	3000	16800	C-25	S-275
S-CFT-5	350 X350	12.5	3000	16800	C-30	S-275
S-CFT-6	350 X350	12.5	3000	16800	C-37	S-275
S-CFT-7	350 X350	12.5	3000	16800	C-50	S-275

Table 4.11: Investigating effect of slenderness ratio on S-CFT columns

Column specimen	Steel section (mm x mm)	Thickness (mm)	Length (mm)	Area of steel (mm^2)	Concrete Strength (fcu) MPa	Steel yield Strength (fyk) MPa
S-CFT-8	350 X350	12.5	2500	16800	C-30	S-275
S-CFT-9	350 X350	12.5	3000	16800	C-30	S-275
S-CFT-10	350 X350	12.5	3500	16800	C-30	S-275
S-CFT-11	350 X350	12.5	4000	16800	C-30	S-275

Table 4.12: Investigating effect of steel yield strength on S-CFT columns

Column specimen	Steel section (mm x mm)	Thickness (mm)	Length (mm)	Area of steel (mm^2)	Concrete Strength (fcu) MPa	Steel yield Strength (fyk) MPa
S-CFT-12	350 x 350	12.5	3000	16800	30	***235***
S-CFT-13	350 x 350	12.5	3000	16800	30	***275***
S-CFT-14	350 x 350	12.5	3000	16800	30	***355***

CHAPTER FIVE

5 RESULTS AND DISCUSSIONS

Numerical analysis of CFST columns were done using ABAQUS 6.14 software. The effect of different parameters on the behaviour of CFST columns under axial and cyclic loading are illustrated below.

5.1 Hysteresis Curves for concrete filled steel tubular column

The plot of lateral load and lateral displacement gives the hysteresis loops for the specimens subjected to cyclic lateral loading. The hysteresis curves for different specimens were plotted.

5.1.1 Diameter to thickness ratio (D/t)

This study was conducted on five circular concrete filled steel tubular columns to investigate the effect of thickness variation on the performance the column. The decrease in D/t ratio may be either due to the decrease in diameter or due to the increase in thickness of the section. However, it is analyzed by keeping the diameter constant and increasing the thickness. For this study, the D/t ratio was varied from 36.8 to 18.4. The decrease in D/t ratio with increased thickness for a constant diameter represents the improvement in cross section of the steel tube and hence produces greater section capacity. When the D/t ratio is decreased from 36.8 to 18.4, ultimate lateral load of the column is increased by 120.8%. The comparison of hysteresis behaviour of the five different D/t ratio is shown in figure 5.1.

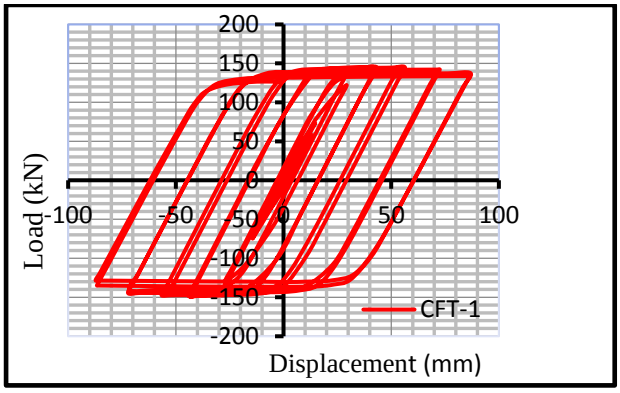

a) Specimen-1

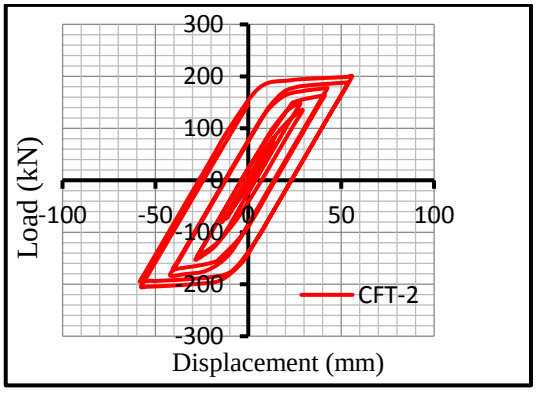

b) Specimen 2

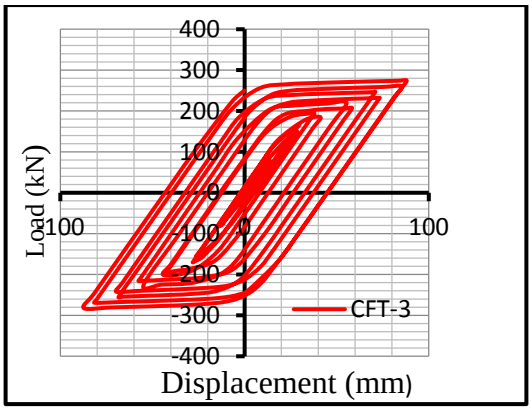

c)specimen-3

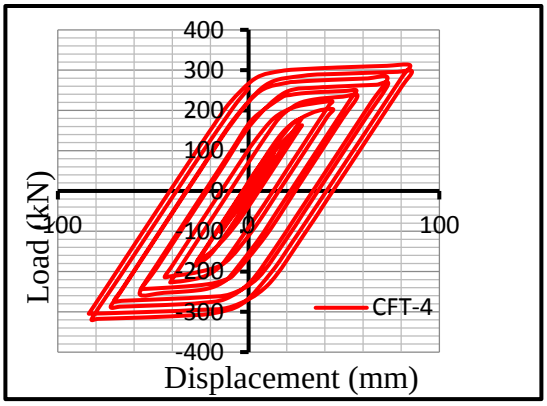

d) specimen-4

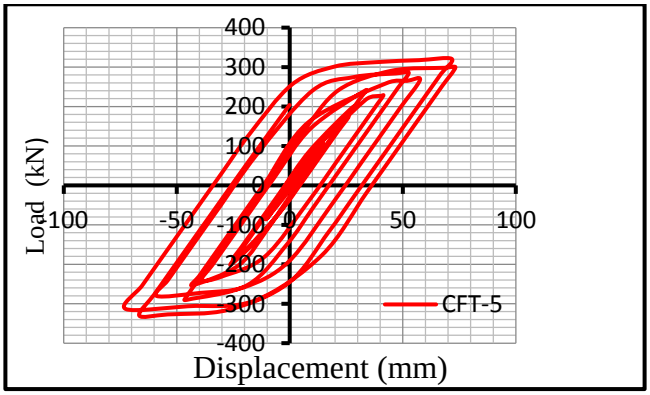

e) Specimen -5

Figure 5.1: Lateral load-displacement hysteresis curves for different D/t ratio (cyclic load alone)

Parametric study with variable diameter to thickness ratio by considering axial load of $0.4P_u$ and cyclic lateral loading.

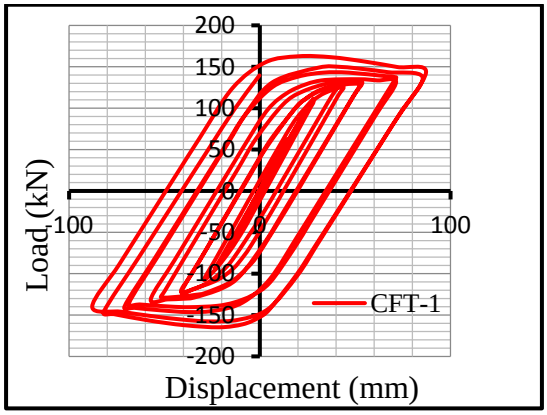

a) specimen 1

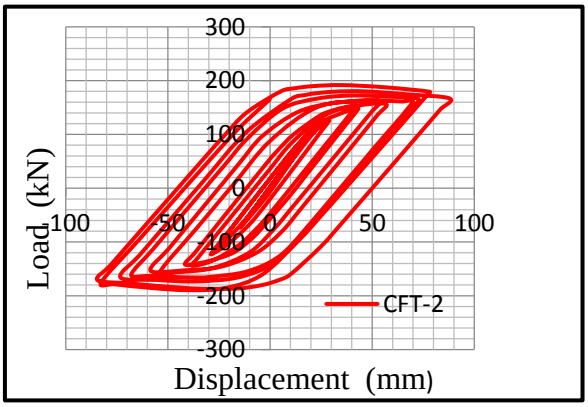

b) Specimen 2

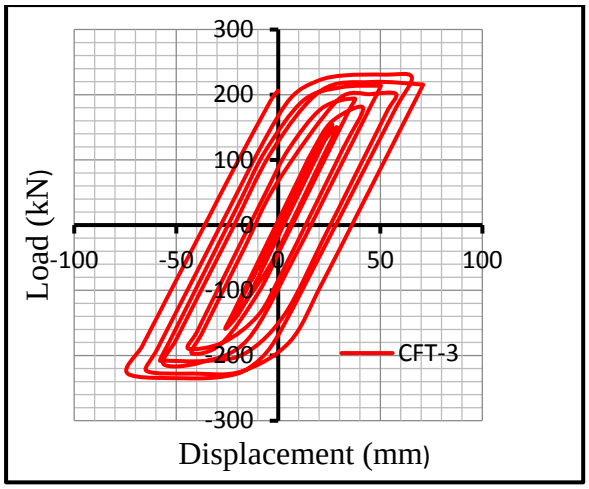

c) specimen 3

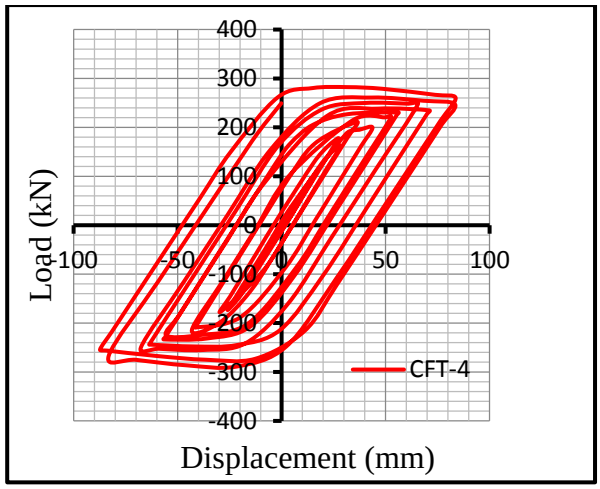

d) Specimen-4

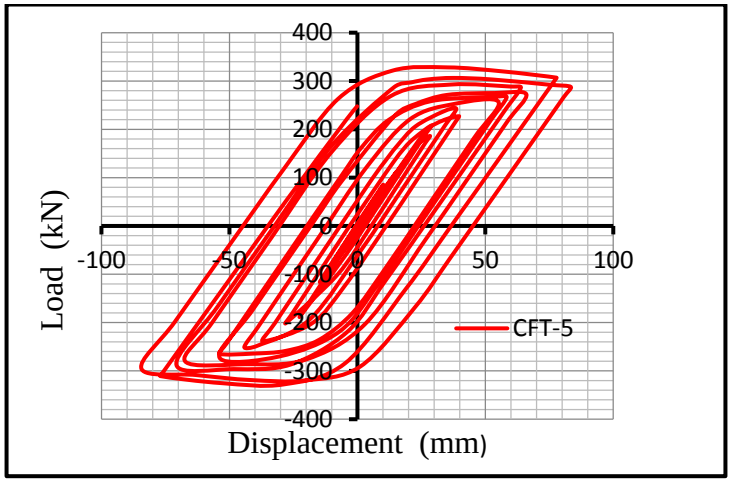

e) Specimen-5

Figure 5.2: Lateral load-displacement hysteresis curves for different D/t ratio (cyclic load +axial load)

Strength Capacity of specimen

The effect of thickness on the ultimate axial load carrying capacity of CFST columns are illustrated below:

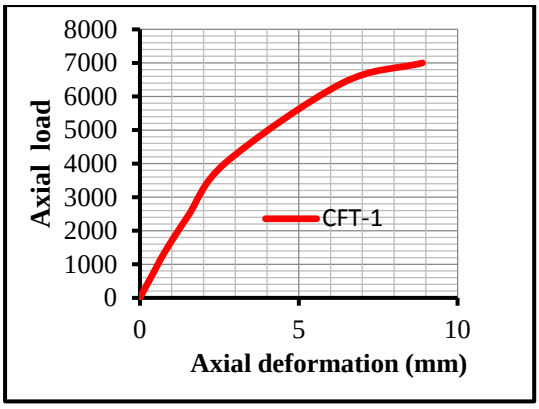

a) Specimen-1

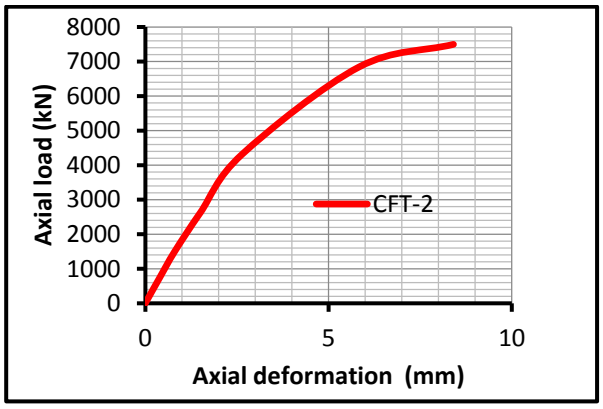

b) Specimen-2

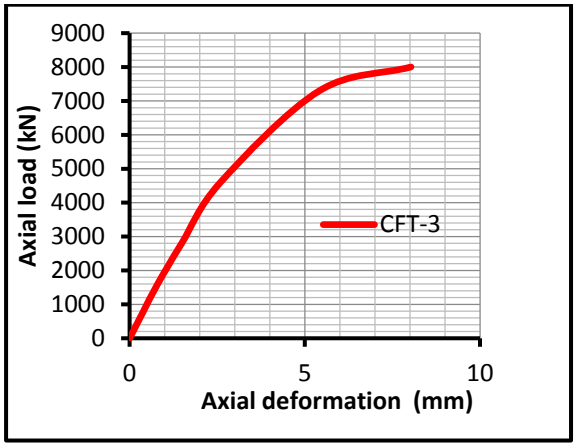

c) specimen-3

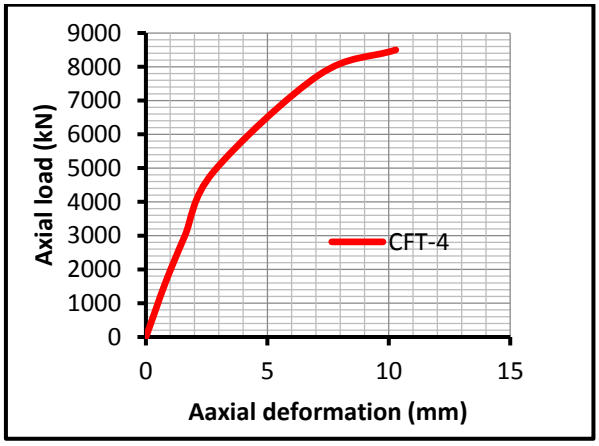

d) Specimen-4

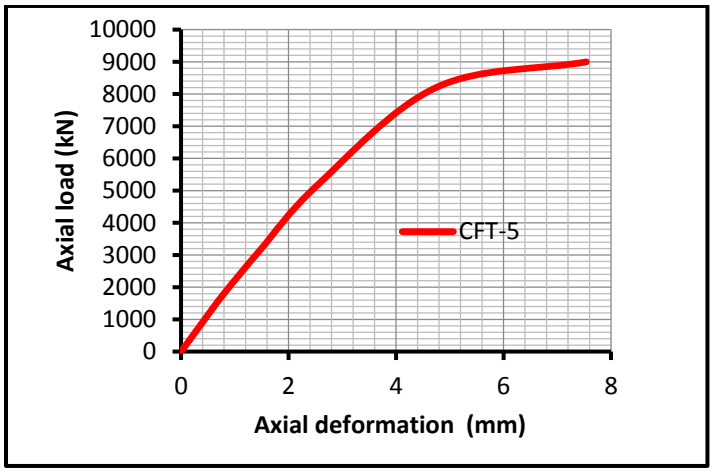

e) Specimen-5

Figure 5.3: axial load- axial deformation curves for different diameter to thickness ratio.

The result indicates that, axial load capacity of CFST column can be significantly increased with increase in thickness of steel tube.

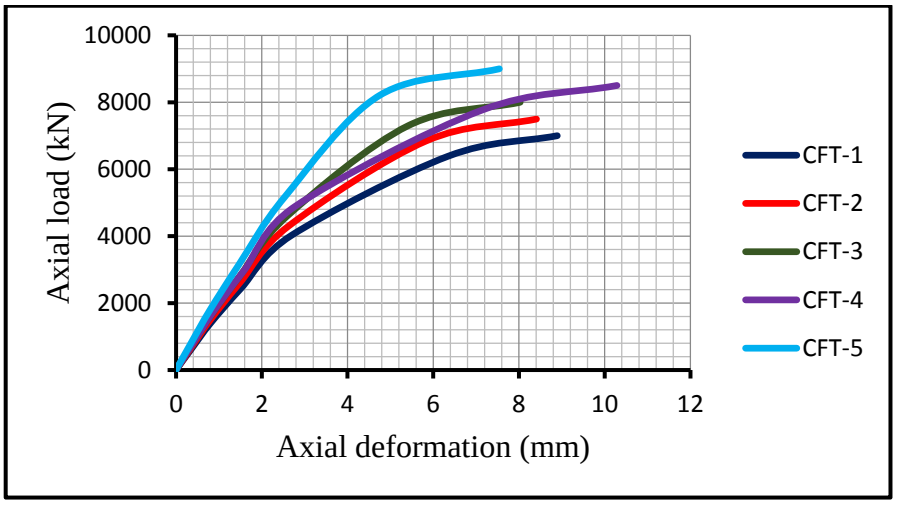

Figure 5.4: skeleton curve for different D/t ratios

5.1.2 Concrete grade effect on CCFT

Different specimens of CFST columns were taken to investigate the effect of variation of concrete on the performances of CFST column. The strength of concrete core depends on stiffness of CFST columns. Stiffness increases with increase in concrete strength but columns fail due to crushing of concrete exhibiting brittle behavior when filled with high strength concrete. However it is a fact that increase in concrete core strength increases the strength of filled columns to a larger extent. The computed cyclic load-deflection curves for CFST columns with different concrete compressive strengths are depicted in Figure 5.4 . The ultimate cyclic lateral loads of CFST columns increase with an increase in the concrete compressive strength. Increasing concrete compressive strength from 25MPa to 50 MPa increases the ultimate cyclic lateral strength by 91%.

Parametric study of CFST subjected to cyclic loading alone considering comcpressive strength as varying parameter keeping others constant.

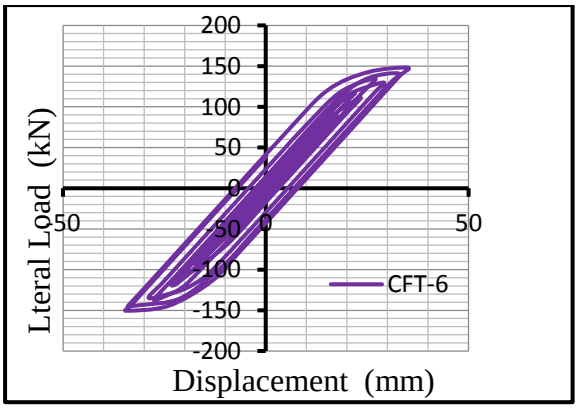

a) specimen-1

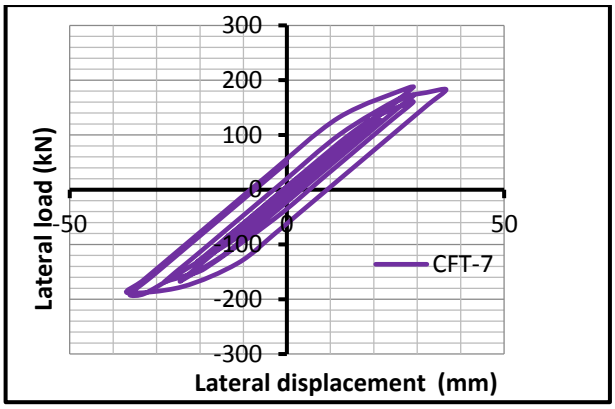

b) specimen-2

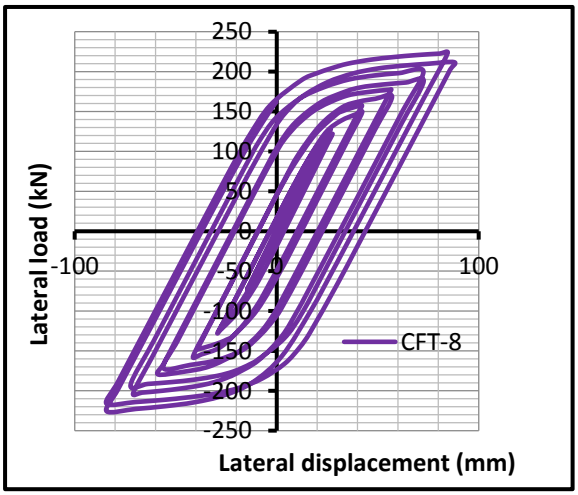

c) specimen-3

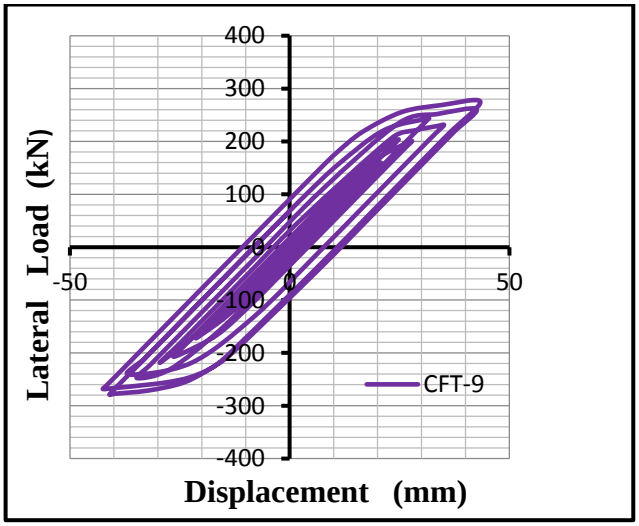

d) specimen-4

Figure 5.5: Lateral load-displacement hysteresis curves for different different concrete grade (cyclic load alone)

Parametric study with variable diameter to thickness ratio by considering axial load of $0.4P_u$ and cyclic lateral loading.

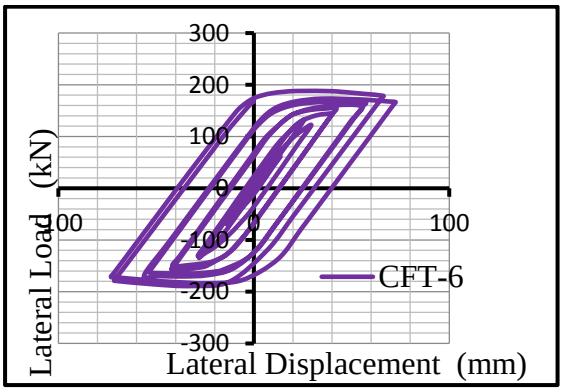

a) specimen-1

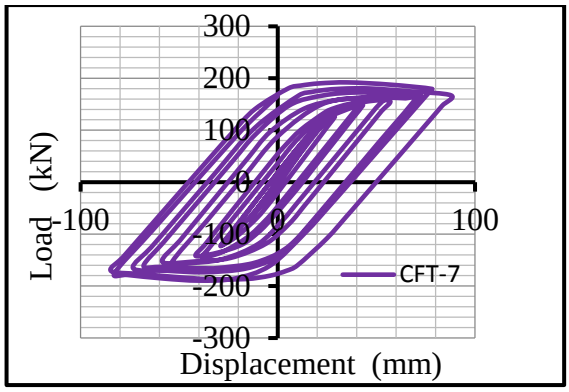

b) specimen-2

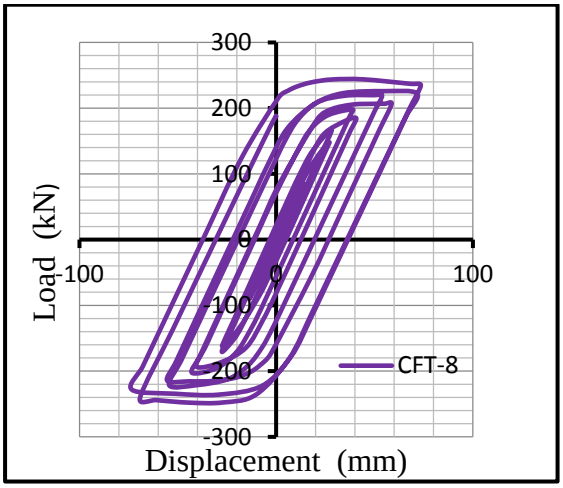

c) specimen-3

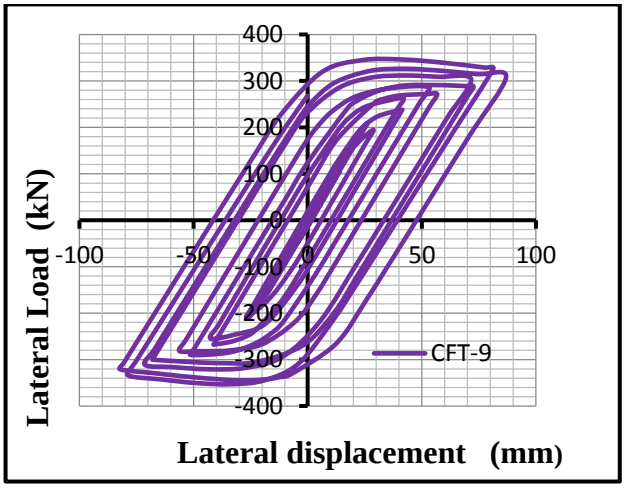

d) specimen-4

Figure 5.6: Lateral load-displacement hysteresis curves for different concrete grade (cyclic load +axial load)

5.1.3 Slenderness effect on CCFT

parametric study was conducted on five circular CFST columns to investigate the effect of slenderness ratio variation on the performances of CFST columns. The length to diameter ratio (Le/D) represents the slenderness of the column. The failure modes of CFST columns are characterized by yielding of steel followed by crushing of concrete. The strength increase will occur only for columns of smaller slenderness ratio (Le/D). Columns with greater slenderness ratio failed by overall buckling. Hence it can be observed from the analytical results that the decrease in Le/D ratio decreases the section capacity of the CFST column. The slenderness ratio was considered from 6.79 to 12.23 for this study. The hysteresis curves

of different slenderness ratios are shown in figure 5.7. Ultimate cyclic lateral load of column decreases by 51.5%.

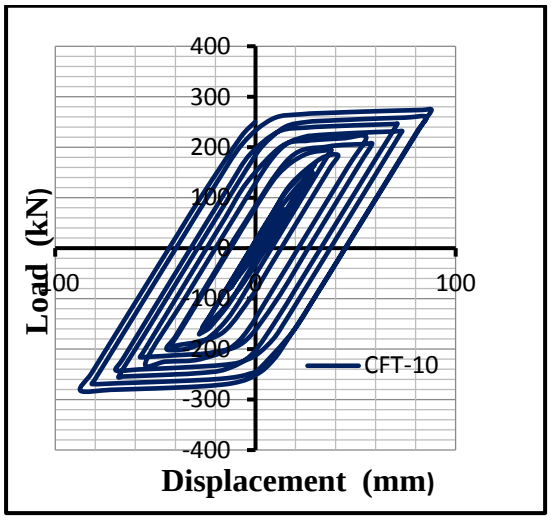

a) Specimen-1

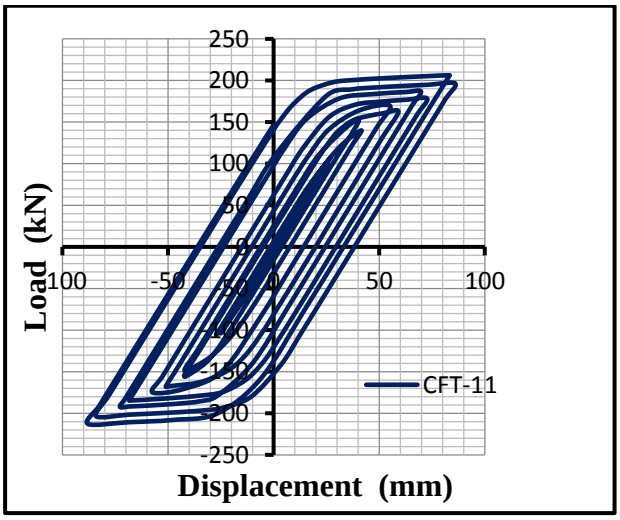

b) Specimen-2

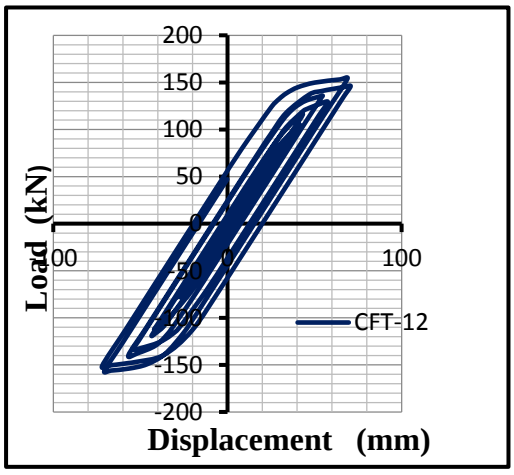

c) Specimen-3

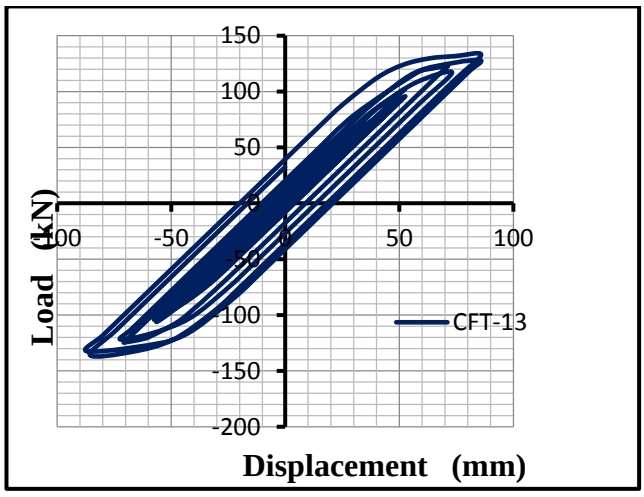

d) specimen-4

Figure 5.7: Lateral load-displacement hysteresis curves for different slenderness ratio (cyclic load alone)

Parametric study with variable diameter to thickness ratio by considering axial load of $0.4P_u$ and cyclic lateral loading.

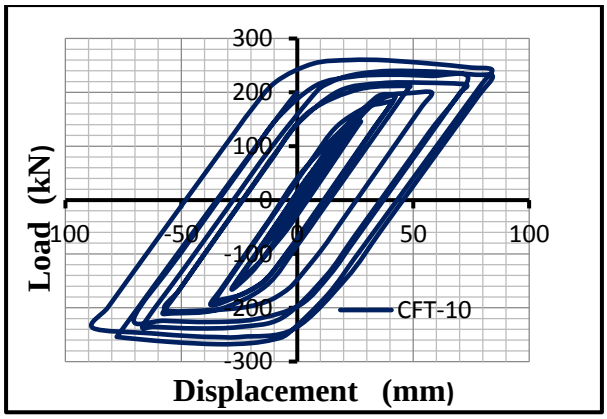

a) specimen-1

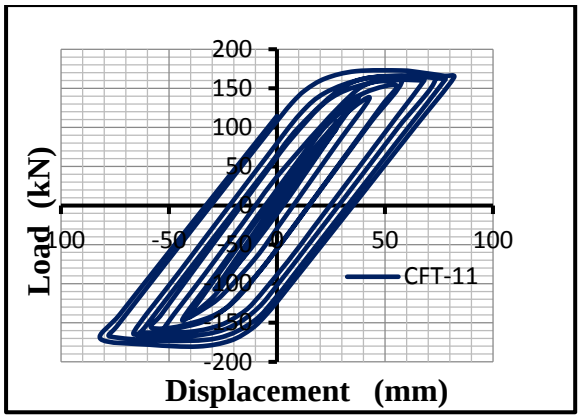

b) specimen-2

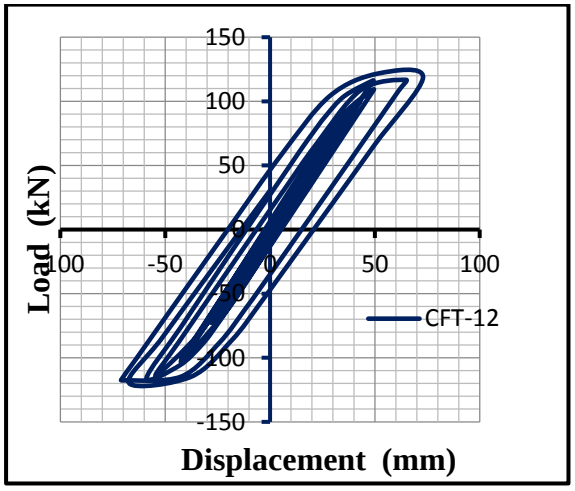

c) specimen-3

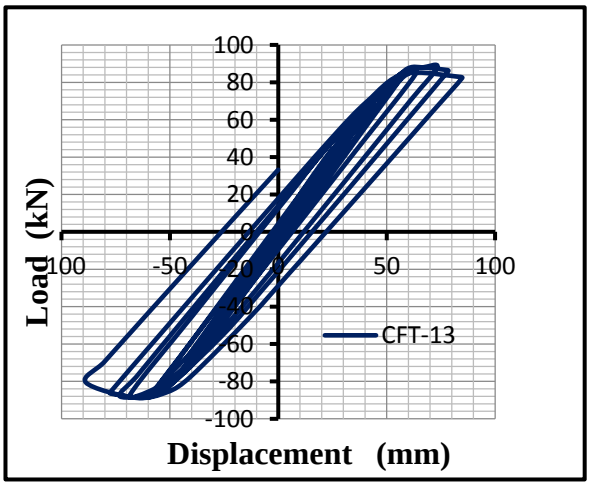

d) specimen-4

Figure 5.8: Lateral load-displacement hysteresis curves for different slenderness ratio (cyclic load +axial load)

5.1.4 Steel grade effect on CCFT

Three circular CFST columns were taken to investigate the effect of grade variation of steel grade on the performances of CFST column. The capacity of CFST column linearly increases with the increase in the steel grade. Figure 5.9 gives the cyclic lateral load-deflection curves for CFST columns with different steel yield strengths. The ultimate cyclic lateral load of columns is found to increase significantly with an increase in the steel yield strength. Ultimate cyclic lateral load of column is found to increase by 39.8% with increment of steel grade S-235 MPa to S-355MPa.

Parametric study of CFST by considering steel grade as varying parameters.

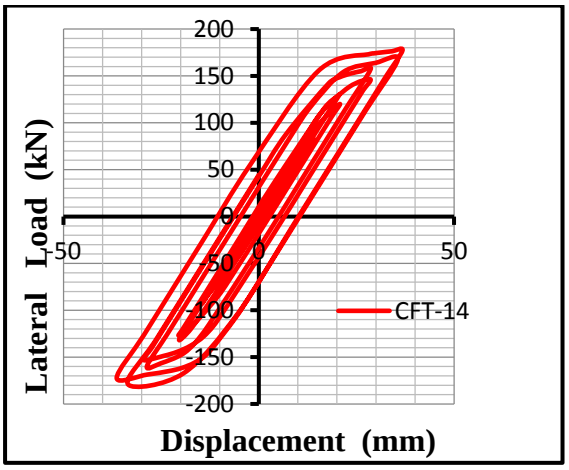

a) specimen-1

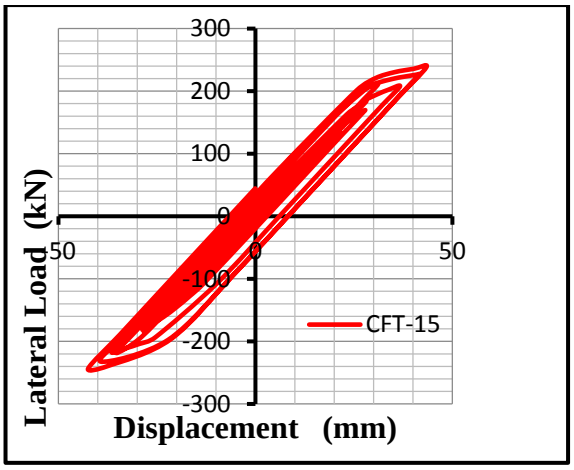

b)Specimen-2

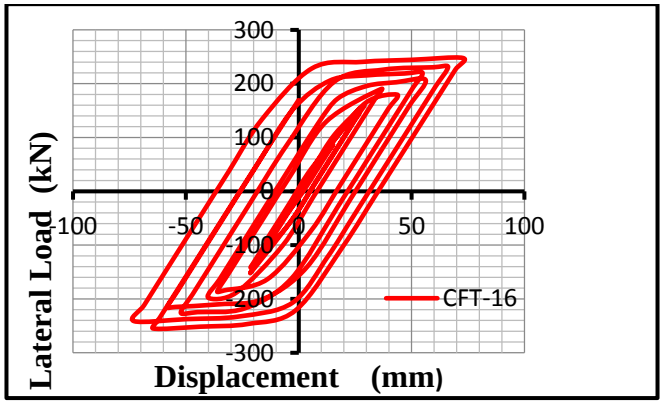

c) specimen-3

Figure 5.9: Lateral load-displacement hysteresis curves for different steel grade (cyclic load alone)

CFST subjected to cyclic lateral loading and 40 % of axial load capacity with steel grade variation. Ultimate cyclic lateral load of column is found to increase by 26 % with increment of steel grade S-235 MPa to S-355MPa

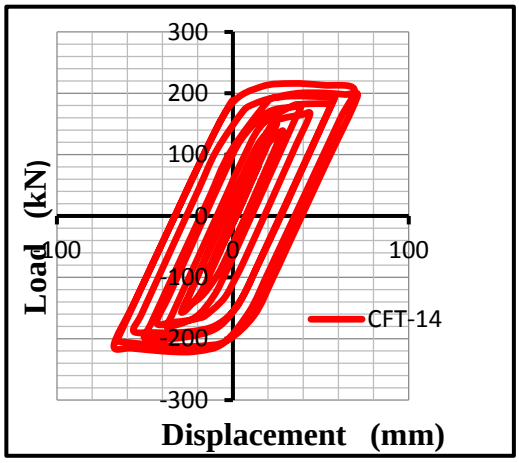

a) specimen-1

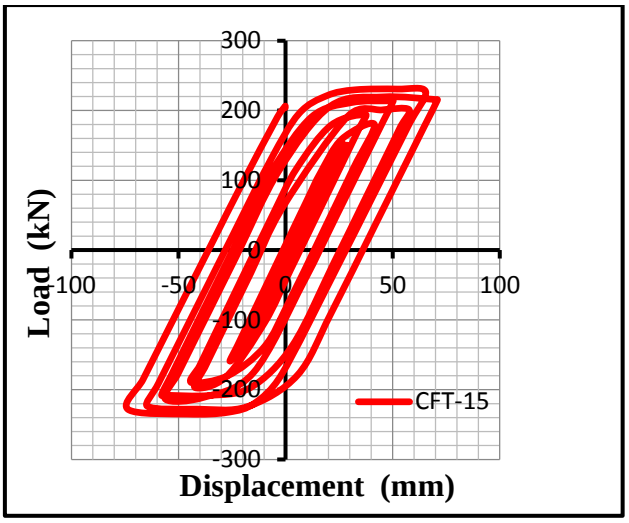

b) Specimen-2

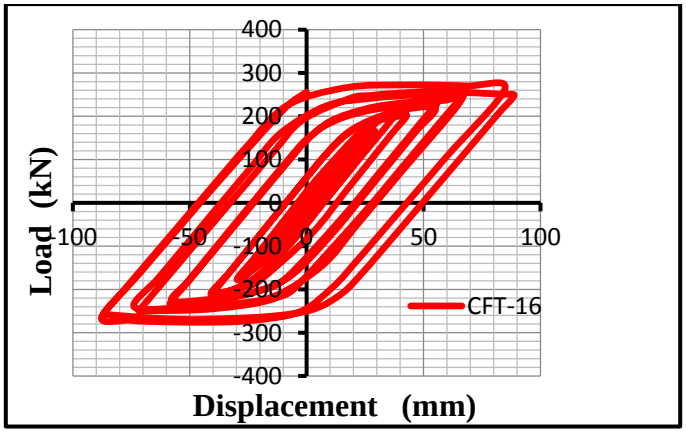

c) specimen-3

Figure 5.10: Lateral load-displacement hysteresis curves for steel grade (cyclic load +axial load)

5.2 Steel reinforced concrete filled filled steel tubular column

5.2.1 Reinforcing steel contribution ratio

Axial load capacity of steel reiforced concrete filled steel tube by considering effect of steel cross sectional area was conducted on four concrete filled steel tubular columns. Finite element modelling of CFST column under axial loading has been carried out. While modeling of column load has been applied axially on the top of the column using rigid steel plate. Figure shows that axial load vs axial deformation curves of different S-RCFT columns.

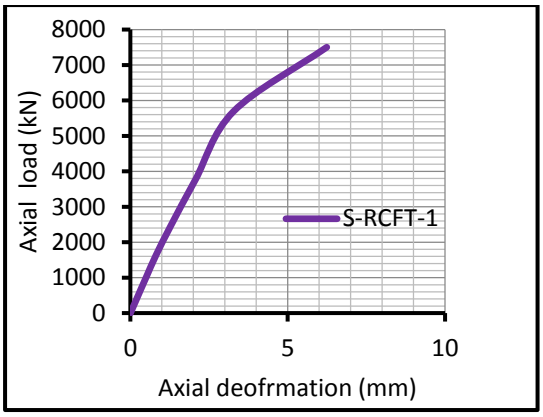

a) specimen-1

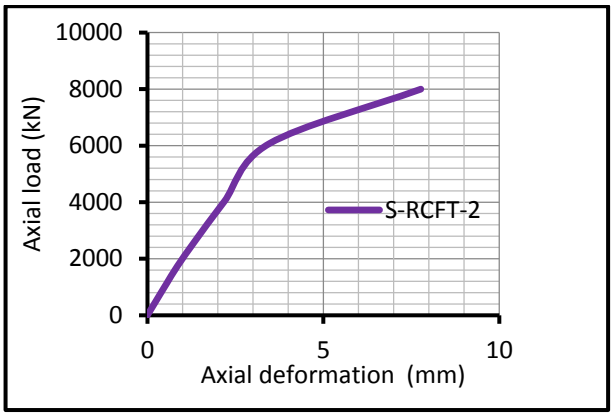

b)specimen-2

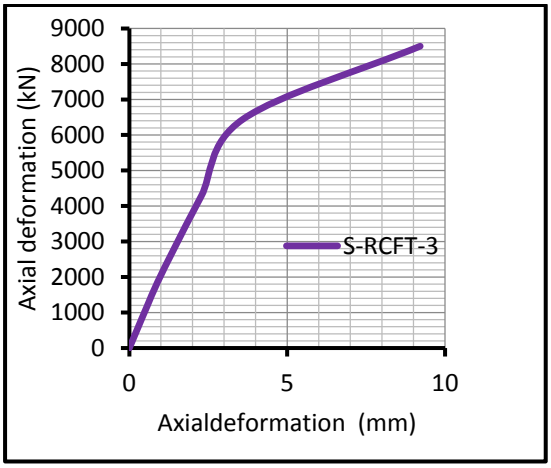

c) specimen-3

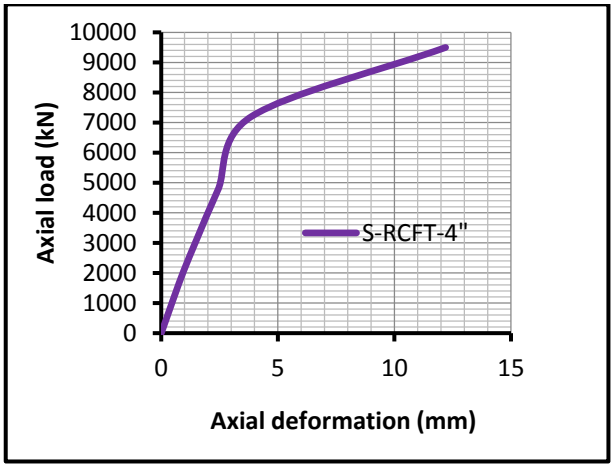

d) specimen-4

Figure 5.11: axial load- axial deformation curves of SRCFT for different steel contribution ratios.

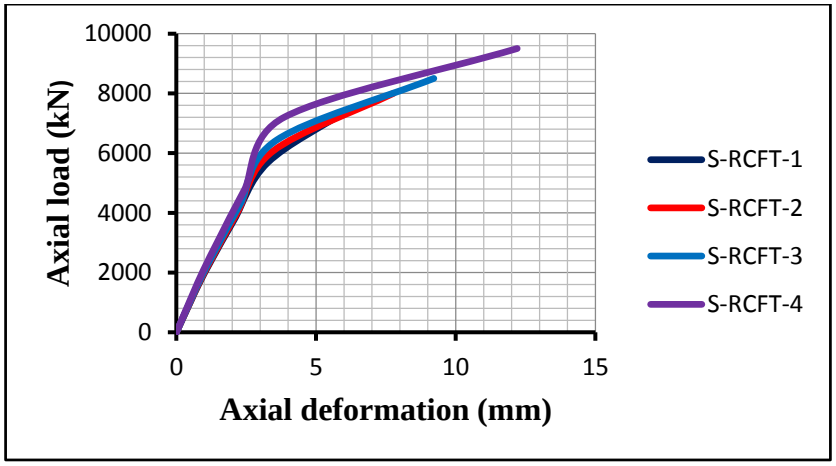

Figure 5.12: Skeleton curve for different diameter to thickness ratio of S-RCFT

Parameteric study on steel reinforced concrete filled steel tube subjected to cyclic loading alone by considering steel contribution ratio as varying parameters.

As shown in figure 5.13, ultimate lateral load of specimen -1, (S-RCFT-1) and specimen 4, (S-RCFT-4), is 309 kN and 354.73 kN respectively. When steel contribution ratio is increased from 0.777 to 0.807, ultimate lateral load capacity of steel reinforced concrete filled steel tubular column is increased by 14.8%.

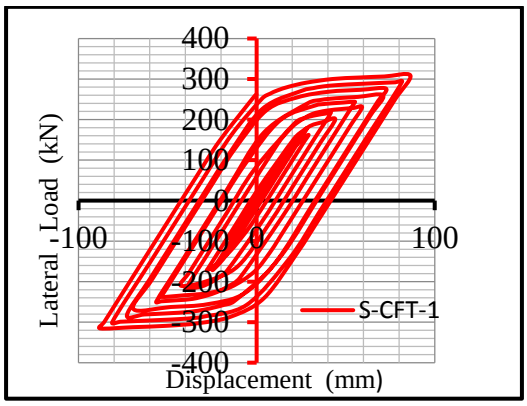

a) specimen-1

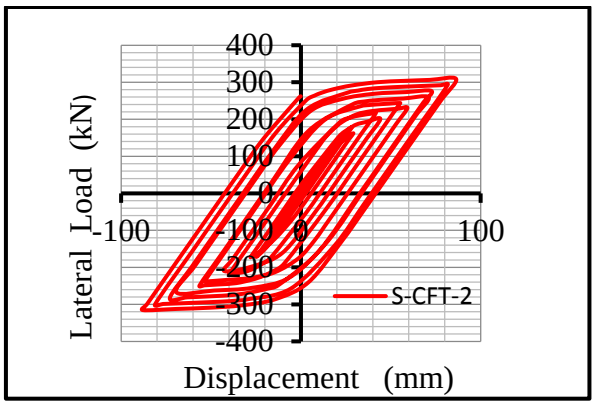

b) specimen-2

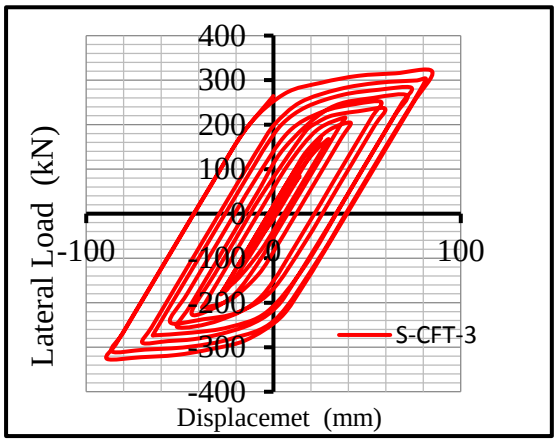

c)specimen-3

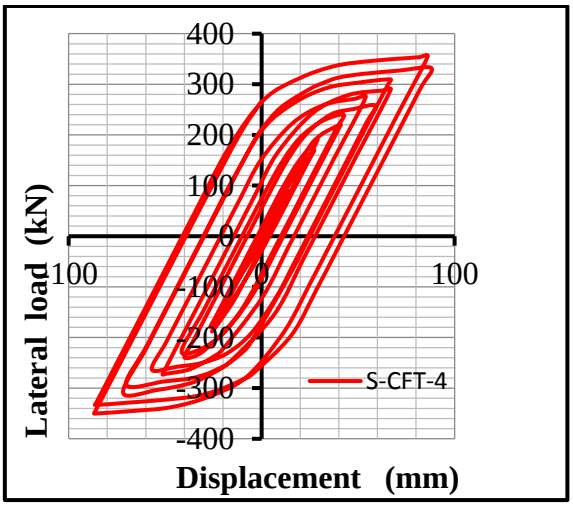

d) specimen-4

Figure 5.13: Lateral load-displacement hysteresis curves of SRCFT with different steel contribution ratio (cyclic load alone)

Parametric study on steel reinforced concrete filled steel tube by considering effect of axial and cyclic loading.

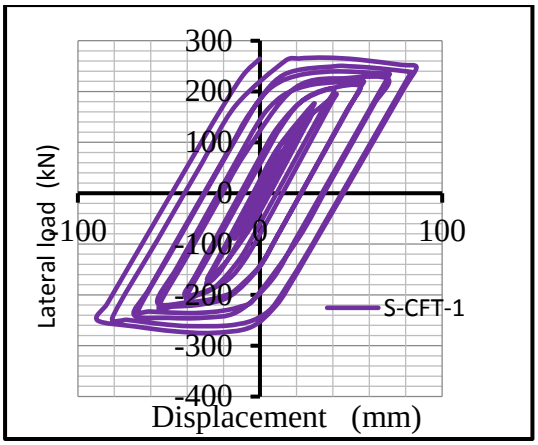

a) specimen-1

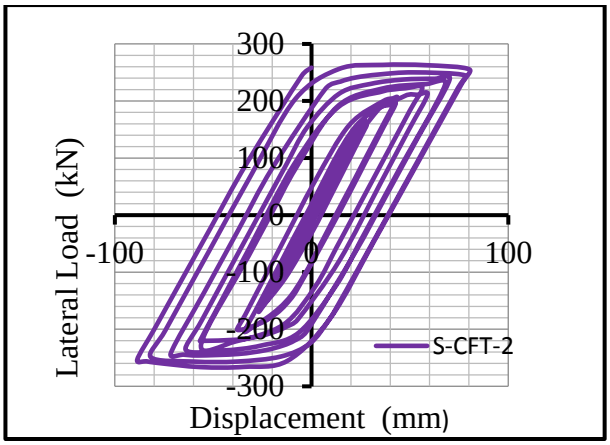

b) specimen-2

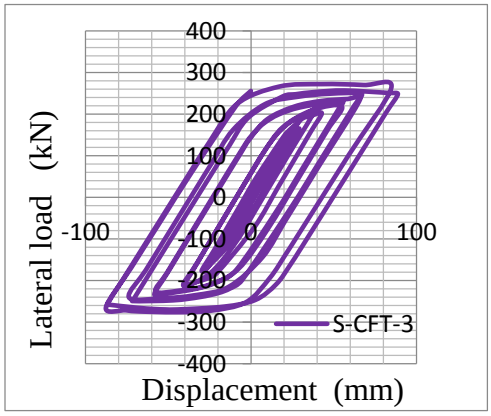

c) specimen-3

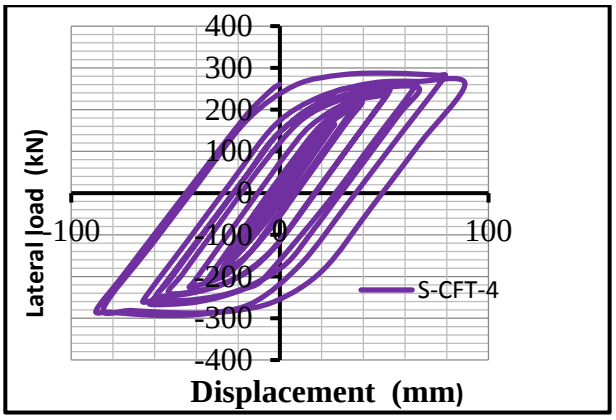

d) specimen-4

Figure 5.14: Lateral load-displacement hysteresis curves of SRCFT with different steel contribution ratio (cyclic load +axial load)

5.2.2 Concrete compressive strength effect on SRCFT

Different specimens of S-RCFT columns were taken to investigate the effect of variation of concrete on the performances of S-RCFT columns. The computed cyclic load-deflection curves for S-RCFT columns with different concrete compressive strengths are depicted in Figure 5.15. The ultimate cyclic lateral loads of S-RCFT columns increase with an increase in the concrete compressive strength. Increasing concrete compressive strength from 25MPa to 50 MPa increases the ultimate cyclic lateral strength by 8 %.

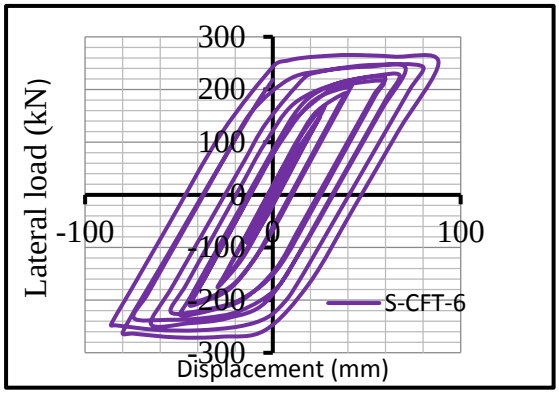

a) specimen-1

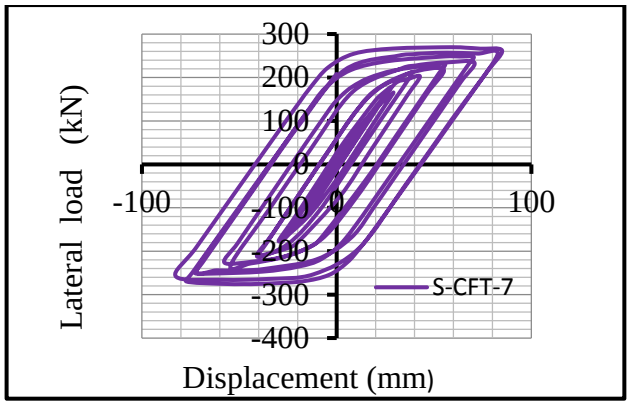

b) specimen-2

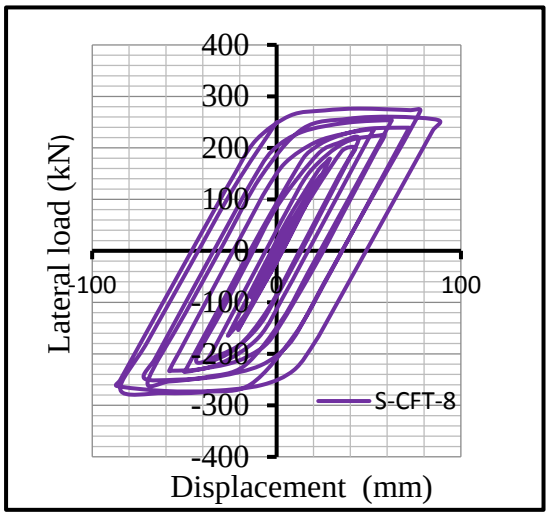

c) specimen-3

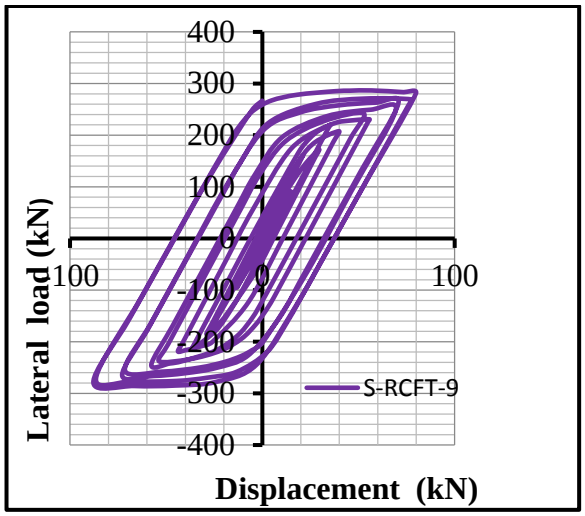

d) specimen-4

Figure 5.15: Lateral load-displacement hysteresis curves of SRCFT with different concrete grade (cyclic load +axial load)

5.2.3 Slenderness ratio effect on S-RCFT column

Parametric study was conducted on four circular S-RCFT columns to investigate the effect of slenderness ratio variation on the performances of S-RCFT columns. It can be observed from the analytical results that the decrease in Le/D ratio decreases the lateral load capacity of the S-CFT column. The slenderness ratio was considered from 6.79 to 12.23 for this study. The hysteresis curves of different slenderness ratios are shown in figure 5.16. Ultimate cyclic lateral load of S-RCFT column decreases by 404.3 kN to 103.45 kN.

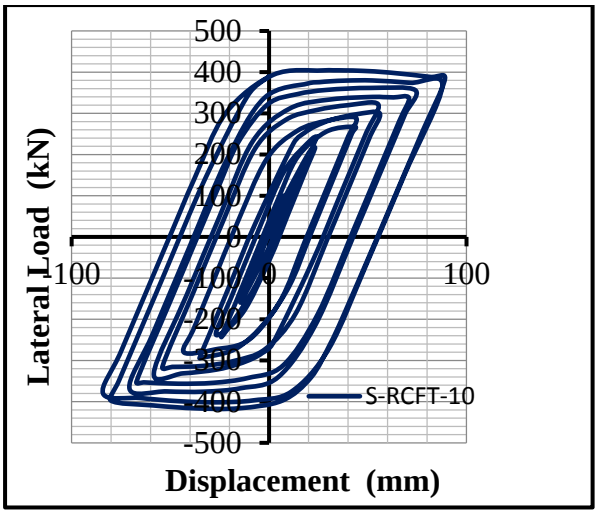

a) specimen-1

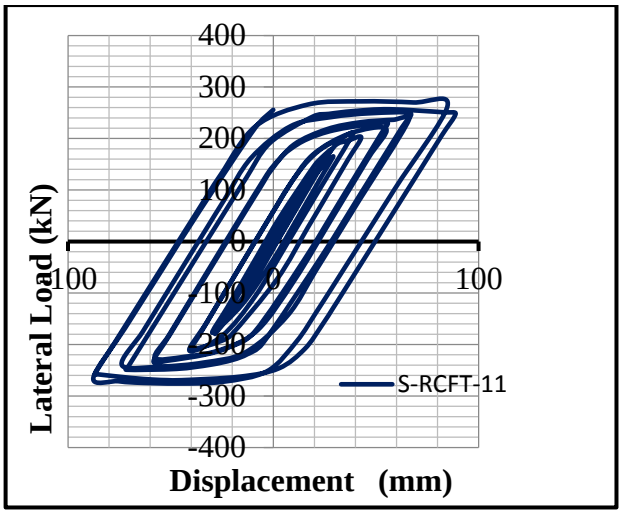

b) specimen-2

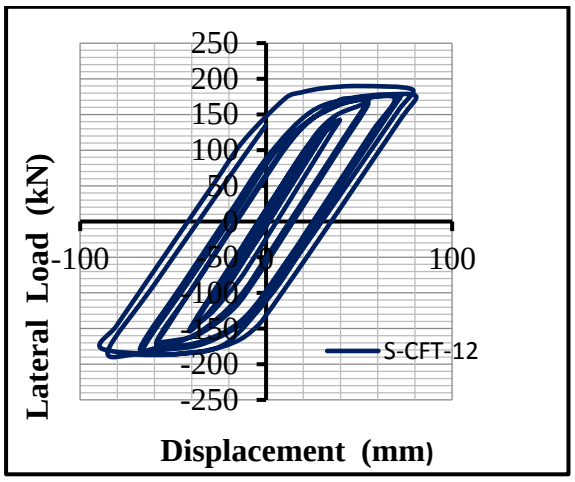

c) specimen-3

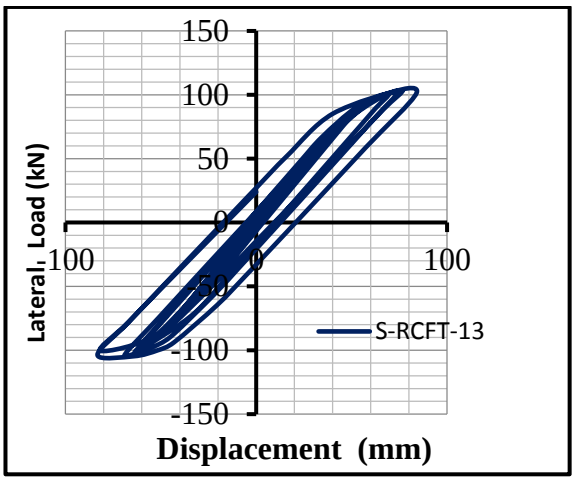

d) specimen-4

Figure 5.16: Lateral load-displacement hysteresis curves of S-RCFT with different steel contribution ratio (cyclic load +axial load)

5.2.4 Steel grade effects on SRCFT

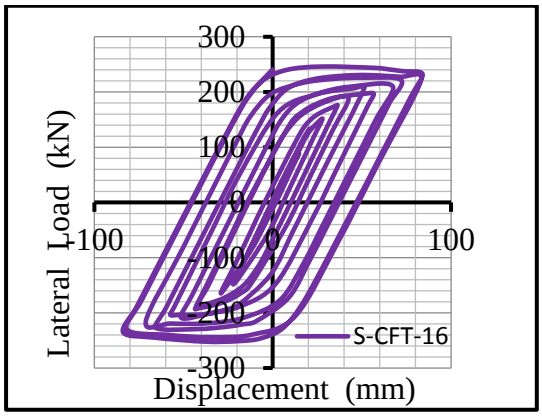

a) specimen-1

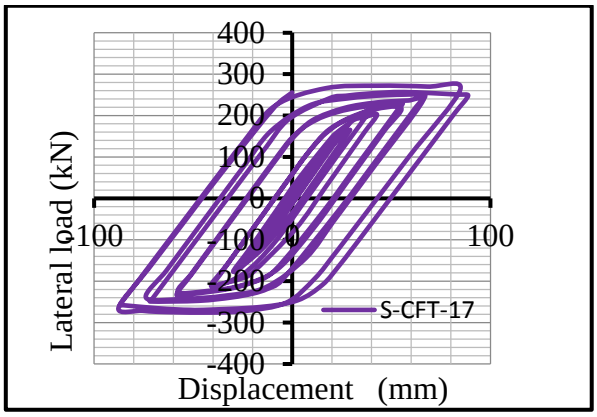

b) specimen-2

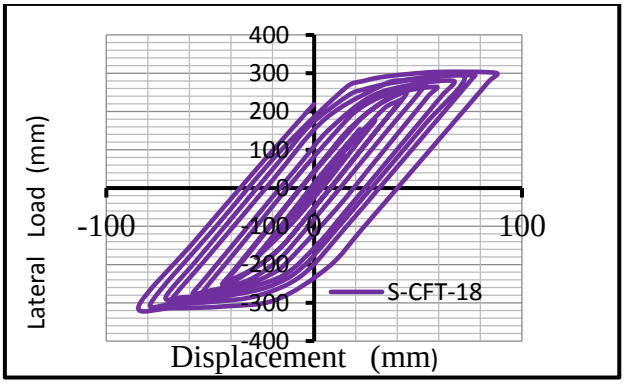

c) specimen-3

Figure 5.17: Lateral load-displacement hysteresis curves of SRCFT with different steel contribution ratio (cyclic load +axial load)

5.3 Hysteretic curves of square concrete filled steel tubular columns

5.3.1 Thickness effect on S-CFT

Parametric study was conducted on three square concrete filled steel tubular columns to investigate the effect of thickness variation on the performance S-CFT columns. The decrease in B/t ratio may be either due to the decrease in width or due to the increase in thickness of the section. However, it was analyzed by keeping the width constant and increasing the thickness. For this study, the B/t ratio was varied from 35 to 21.875. The decrease in B/t ratio with increased thickness for a constant width represents the improvement in cross section of the steel tube and hence produces greater section capacity. The comparisons of hysteresis behaviour of the three different B/t ratio are shown in figure 5.18.

Ultimate lateral load capacity of square concrete filled steel tubular column is increased by 65%.

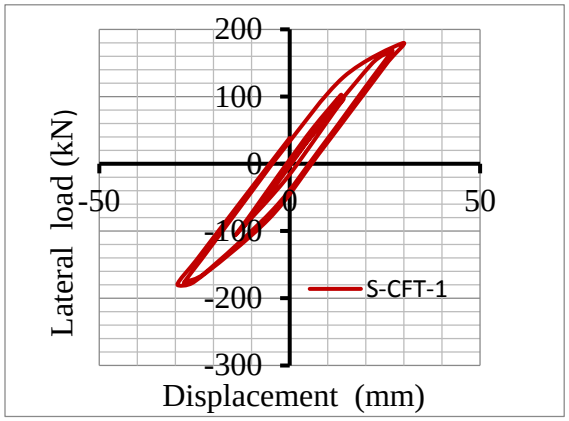

a) Specimen-1

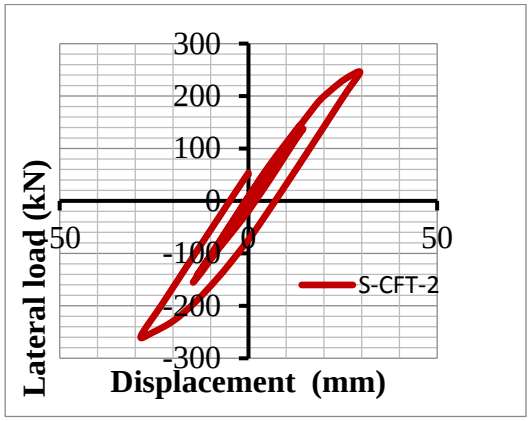

b) specimen-2

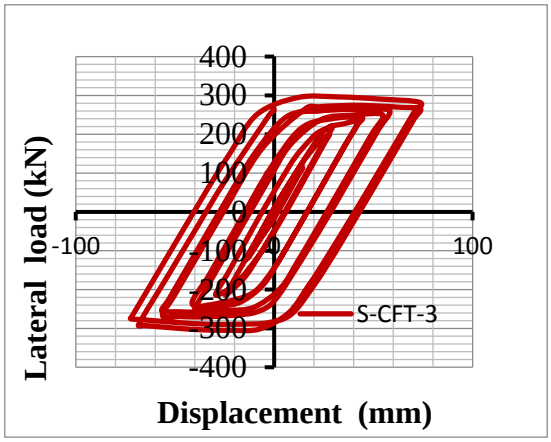

c) Specimen-3

Figure 5.18: Lateral load-displacement hysteresis curves of S-CFT with different steel contribution ratio (cyclic load +axial load)

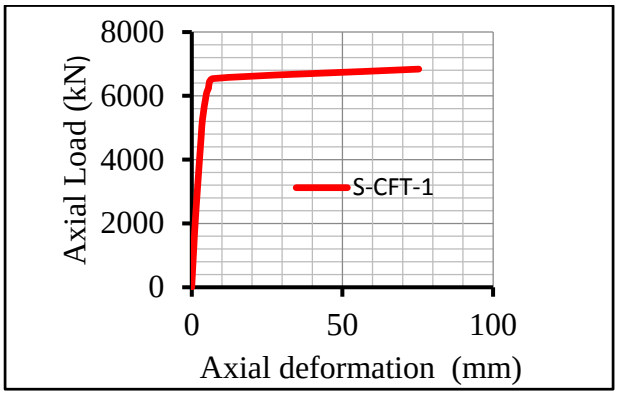

a) Specimen-1

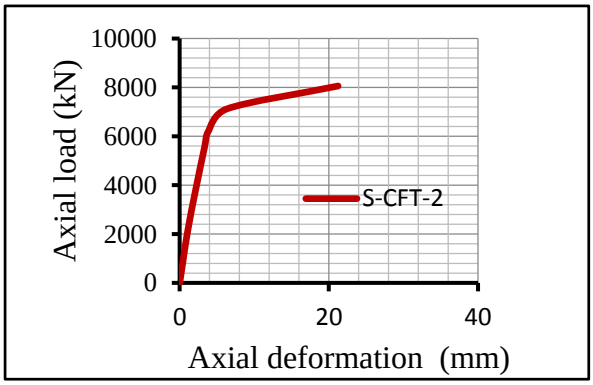

b) specimen-2

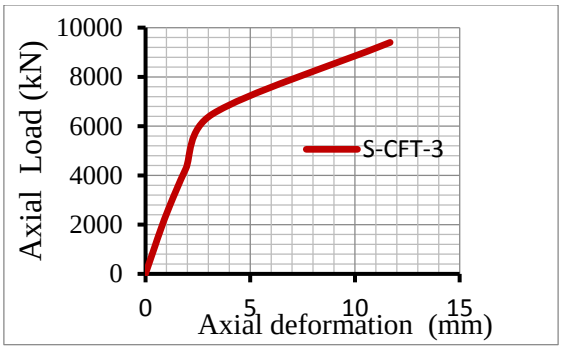

c) Specimen-3

Figure 5.19: axial load- axial deformation curves of S-CFT for different steel contribution ratios.

5.3.2 concrete compressive strength effect on S-CFT

As concrete compressive strength varies from 25 MPa to 50 MPa peak lateral load increased by 12.54 %.

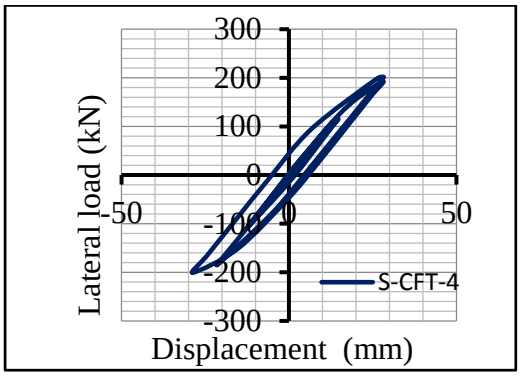

a) specimen-1

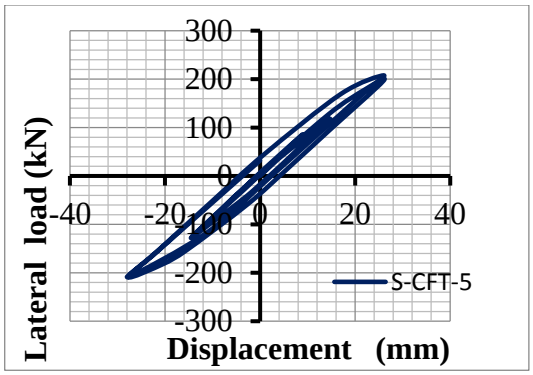

b) specimen-2

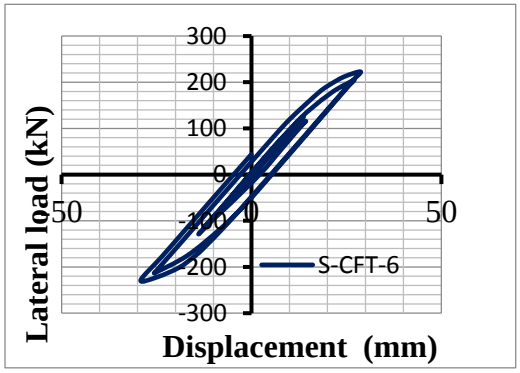

c) specimen-3

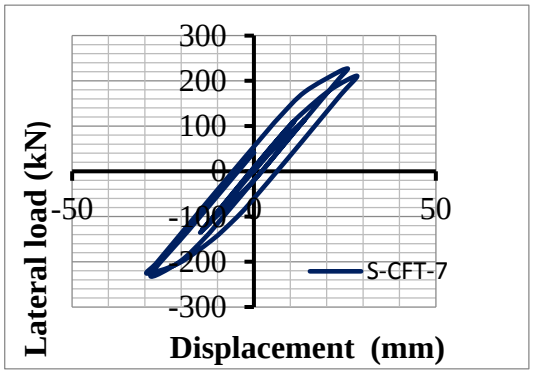

d) specimen-4

Figure 5.20:Lateral load-displacement hysteresis curves of S-CFT with different concrete grade (cyclic load +axial load)

5.3.3 Slenderness ratio effect on S-CFT

As slenderness ratio varies from 35 to 21.875, peak lateral load decreased by 56 %.

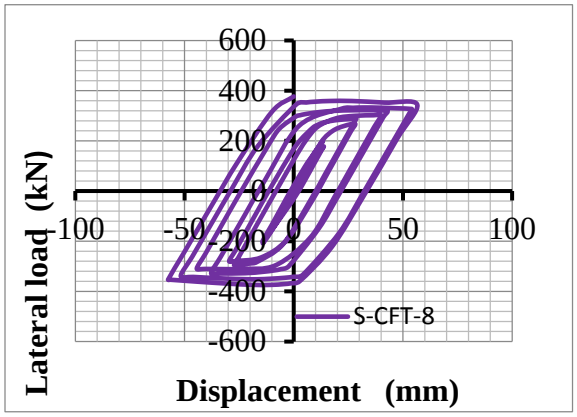

a) specimen-1

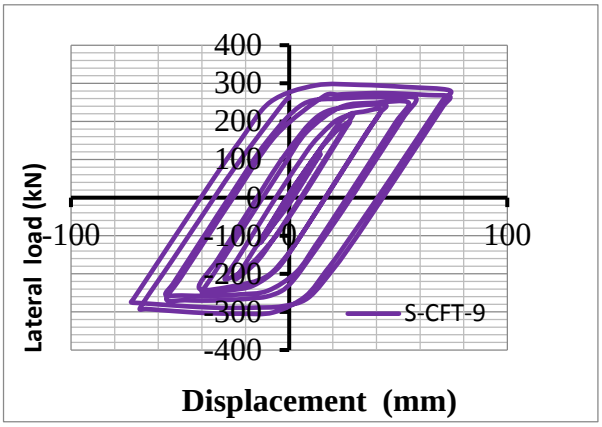

b) specimen-2

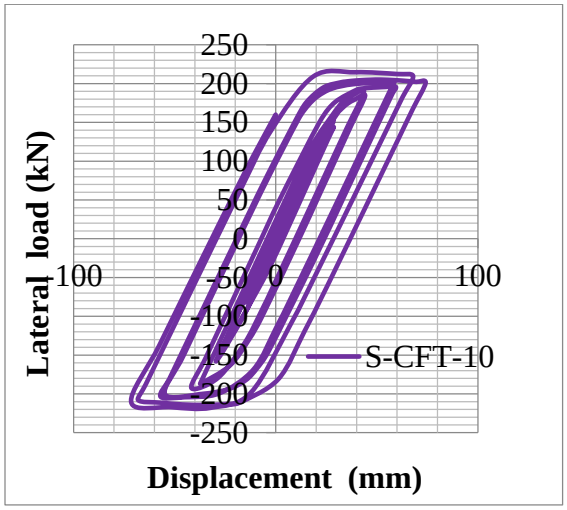

c) specimen-3

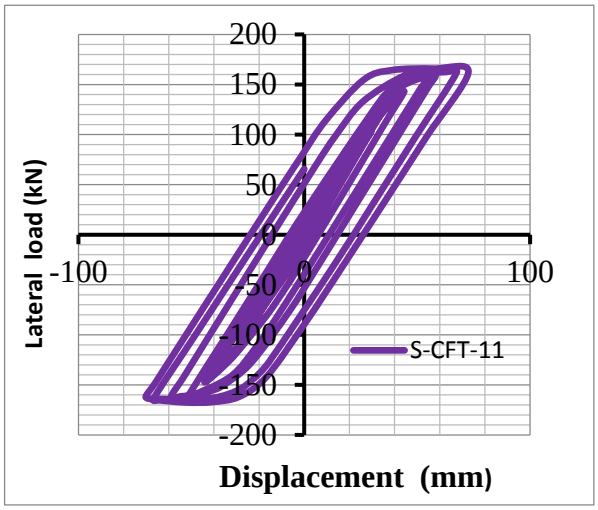

d) specimen-4

Figure 5.21: Lateral load-displacement hysteresis curves of S-CFT with different slenderness ratios (cyclic load +axial load)

5.3.4 Steel grade effect on S-CFT

As steel grade varies from S-235 to S-355, peak lateral load decreased by 31.2 %.

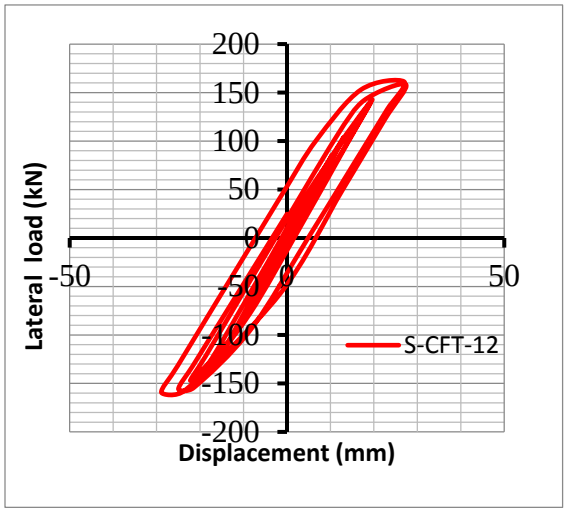

a) specimen-1

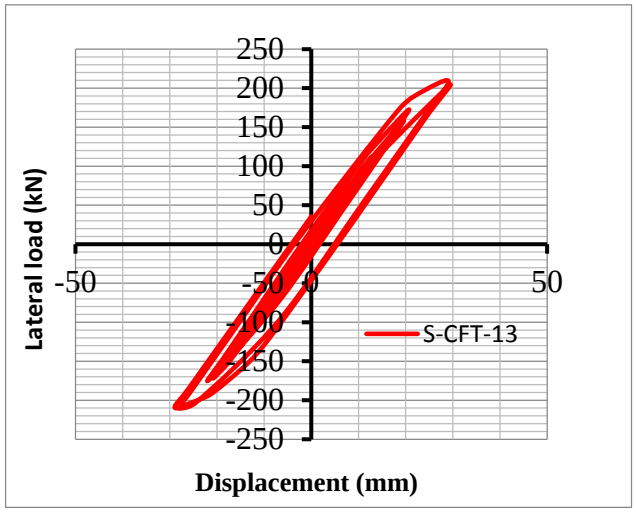

b) specimen-2

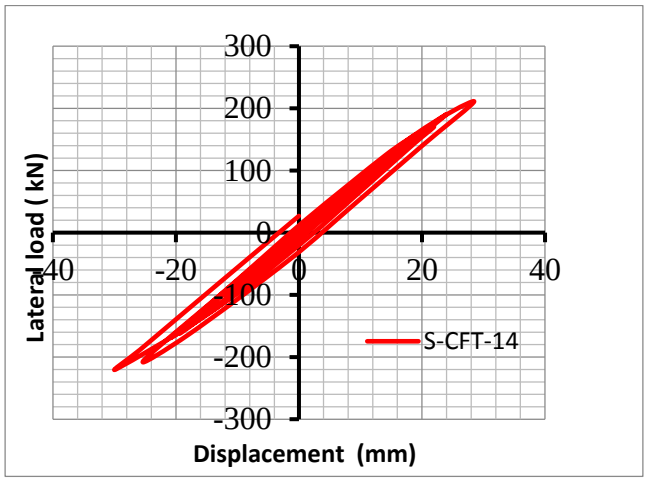

c) specimen-3

Figure 5.22: Lateral load-displacement hysteresis curves of S-CFT with different steel grade (cyclic load +axial load)

CHAPTER SIX

6 Conclusion and Recommendation

6.1 Conclusion

The mechanical performance of CFST columns under cyclic loading was investigated through the ABAQUS/Standard solver. The feasibility and accuracy of the numerical method was verified by comparing the calculated results with the experimental observations. Based on parametric study on three types of CFST, the following conclusion have been drawn.

- The cyclic lateral load capacity of a CFST columns are significantly increased by increase in D/t ratios.
- The ultimate cyclic lateral load is directly proportional with steel yield strength.
- The lateral deflection at the ultimate cyclic lateral load is proportional to the column slenderness ratio and ultimate load capacity of the colums is indirectly proportional to slenderness ratio.
- The presence of the section steel can carry the lateral load and reduce the tensile zone of the concrete section. As a result, the S-RCFST columns have higher stiffness and peak lateral load than the common CFST columns even with the same geometrical and material parameters. The steel section can also enhance the deformation ability of a SRCFST column.
- The flanges of the steel section can also offer some confining effect on the concrete inner. The highest longitudinal stress in the concrete section for S-RCFST column is in the flanges of the steel section.
- The parametric study is also conducted to analyze the effects of ratio of steel section, yield strength of steel section, axial load level, thickness of steel tube and concrete strength on peak lateral load of S-RCFST columns.
- By the investigation of envelope curves of hysteresis loops of SRCFST columns, it is observed that reinforcing CFT column by a steel section causes less degradation of load at large defections, increase of energy absorption capacity.

6.2 Recommendations

The following directions could be taken to extend this research, address some of the issues encountered, and improve the quality of predictions provided by the FE model:

- The effects of load eccentricity in combination with cyclic loading on the behaviour of concrete filled steel tubular column should be investigated.
- This study did not draw comparisons between CFST columns with other types of composite column. Comparison between CFST columns and composite columns, showing advantages and disadvantages could go along way in promoting the use of concrete filled steel tubular column in our country.
- Behavior of CFST columns in the assemblies of frame should be studied.
- Extend numerical investigation of CFST by considering the following:
    - Effects of longitudinal and transverse reinforcement should be considered.
    - Built up reinforcing steel on cyclic behavior of CSFT should be incorporated.
    - Since this research covers CFST with normal concrete, effect of high strength should investigated.

REFERENCES

A.H. Varma, J.M. Ricles, R. Sause, LW. Lu. (2004). Seismic behavior and design of High-Strength Square Concrete-Filled Steel Tube Beam Columns, Journal of Structural Engineering ASCE, 130(2): 169-179.

ABAQUS, 2009. Version 6.8, ABAQUS documentation. USA: ABAQUS Inc.

ACI. (2011). Building code requirements for structural concrete and commentary. ACI, USA: American Concrete Institute.

Desayi, P. and Krishnan, S., (1964). Discussion of 'Equation for the stress–strain curve of concrete', vol. 61, ACI Journal, 1229–1235.

Ellobody, E. and Young, B. (2006). Nonlinear analysis of concrete-filled steel SHS and RHS columns. Thin-walled structures. 44 (8): 919-930.

Ellobody, E., Young, B. and Lam, D. (2006). Behaviour of normal and high strength concrete-filled compact steel tube circular stub columns. Journal of Constructional Steel Research. 62 (7): 706-715.

Ellobody, E., Young, B. and Lam, D., (2006). Behaviour of normal and high strength concrete-filled compact steel tube circular stub columns, *Journal of Constructional Steel Research,* 62, 706–715.

Elremaily A, Azizinamini A. (2002). Behavior and strength of circular concrete-filled steel tube columns. Journal of Construction Steel Research. 58: 1567–1591.

Evirgen, B.; Tuncan, A.; Taskin, K. (2014). Structural behavior of concrete filled steel tubular sections under axial compression. Thin walled structures, 80, 46-56.

Farajpourbonab E., Sunil Y. Kute, Vilas M. Inamdar. (2018). Steel-reinforced concrete-filled steel tubular columns under axial and lateral cyclic loading. International Journal of Advanced Structural Engineering. 10:61–72

Gupta, P,K.; Sarda, S,M; Kumar, M,S.(2007), "Experimental and computational study of concrete filled steel tubular columns under axial loads", journal of constructional steel research, 63,182-193.

H. Hu, C. Huang, M. Wu and Y. Wu, (2003). "Nonlinear Analysis of Axially Loaded Concrete-Filled Tube Columns with Confinement Effect," *Journal of Structural Engineering,* 129(10): 1322-1329.

Han LH, Yang YF, Tao Z. (2003). Concrete-filled thin-walled steel SHS and RHS beam columns subjected to cyclic loading. Thin-Walled Structure. 41: 801–33.

Hu, HT.; Huang, S, C.; Chen, Z, L. (2005), "Finite element analysis of CFT columns subjected to an axial compressive force and bending moment in combination", journal of constructional steel research, 61,1692-1712.

Inai E, Mukai A, Kai M, Tokinoya H, Fukumoto T, Mori K. (2004). Behavior of concrete filled steel tube beam columns. Journal Structural Engineering, ASCE ,130(2):189–202.

Keigo Tsuda, Chiaki Matsui. (1998): Strength of Square Steel Tubular Beam-Columns under Constant Vertical and Horizontal Loads. Journal of Structure and Construction Engineering AIJ, 512,149-156.

Kuranovas, A.; Kvedaras, A. K. (2007). Behaviour of hollow concrete steel tubular composite elements, Journal of Civil Engineering and Management. 13(2): 131–14.

L. H. Han, H. Huang and X. L. Zhao, (2009). Analytical behavior of concrete filled double skin steel tubular beam-columns under cyclic loading. Thin walled structures. 47(6-7):668-680.

L.H. Han, H. Huang and X.L. Zhao, (2009), analytical behavior of concrete filled double skin steel tubular beam columns under cyclic loading thin walled structures, 47(6-7): 668-680.

Lin-Hai Han, Wei Li and Reidar Bjorhovde (2014). Developments and advanced applications of concrete-filled steel tubular (CFST) structures: Journal of Construction Steel Research. 100, 211-228.

M. Dundu (2012). Compressive strength of circular concrete filled steel tube columns. Thin-Walled Structures. 56, 62-70.

Mander, J. B., Priestley, M. J. N. and Park, R., (1988). "Theoretical stress–strain model for confined concrete," *Journal of Structural Engineering.* 8(114): 1804-1826.

Mander,J.B., prestley, M.J.N. and Park, R., (1988). " Theoritical stress-strain model for confined concrete,". Journal of Structural Engineering. 8(114): 1804-1826.

Marson J, Bruneau M. (2004). Cyclic testing of concrete-filled circular steel bridge piers having encased fixed-based detail. Journal of Bridge Engineering. ASCE; 1:14–23.

Md. Soebur Rahman, Mahbuba. B. and Raquib, A., 2016. Comparison between Experimental and Numerical Studies of Fully Encased Composite Columns. International Journal of Structural and Construction Engineering, 10(6).

Montoya E., Vecchio F. and Sheikh S., (2006). Compression field modeling of confined concrete: constitutive models," *Journal of Materials in Civil Engineering,* 18, 510-517.

N. K. Brown, M. J. Kowalsky and J. M. Nau (2015), Impact of D/t on seismic behavior of reinforced concrete filled steel.

Nakanishi Katsuyoshi, Kitada Toshiyuki, Nakai Hiroshi. (1999) Experimental study on ultimate strength and ductility of concrete filled steel columns under strong earthquake. Journal of Construction Steel Res 51: 297–319.

P. K. Gupta, S. M. Sarda and M. S. Kumar (2007). Experimental and computational study of concrete filled steel tubular columns under axial loads. Journal of construction of steel research, 182-193.

Papanikolaou VK,Kappos AJ. (2007). Confinement sensitive plasticity constitutive model for concrete in triaxial compression. International Journal of Solids structure. 44(21): 7021-48.

Raghabendra Yadav, Baochun Chen, Huihui Yuan, Subhash Pantha, (2017). Parametric Study on the Lateral Load Carrying Capacity of CFST Columns. International Journal of Civil Engineering and Construction Science.Vol. 4, (5) , pp. 57-66.

Raghabendra Yadav, Baochun Chen, Huihui Yuan and Zhibin Lian, (2017). Analytical behavior of CFST bridge piers under cyclic loading. 11th international symposium on plasticty and Impact Mechanics, Procedia Engineering , (173), 1731-1738

S. J. Richard and S. H. Perry, (2000). "The impact behaviour of sleeved concrete cylinders," *The Structural Engineer*, 68(17): 23-27.

Sakino K, Tomii M. (1981). Hysteretic behavior of concrete filled square steel tubular beam-column failed in flexure. Trans Jpn Concr Inst. (3) 439–446.

Singh, H,; Gupta, P, K. (2013)," Numerical modeling of rectangular concrete filled steel tubular short columns", International journal of scientific and engineering research, 4,(5), pp. 170-173

Sugano S, Nagashima T, Kei T., (1992). Seismic behaviour of concrete-filled tubular steel columns. Morgan Jim, editor. Tenth structures congress. San Antonio: ASCE; pp. 914–917.

Tao Z, Wang XQ, Uy B (2013. Stress-strain curves of structural steel and reinforcing steel after exposure to elevated temperatures. J Mater Civil Eng (in press).

Tao, Z.; Wang, Z,B.; Yu, Q.(2013), " Finite element modelling of concrete filled steel stub columns under axial compression", journal of constructional steel research, 89, 121-131.

Varma AH, Ricles JM, Sause R, Lu LW. (2002). Seismic behavior and modeling of high strength composite concrete-filled steel tube (CFST) beam columns. Journal of Construction and Steel Research. 58(5–8):725–58.

Varma AH, Ricles JM, Sause R, Lu LW. (2004). Seismic behavior and design of high strength square concrete-filled steel tube beam columns. Journal of structural engineering, ASCE 130(2):169–79.

Wang W. and Li T., (2012). Hysteresis curve simulation of reinforced concrete frame based on finite element software ABAQUS. 2nd International Conference on Electronic & Mechanical Engineering and Information Technology. Published by Atlantis Press, Paris, France. pp.405-408.

Yadav R., Chen B., Yuan H. and Lian Z., (2017). Analytical Behaviour of CFST Bridge Piers under Cyclic Loading. Procedia Engineering, 173: 1731-1738.

Yu T., Teng JG, Wong YL, Dong SL. (2010). Finite element modeling of confined concrete-I: Drucker-Prager type plasticity model. Journal of structural Engineering. 32(3):665-679.

Zhu, M., Liu, J. and Wang, Q., (2010). Experimental Research on Square Steel Tubular Columns Filled with Steel-reinforced Self-consolidating High-strength Concrete under Axial Load. Journal of Engineering Structures. 32(8): 2278-2286.

ZHUANG Zhuo, ZHANG Fan, CEN Song, (2005). ABAQUS Nonlinear Finite Element Analysis and Examples[M]. Beijing: Science Press, 123-139.

Schneider S.P., (1998). Axially loaded concrete-filled steel tubes, Journal of Structural Engineering. 124(10):1125-1138.

Huang C.S, Yeh Y., Liu G,Y., and Hu H.T. (2002). Axial load behavior of stiffened concrete filled steel columns, Journal of structural Engineering. 128(9): 1222-1230.

JChen, W. X. Zhang, . H. Shan, R. Y. Xiao, W. J. Yi and F. Y. Lu, (2007). "Behavior of Concrete Filled Tubes and Confined Concrete Filled Tubes under High Speed Impact," Advances in Structural Engineering. 10(2): 209-218.

Tort, Cenk & M Asce, A & Hajjar, Jerome & Asce, F. (2010). Mixed Finite-Element Modeling of Rectangular Concrete-Filled Steel Tube Members and Frames under Static and Dynamic Loads. Journal of Structural Engineering-ASCE. 136: 654-664.

Moon J, Lehman DE, Roeder CW and Lee H-E (2013). Strength of circular concrete-filled tubes (CFT) with and without internal reinforcement under combined loading. Journal of Structural Engineering, ASCE.

APPENDICES

Appendix A: Analysis of concrete filled steel tubular column according to Eurocode-4, 2004

Simplified method of design is applied in determination of resistance of cross-sections.

Steps to calculate axial load capacity of concrete filled steel column

Material data:

Concrete grade: , characteristic concrete compressive strength

Secant modulus for short term loading Ecm

Steel grade: characteristics yield strength

Modulus of Elasticity, Es = 210 GPa

Partial safety factor for ultimate limit state:

Concrete $\gamma_c = 1.5$

Structural steel, $\gamma_a = 1.1$

Reinforcing steel $\gamma_s = 1.15$

Column cross section data:

D = outer diameter

t = thickness of steel tube

I_{xx} = Moment of inertia along x-x axis

I_{yy} = moment of inertia along y-y axis

Aa = cross sectional area of steel tube

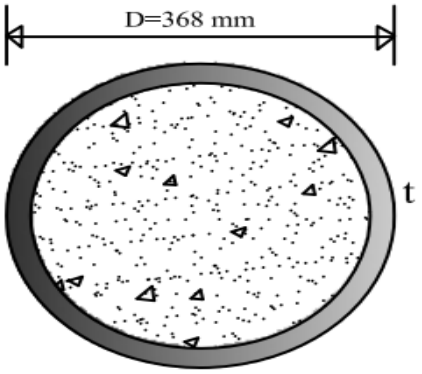

(1) effective flexural stiffness of a cross section of a composite column should be calculated as:

$$(EI)_{eff} = E_a I_a + E_s I_s + K_e E_{cm} I_c$$

where, K_e is a correction factor that should be taken as 0.6

I_a, I_c and I_s are the second moments of area of the structural steel section, the uncracked concrete sectionand the reinforcement for the bending plane being considered

(2) Related Slenderness ratio $\bar{\lambda}$ for the plane of bending being considered is given by:

$$\bar{\lambda} = \sqrt{\frac{N_{pl,Rk}}{N_{cr}}},$$

$Where,\ \ N_{pl,Rk}\ , is\ \ the\ characteristic\ value\ of\ the\ plastic\ resistance$ to compression

$$N_{pl,Rk} = A_a * f_{yk} + A_c * (0.85 * f_{ck}) + A_s * f_{yk}$$

$N_{cr}\ ,\ is\ the\ elastic\ critical\ normal\ force\ for\ the\ relevant\ buckling\ mode$

$$Along\ x-axis\ , \quad N_{cr,xx} = \frac{\pi^2 * EI_{xx}}{L^2}$$

$$Along\ y-axis \quad N_{cr,yy} = \frac{\pi^2 * EI_{yy}}{L^2}$$

(3) The plastic resistance to compression may then be calculated from the following expression:

$$N_{pl,Rd} = \eta_{ao}\frac{Aa * fy}{\gamma_a} + A_c * \frac{0.85 * f_{ck}}{\gamma_c}\left(1 + \eta_{ac}\frac{t}{D}\frac{f_y}{f_{ck}}\right) + \frac{\left(A_s * f_{yk}\right)}{\gamma_s}$$

where, t is the wall thickness of the steel tube

For members with eccentricity e =0,

$$\eta_{ao} = 0.25\left(3 + 2\bar{\lambda}\right) \leq 1$$

$$\eta_{c0} = 4.9 - 18.5\bar{\lambda} + 17\left(\bar{\lambda}\right)^2 \geq 0$$

(4) The steel contribution ratio δ is defined as:

$$\delta = \frac{\frac{A_a * f_y}{\gamma_a}}{N_{pl,Rd}} \rightarrow 0.2 < \delta < 0.9 \quad ok.$$

Column designation **1: CFT-S-1**

Material data:

Concrete: C-30, characteristic concrete compressive strength, fck = 25 MPa

Secant modulus for short term loading Ecm = 26222.34 MPa

Steel: S-275, characteristics yield strength fy = 275 MPa $(t \leq 40\ mm)$

Modulus of Elasticity, Es = 210 GPa

Partial safety factor for ultimate limit state:

Concrete $\gamma_c = 1.5$

Structural steel, $\gamma_a = 1.1$

Column cross section data:

Specimen Designation: CFT-S-1

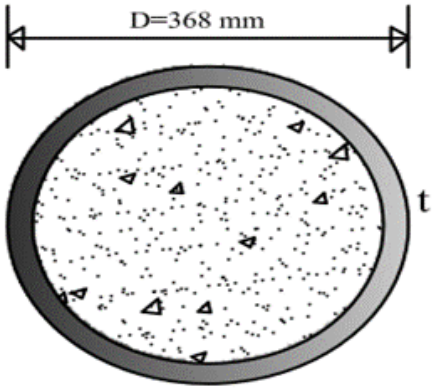

D =368 mm Aa = 112 cm^2

t = 10 mm $I_{xx} = I_{yy} = 18030\ cm^4$

(1) Effective bending stiffness

$EI_e = E_a I_a + 0.6 * E_{cd} I_c + E_s I_s$

$$(EI)_e = 210 * 18030 * 10^4 + 0.6 * \frac{26.222}{1.35} * \pi \frac{348^4}{64}$$

$$\boldsymbol{(EI)_e = 4.625 * 10^{10} kN/mm^2}$$

(2) Related Slenderness ratios:

$$\bar{\lambda} = \sqrt{\frac{N_{pl,Rk}}{N_{cr}}}, \qquad N_{pl,Rk} = A_a * f_{yk} + A_c * (0.85 * f_{ck}) + A_s * f_{yk}$$

$$N_{pl,Rk} = 112 * 10^2 * 275 + \left(\pi * \frac{348^2}{4}\right) * 0.85 * 25$$

$$N_{pl,Rk} = 5459\ kN$$

$$N_{cr,xx} = N_{cr,yy} = \frac{\pi^2 * EI_{xx}}{L^2} = \pi^2 * \frac{(4.625) * 10^{10}}{(3000)^2} = 507222.3\ kN$$

$$\bar{\lambda}_{xx} = \bar{\lambda}_{yy} = \sqrt{\frac{5459}{507222.3}} = 0.328, \qquad 0.328 < 2\ \ ok$$

(3) Plastic axial load capacity of cross section

$$N_{pl,Rd} = \eta_{ao} \frac{Aa * fy}{\gamma_a} + A_c * \frac{0.85 * f_{ck}}{\gamma_c}\left(1 + \eta_{ac} \frac{t}{D} \frac{f_y}{f_{ck}}\right) + \frac{(A_s * f_{yk})}{\gamma_s}$$

For eccentricity e = 0, $\eta_{ao} = 0.25(3 + 2\bar{\lambda}) \leq 1$

$$\eta_{c0} = 4.9 - 18.5\bar{\lambda} + 17(\bar{\lambda})^2 \geq 0$$

$\eta_{ao} = 0.25(3 + 2 * 0.328) = 0.914$

$\eta_{c0} = 4.9 - 18.5 * 0.3228 + 17 * 0.3228^2 = 0.661$

$$N_{pl,Rd} = 0.914 * 11200 * \frac{275}{1.1} + \pi * \frac{348^2}{4} * 0.85 * \frac{25}{1.5}\left[1 + 0.661 * \frac{1}{36.8} * \frac{275}{25}\right]$$

$N_{pl,Rd} = 4173kN$

Steel contribution ratio:

$$\delta = \frac{\frac{A_a * f_y}{\gamma_a}}{N_{pl,Rd}} = \frac{2800}{4173} = 0.67 \rightarrow 0.2 < \delta < 0.9 \quad ok.$$

Column cross section properties: (Columns with different thickness)

Column designation	Diameter (D) (mm)	Thickness (t) (mm)	Area of cross section (mm^2)	Moment of inertia (mm^4)	
				I_{xx} (mm^4)	I_{yy} (mm^4)
CFT-1	368	10	11200	$18030 * 10^4$	$18030 * 10^4$
CFT-2	368	12	13400	$21290 * 10^4$	$21290 * 10^4$
CFT-3	368	14	15600	$24430 * 10^4$	$24430 * 10^4$
CFT-4	368	16	17700	$27460 * 10^4$	$27460 * 10^4$
CFT-5	368	20	21900	$33210 * 10^4$	$33210 * 10^4$

Column designation	Material Data		EI_{eff} (kN/mm^2)	Slenderness Ratio ($\bar{\lambda}$)	$N_{pl,Rd}$ (kN)	Steel contribution ratio (δ)
	concrete	steel				
CFT-1	C-30	S-275	$4.625 * 10^{10}$	0.328	4173	0.67
CFT-2	C-30	S-275	$5.288 * 10^{10}$	0.322	4702	0.71
CFT-3	C-30	S-275	$5.924 * 10^{10}$	0.318	5228	0.746
CFT-4	C-30	S-275	$6.538 * 10^{10}$	0.314	5730	0.772
CFT-5	C-30	S-275	$7.69 * 10^{10}$	0.310	6723.5	0.814

Axial load capacity determination by considering (**Compressive strengths)** as varying parameters.

Material data:

Concrete: C-25, characteristic concrete compressive strength, fck = 20 MPa

Secant modulus for short term loading Ecm = 25.127 GPa

Steel: S-275, characteristics yield strength fy = 275 MPa ($t \leq 40\ mm$)

Modulus of Elasticity, Es = 210 GPa

Partial safety factor for ultimate limit state:

Concrete $\gamma_c = 1.5$

Structural steel, $\gamma_a = 1.1$

Column cross section data:

Specimen Designation: CFT-S-3

D =368 mm Aa = 156 cm^2

t = 14 mm $I_{xx} = I_{yy}$ = 24430 cm^4

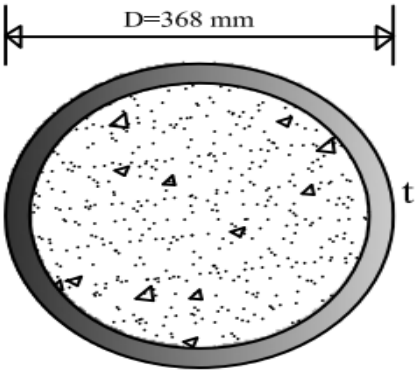

(1) Effective bending stiffness

$$EI_e = E_a I_a + 0.6 * E_{cd} I_c + E_s I_s$$

$$(EI)_e = 210 * 24430 * 10^4 + 0.6 * \frac{25.127}{1.35} * \pi \frac{340^4}{64}$$

$$\boldsymbol{(EI)_e = 5.86 * 10^{10} kN/mm^2}$$

(2) Related Slenderness ratios:

$$\bar{\lambda} = \sqrt{\frac{N_{pl,Rk}}{N_{cr}}}, \qquad N_{pl,Rk} = A_a * f_{yk} + A_c * (0.85 * f_{ck}) + A_s * f_{yk}$$

$$N_{pl,Rk} = 156 * 10^2 * 275 + \left(\pi * \frac{340^2}{4}\right) * 0.85 * 20$$

$$N_{pl,Rk} = 5833.5 \text{ kN}$$

$$N_{cr,xx} = N_{cr,yy} = \frac{\pi^2 * EI_{xx}}{L^2} = \pi^2 * \frac{(5.86) * 10^{10}}{(3000)^2} = 64262\ kN$$

$$\bar{\lambda}_{xx} = \bar{\lambda}_{yy} = \sqrt{\frac{5833.5}{64968}} = 0.301, \qquad 0.301 < 2\ \ ok$$

(3) Plastic axial load capacity of cross section

$$N_{pl,Rd} = \eta_{ao} \frac{Aa * fy}{\gamma_a} + A_c * \frac{0.85 * f_{ck}}{\gamma_c}\left(1 + \eta_{ac} \frac{t}{D} \frac{f_y}{f_{ck}}\right) + \frac{(A_s * f_{yk})}{\gamma_s}$$

For eccentricity e = 0, $\eta_{ao} = 0.25(3 + 2\bar{\lambda}) \leq 1$

$$\eta_{c0} = 4.9 - 18.5\bar{\lambda} + 17(\bar{\lambda})^2 \geq 0$$

$$\eta_{ao} = 0.25(3 + 2 * 0.301) = 0.9$$

$$\eta_{c0} = 4.9 - 18.5 * 0.301 + 17 * 0.301^2 = 0.736$$

$$N_{pl,Rd} = 0.9 * 15600 * \frac{275}{1.1} + \pi * \frac{340^2}{4} * 0.85 * \frac{20}{1.5}\left[1 + 0.76 * \frac{1}{26.25} * \frac{275}{20}\right]$$

$$\boldsymbol{N_{pl,Rd} = 4949\ kN}$$

Steel contribution ratio:

$$\delta = \frac{\frac{A_a * f_y}{\gamma_a}}{N_{pl,Rd}} = \frac{3900}{4949} = 0.788 \rightarrow 0.2 < \delta < 0.9 \quad ok.$$

Column cross-section properties:

Column designation	Diameter (D) (mm)	Thickness (t) (mm)	Area of cross section (mm^2)	Moment of inertia (mm^4)	
				I_{xx} (mm^4)	I_{yy} (mm^4)
CFT-6	368	14	15600	$24430 * 10^4$	$24430 * 10^4$
CFT-7	368	14	15600	$24430 * 10^4$	$24430 * 10^4$
CFT-8	368	14	15600	$24430 * 10^4$	$24430 * 10^4$
CFT-9	368	14	15600	$24430 * 10^4$	$24430 * 10^4$

According to EN-EBCS-4,2015, the valus of plastic resistance to compression can be expressed in tabular form.

Column designation	Material Data		EI_{eff} (kN/mm^2)	Slenderness Ratio ($\bar{\lambda}$)	$N_{pl,Rd}$ (kN)	Steel contribution ratio (δ)
	concrete	steel				
CFT-6	C-25	S-275	$5.86 * 10^{10}$	0.301	4949	0.788
CFT-7	C-30	S-275	$5.924 * 10^{10}$	0.309	5248	0.743
CFT-8	C-37	S-275	$5.982 * 10^{10}$	0.317	5489	0.71
CFT-9	C-50	S-275	$6.085 * 10^{10}$	0.332	5971	0.653

Plastic resistance to axial compression by considering Slenderness Effect

Concrete Filled steel tube capacity determination

For Specimen **CFT-S-1** axial load capacity determination.

Material data:

Concrete: C-30, characteristic concrete compressive strength, fck = 25 MPa

Secant modulus for short term loading Ecm = 27.236 GPa

Steel: S-275, characteristics yield strength fy = 275 MPa ($t \leq 40\ mm$)

Modulus of Elasticity, Es = 210 GPa

Partial safety factor for ultimate limit state:

Concrete $\gamma_c = 1.5$

Structural steel, $\gamma_a = 1.1$

Column cross section data:

Specimen Designation: CFT-S-3

D =368 mm Aa = 156 cm^2

t = 14 mm $I_{xx} = I_{yy} = 24430\ cm^4$

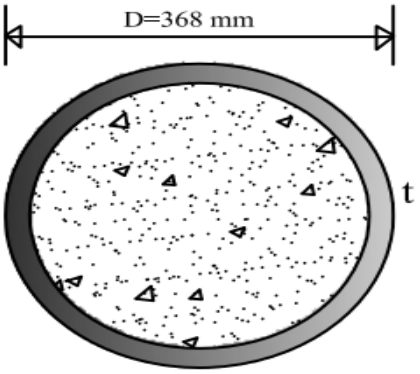

(4) Effective bending stiffness

$$EI_e = E_a I_a + 0.6 * E_{cd} I_c + E_s I_s$$

$$(EI)_e = 210 * 24430 * 10^4 + 0.6 * \frac{27.236}{1.35} * \pi \frac{340^4}{64}$$

$$\boldsymbol{(EI)_e = 5.924 * 10^{10} kN/mm^2}$$

(5) Related Slenderness ratios:

$$\bar{\lambda} = \sqrt{\frac{N_{pl,Rk}}{N_{cr}}}, \qquad N_{pl,Rk} = A_a * f_{yk} + A_c * (0.85 * f_{ck}) + A_s * f_{yk}$$

$$N_{pl,Rk} = 156 * 10^2 * 275 + \left(\pi * \frac{340^2}{4}\right) * 0.85 * 25$$

$$N_{pl,Rk} = 6559\ \text{kN}$$

$$N_{cr,xx} = N_{cr,yy} = \frac{\pi^2 * EI_{xx}}{L^2} = \pi^2 * \frac{(5.924) * 10^{10}}{(2500)^2} = 93548kN$$

$$\bar{\lambda}_{xx} = \bar{\lambda}_{yy} = \sqrt{\frac{6559}{64968}} = 0.265, \qquad 0.265 < 2 \ \ ok$$

(6) Plastic axial load capacity of cross section

$$N_{pl,Rd} = \eta_{ao} \frac{Aa * fy}{\gamma_a} + A_c * \frac{0.85 * f_{ck}}{\gamma_c}\left(1 + \eta_{ac} \frac{t}{D} \frac{f_y}{f_{ck}}\right) + \frac{(A_s * f_{yk})}{\gamma_s}$$

For eccentricity e = 0, $\eta_{ao} = 0.25(3 + 2\bar{\lambda}) \leq 1$

$$\eta_{c0} = 4.9 - 18.5\bar{\lambda} + 17(\bar{\lambda})^2 \geq 0$$

$$\eta_{ao} = 0.25(3 + 2 * 0.265) = 0.882$$

$$\eta_{c0} = 4.9 - 18.5 * 0.265 + 17 * 0.265^2 = 1.191$$

$$N_{pl,Rd} = 0.882 * 15600 * \frac{275}{1.1} + \pi * \frac{340^2}{4} * 0.85 * \frac{25}{1.5}\left[1 + 1.191 * \frac{1}{26.25} * \frac{275}{25}\right]$$

$$N_{pl,Rd} = 5368\ kN$$

Steel contribution ratio:

$$\delta = \frac{\frac{A_a * f_y}{\gamma_a}}{N_{pl,Rd}} = \frac{3900}{5368} = 0.7265 \rightarrow 0.2 < \delta < 0.9 \quad ok.$$

Column cross-section properties

Column designation	Diameter (D) (mm)	Thickness (t) (mm)	Area of steel tube (mm^2)	Moment of inertia (mm^4)	
				I_{xx} (mm^4)	I_{yy} (mm^4)
CFT-10	368	14	15600	$24430 * 10^4$	$24430 * 10^4$
CFT-11	368	14	15600	$24430 * 10^4$	$24430 * 10^4$
CFT-12	368	14	15600	$24430 * 10^4$	$24430 * 10^4$
CFT-13	368	14	15600	$24430 * 10^4$	$24430 * 10^4$

According to EN-EBCS-4,2015, the values of plastic resistance to compression can be expressed in tabular form.

Column designation	Material Data		Height (mm)	EI_{eff} (kN/mm^2)	Slenderness Ratio ($\bar{\lambda}$)	$N_{pl,Rd}$ (kN)	(δ)
	concrete	steel					
CFT-10	C-30	S-275	2500	$5.924 * 10^{10}$	0.265	5368	0.7265
CFT-11	C-30	S-275	3000	$5.924 * 10^{10}$	0.318	5228	0.746
CFT-12	C-30	S-275	3500	$5.924 * 10^{10}$	0.37	5138.8	0.76
CFT-13	C-30	S-275	4500	$5.924 * 10^{10}$	0.478	5143.3	0.76

Plastic resistance to axial compression capacity by considering steel yield strength

Material data:

Concrete: C-30, characteristic concrete compressive strength, fck = 25 MPa

Secant modulus for short term loading Ecm = 27.236 GPa

Steel: S-235, characteristics yield strength fy = 235 MPa ($t \leq 40\ mm$)

Modulus of Elasticity, Es = 210 GPa

Partial safety factor for ultimate limit state:

Concrete $\gamma_c = 1.5$

Structural steel, $\gamma_a = 1.1$

Column cross section data:

Specimen Designation: CFT-S-1

D =368 mm Aa = 156 cm^2

t = 14 mm $I_{xx} = I_{yy}$ = 24430 cm^4

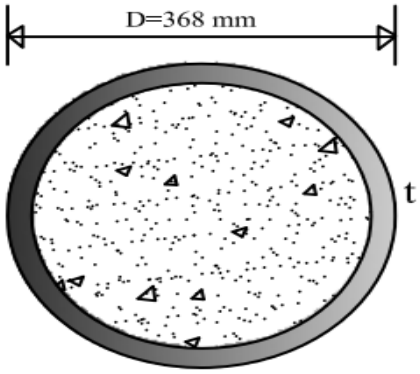

(1) Effective bending stiffness

$EI_e = E_a I_a + 0.6 * E_{cd} I_c + E_s I_s$

$$(EI)_e = 210 * 24430 * 10^4 + 0.6 * \frac{27.236}{1.35} * \pi \frac{340^4}{64}$$

$$\boldsymbol{(EI)_e = 5.924 * 10^{10} kN/mm^2}$$

(2) Related Slenderness ratios:

$$\bar{\lambda} = \sqrt{\frac{N_{pl,Rk}}{N_{cr}}}, \qquad N_{pl,Rk} = A_a * f_{yk} + A_c * (0.85 * f_{ck}) + A_s * f_{yk}$$

$$N_{pl,Rk} = 156 * 10^2 * 235 + \left(\pi * \frac{340^2}{4}\right) * 0.85 * 25$$

$$N_{pl,Rk} = 5595.33 \text{ kN}$$

$$N_{cr,xx} = N_{cr,yy} = \frac{\pi^2 * EI_{xx}}{L^2} = \pi^2 * \frac{(5.924) * 10^{10}}{(3000)^2} = 64964\ kN$$

$$\bar{\lambda}_{xx} = \bar{\lambda}_{yy} = \sqrt{\frac{5595.33}{64964}} = 0.293, \qquad 0.293 < 2\ \ ok$$

(3) Plastic axial load capacity of cross section

$$N_{pl,Rd} = \eta_{ao} \frac{Aa * fy}{\gamma_a} + A_c * \frac{0.85 * f_{ck}}{\gamma_c}\left(1 + \eta_{ac} \frac{t}{D} \frac{f_y}{f_{ck}}\right) + \frac{(A_s * f_{yk})}{\gamma_s}$$

For eccentricity e = 0, $\eta_{ao} = 0.25(3 + 2\bar{\lambda}) \leq 1$

$$\eta_{c0} = 4.9 - 18.5\bar{\lambda} + 17(\bar{\lambda})^2 \geq 0$$

$\eta_{ao} = 0.25(3 + 2 * 0.293) = 0.897$

$\eta_{c0} = 4.9 - 18.5 * 0.293 + 17 * 0.293^2 = 0.94$

$$N_{pl,Rd} = 0.897 * 15600 * \frac{235}{1.1} + \pi * \frac{340^2}{4} * 0.85 * \frac{25}{1.5}\left[1 + 0 * \frac{1}{26.25} * \frac{235}{25}\right]$$

$N_{pl,Rd} = 4708.63\ kN$

Steel contribution ratio:

$$\delta = \frac{\frac{A_a * f_y}{\gamma_a}}{N_{pl,Rd}} = \frac{3333}{4708.63} = 0.71 \rightarrow 0.2 < \delta < 0.9 \quad ok.$$

Column cross-section properties:

Column designation	Diameter (D) (mm)	Thickness (t) (mm)	Area of cross section (mm^2)	Moment of inertia (mm^4)	
				I_{xx} (mm^4)	I_{yy} (mm^4)
CFT-10	368	14	15600	$24430 * 10^4$	$24430 * 10^4$
CFT-11	368	14	15600	$24430 * 10^4$	$24430 * 10^4$
CFT-12	368	14	15600	$24430 * 10^4$	$24430 * 10^4$
CFT-13	368	14	15600	$24430 * 10^4$	$24430 * 10^4$

According to EN-EBCS-4, 2015, the values of plastic resistance to compression can be expressed in tabular form.

Column designation	Material Data		Height (mm)	EI_{eff} (kN/mm^2)	Slenderness Ratio ($\bar{\lambda}$)	$N_{pl,Rd}$ (kN)	(δ)
	concrete	steel					
CFT-14	C-30	S-235	3000	$5.924 * 10^{10}$	0.293	4708.63	0.71
CFT-15	C-30	S-275	3000	$5.924 * 10^{10}$	0.318	5228	0.746
CFT-16	C-30	S-355	3000	$5.924 * 10^{10}$	0.34	6318.22	0.797

Axial load capacity determination for steel reinforced concrete filled tube (SCFT)

For Specimen **S-CFT-S-1** axial load capacity determination.

Material data:

Concrete: C-30, characteristic concrete compressive strength, fck = 25 MPa

Secant modulus for short term loading Ecm = 27.236 GPa

Steel: S-275, characteristics yield strength fy = 275 MPa ($t \leq 40\ mm$)

Modulus of Elasticity, Es = 210 GPa

Partial safety factor for ultimate limit state:

Concrete $\gamma_c = 1.5$

Structural steel, $\gamma_a = 1.1$

Column cross section data:

Specimen Designation: S-CFT-S-1

Steel tube D =368 mm Aa = 156 cm^2

t = 14 mm $I_{xx} = I_{yy} = 24430\ cm^4$

I-section Aa = 25 cm^2 , h =114mm, b = 120 mm,

tw = 5 mm, tf = 8 mm, $I_{xx} = 606\ cm^2$, $I_{yy} = 231\ cm^2$

(1) Effective bending stiffness

$EI_e = E_a I_a + 0.6 * E_{cd} I_c + E_s I_s$

Along X-axis:

$$(EI)_e = 210 * (24430 + 606) * 10^4 + 0.6 * \frac{27.236}{1.35} * \pi \frac{340^4}{64}$$

$$\boldsymbol{(EI)_e = 6.051 * 10^{10} kN/mm^2}$$

Along Y-axis:

$$(EI)_e = 210 * (24430 + 231) * 10^4 + 0.6 * \frac{27.236}{1.35} * \pi \frac{340^4}{64}$$

$$\boldsymbol{(EI)_e = 5.9722 * 10^{10} kN/mm^2}$$

(2) Related Slenderness ratios:

$$\bar{\lambda} = \sqrt{\frac{N_{pl,Rk}}{N_{cr}}}, \qquad N_{pl,Rk} = A_a * f_{yk} + A_c * (0.85 * f_{ck}) + A_s * f_{yk}$$

$$N_{pl,Rk} = (156 + 25) * 10^2 * 275 + \left(\pi * \frac{340^2}{4}\right) * 0.85 * 25$$

$$N_{pl,Rk} = 6907 \text{ kN}$$

$$N_{cr,xx} = \frac{\pi^2 * EI_{xx}}{L^2} = \pi^2 * \frac{(6.051) * 10^{10}}{(3000)^2} = 66356.6\ kN$$

$$N_{cr,yy} = \frac{\pi^2 * EI_{yy}}{L^2} = \pi^2 * \frac{(5.9722) * 10^{10}}{(3000)^2} = 65492.5$$

$$\bar{\lambda}_{xx} = \sqrt{\frac{6907}{66356.6}} = 0.3226, \qquad 0.323 < 2\ \ ok$$

$$\bar{\lambda}_{yy} = \sqrt{\frac{6907}{65492.5}} = 0.325$$

(3) Plastic axial load capacity of cross section

$$N_{pl,Rd} = \eta_{ao}\frac{Aa * fy}{\gamma_a} + A_c * \frac{0.85 * f_{ck}}{\gamma_c}\left(1 + \eta_{ac}\frac{t}{D}\frac{f_y}{f_{ck}}\right) + \frac{(A_s * f_{yk})}{\gamma_s}$$

For eccentricity e = 0, $\eta_{ao} = 0.25(3 + 2\bar{\lambda}) \leq 1$

$$\eta_{c0} = 4.9 - 18.5\bar{\lambda} + 17(\bar{\lambda})^2 \geq 0$$

$\eta_{ao} = 0.25(3 + 2 * 0.325) = 0.9125$

$\eta_{c0} = 4.9 - 18.5 * 0.325 + 17 * 0.325^2 = 0.683$

$$N_{pl,Rd} = 0.9125 * 18100 * \frac{275}{1.1} + \pi * \frac{340^2}{4} * 0.85 * \frac{25}{1.5}\left[1 + 0.683 * \frac{1}{26.25} * \frac{275}{25}\right]$$

$N_{pl,Rd} = 5783.5kN$

Steel contribution ratio:

$$\delta = \frac{\frac{A_a * f_y}{\gamma_a}}{N_{pl,Rd}} = \frac{4525}{5783.5} = 0.782 \rightarrow 0.2 < \delta < 0.9 \quad ok.$$

Column cross section properties

Column designation	Steel tube properties				Reinforcing steel properties (I-section)						
	D	t	Aa	$I_{xx}=I_{yy}$	h	b	t_w	t_f	A_a	I_{xx}	I_{yy}
	(mm)	(mm)	(cm^2)	(cm^4)	mm	mm	mm	mm	cm^2	cm^4	cm^4
SCFT-1	368	14	156	24430	96	100	5	8	21.2	349	134
SCFT-2	368	14	156	24430	114	120	5	8	25	606	231
SCFT-3	368	14	156	24430	133	140	5.5	8.5	31.4	1030	389
SCFT-4	368	14	156	24430	171	180	6	9.5	45.3	2510	925

According to EN-EBCS-4, 2015, the values of plastic resistance to compression can be expressed in tabular form.

Column designation	Material		Height	EI_{eff}		Slenderness ratio		Npl,Rd	Steel contribution ratio (δ)
				x-axis	y-axis				
	concrete	steel		(10^{10})	(10^{10})	x-axis	y-axis		
	MPa	MPa	mm	kNm^2				kN	
SCFT-1	C-30	S-275	3000	6	5.952	0.321	0.323	5700	0.777
SCFT-2	C-30	S-275	3000	6.051	5.972	0.323	0.325	5783.5	0.782
SCFT-3	C-30	S-275	3000	6.14	6.006	0.324	0.328	5924.5	0.79
SCFT-4	C-30	S-275	3000	6.451	6.119	0.33	0.333	6235	0.807

Axial load capacity determination for square filled steel tube

For Specimen **SFT-S-1** axial load capacity determination. (Thickness effect)

Material data:

Concrete: C-30, characteristic concrete compressive strength, fck = 25 MPa

Secant modulus for short term loading Ecm = 23.5 MPa

Steel: S-275, characteristics yield strength fy = 275 MPa ($t \leq 40\ mm$)

Modulus of Elasticity, Es = 210 GPa

Partial safety factor for ultimate limit state:

Concrete $\gamma_c = 1.5$

Structural steel, $\gamma_a = 1.1$

Column cross section data:

Specimen Designation: CFT-S-1

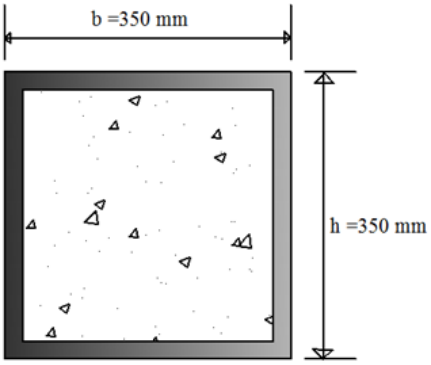

B =350 mm Aa = 136 cm^2

t = 10 mm $I_{xx} = I_{yy} = 26050\ cm^4$

(1) Effective bending stiffness

$EI_e = E_a I_a + 0.6 * E_{cd} I_c + E_s I_s$

$$(EI)_e = 210 * 26050 * 10^4 + 0.6 * \frac{23.5}{1.35} * \frac{330^4}{12}$$

$$\boldsymbol{(EI)_e = 6.503 * 10^{10} kN/mm^2}$$

(2) Related Slenderness ratios:

$$\bar{\lambda} = \sqrt{\frac{N_{pl,Rk}}{N_{cr}}}, \qquad N_{pl,Rk} = A_a * f_{yk} + A_c * (0.85 * f_{ck}) + A_s * f_{yk}$$

$$N_{pl,Rk} = 136 * 10^2 * 275 + (330^2) * 0.85 * 25$$

$$N_{pl,Rk} = 6054.125\ kN$$

$$N_{cr,xx} = N_{cr,yy} = \frac{\pi^2 * EI_{xx}}{L^2} = \pi^2 * \frac{(6.503) * 10^{10}}{(3000)^2} = 71313.4\ kN$$

$$\bar{\lambda}_{xx} = \bar{\lambda}_{yy} = \sqrt{\frac{6054.125}{71313.4}} =, \qquad 0.291 < 2\ \ ok$$

(3) Plastic axial load capacity of cross section

$$N_{pl,Rd} = \frac{Aa * fy}{\gamma_a} + A_c * \frac{0.85 f_{ck}}{\gamma_c} + \frac{(A_s * f_{yk})}{\gamma_s}$$

$$N_{pl,Rd} = 13600 * \frac{275}{1.1} + 330^2 * 0.85 * \frac{25}{1.5} + 0$$

$$N_{pl,Rd} = 4942.75kN$$

Steel contribution ratio:

$$\delta = \frac{\frac{A_a * f_y}{\gamma_a}}{N_{pl,Rd}} = \frac{3400}{4942.75} = 0.69 \rightarrow 0.2 < \delta < 0.9 \quad ok.$$

Column cross-section properties

Column designation	Width (mm)	Thickness (mm)	Area of steel Tube (cm^2)	Moment of inertia (cm^4)
SFT-1	350x350	10	136	26050
SFT-2	350x350	12.5	168	31810
SFT-3	350x350	16	213	39370

According to EN-EBCS-4, 2015, the values of plastic resistance to compression can be expressed in tabular form.

Column designation	Material data		Height (mm)	EI_{eff} (kNm^2) ($*10^{10}$)	Slenderness Ratio ($\bar{\lambda}$)	$N_{pl,Rd}$ (kN)	Steel contribution ratio
	concrete	steel					
SFT-1	C-30	S-275	3000	6.503	0.291	4942.75	0.69
SFT-2	C-30	S-275	3000	7.651	0.286	5696.35	0.737
SFT-3	C-30	S-275	3000	9.16	0.282	6757.6	0.79

Compressive strength effect

For Specimen **SFT-S-1** axial load capacity determination. **Compressive strength effect**

Material data:

Concrete: C-25, characteristic concrete compressive strength, fck = 20 MPa

Secant modulus for short term loading Ecm = 22.3 GPa

Steel: S-275, characteristics yield strength fy = 275 MPa ($t \leq 40\ mm$)

Modulus of Elasticity, Es = 210 GPa

Partial safety factor for ultimate limit state:

Concrete $\gamma_c = 1.5$

Structural steel, $\gamma_a = 1.1$

Column cross section data:

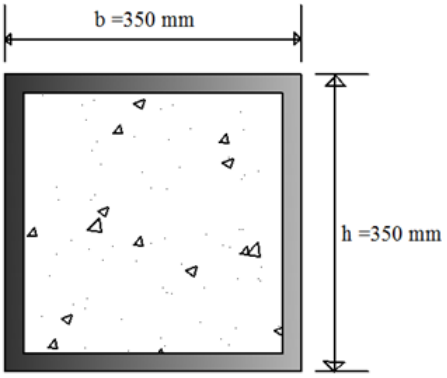

Specimen Designation: CFT-S-3

D =350 mm Aa = 168 cm^2

t = 12.5 mm $I_{xx} = I_{yy} = 31810\ cm^4$

(1) Effective bending stiffness

$EI_e = E_a I_a + 0.6 * E_{cd} I_c + E_s I_s$

$$(EI)_e = 210 * 31810 * 10^4 + 0.6 * \frac{22.3}{1.35} * \frac{325^4}{12}$$

$$\boldsymbol{(EI)_e = 7.6 * 10^{10} kN/mm^2}$$

(2) Related Slenderness ratios:

$$\bar{\lambda} = \sqrt{\frac{N_{pl,Rk}}{N_{cr}}}, \qquad N_{pl,Rk} = A_a * f_{yk} + A_c * (0.85 * f_{ck}) + A_s * f_{yk}$$

$$N_{pl,Rk} = 168 * 10^2 * 275 + 325^2 * 0.85 * 20$$
$$N_{pl,Rk} = 6415.625 \text{ kN}$$

$$N_{cr,xx} = N_{cr,yy} = \frac{\pi^2 * EI_{xx}}{L^2} = \pi^2 * \frac{(7.6) * 10^{10}}{(3000)^2} = 83343\ kN$$

$$\bar{\lambda}_{xx} = \bar{\lambda}_{yy} = \sqrt{\frac{6415.625}{83343}} =, \qquad 0.277 < 2\ \ ok$$

(3) Plastic axial load capacity of cross section

$$N_{pl,Rd} = \frac{Aa * fy}{\gamma_a} + A_c * \frac{0.85 * f_{ck}}{\gamma_c} + \frac{(A_s * f_{yk})}{\gamma_s}$$

$$N_{pl,Rd} = 16800 * \frac{275}{1.1} + 325^2 * 0.85 * \frac{20}{1.5}$$

$$\boldsymbol{N_{pl,Rd} = 5397.1\ kN}$$

Steel contribution ratio:

$$\delta = \frac{\frac{A_a * f_y}{\gamma_a}}{N_{pl,Rd}} = \frac{4200}{5397} = 0.78 \rightarrow 0.2 < \delta < 0.9 \quad ok$$

Column cross section properties

Column designation	Width (mm)	Thickness (mm)	Area of steel tube (cm^2)	Moment of inertia (cm^4)
SFT-4	350 x350	12.5	168	31810
SFT-5	350 x350	12.5	168	31810
SFT-6	350 x350	12.5	168	31810
SFT-7	350 x350	12.5	168	31810
SFT-8	350 x350	12.5	168	31810

According to EN-EBCS-4, 2015, the values of plastic resistance to compression can be expressed in tabular form.

Column designation	Material data		Height (mm)	EI_{eff} (kNm^2) ($*10^{10}$)	Slenderness Ratio ($\bar{\lambda}$)	$N_{pl,Rd}$ (kN)	Steel contribution ratio
	concrete	steel					
SFT-4	C-25	S-275	3000	7.6	0.277	5397.1	0.78
SFT-5	C-30	S-275	3000	7.7	0.29	5696.4	0.74
SFT-6	C-37	S-275	3000	7.79	0.293	5995.6	0.7
SFT-7	C-45	S-275	3000	7.87	0.3	6295	0.67
SFT-8	C-50	S-275	3000	7.95	0.306	6594	0.653

Plastic resistance to axial compression by considering Slenderness Effect

Concrete Filled steel tube capacity determination

For Specimen **CFT-S-1** axial load capacity determination.

Material data:

Concrete: C-30, characteristic concrete compressive strength, fck = 25 MPa

Secant modulus for short term loading Ecm = 27.236 GPa

Steel: S-275, characteristics yield strength fy = 275 MPa ($t \leq 40\ mm$)

Modulus of Elasticity, Es = 210 GPa

Partial safety factor for ultimate limit state:

Concrete $\gamma_c = 1.5$

Structural steel, $\gamma_a = 1.1$

Column cross section data:

Specimen Designation: CFT-S-3

B=350 mm Aa = 168cm^2

t = 12.5 mm $I_{xx} = I_{yy}$ = 31810 cm^4

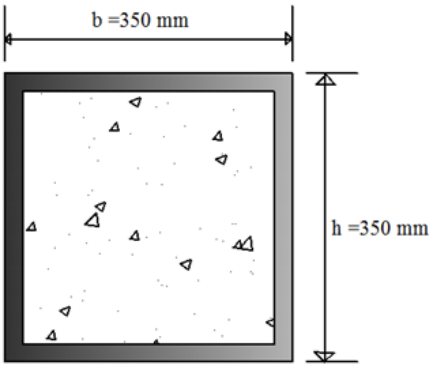

(1) Effective bending stiffness

$EI_e = E_a I_a + 0.6 * E_{cd} I_c + E_s I_s$

$$(EI)_e = 210 * 31810 * 10^4 + 0.6 * \frac{27.236}{1.35} * \frac{325^4}{12}$$

$$\boldsymbol{(EI)_e = 7.806 * 10^{10} kN/mm^2}$$

(2) Related Slenderness ratios:

$$\bar{\lambda} = \sqrt{\frac{N_{pl,Rk}}{N_{cr}}}, \qquad N_{pl,Rk} = A_a * f_{yk} + A_c * (0.85 * f_{ck}) + A_s * f_{yk}$$

$$N_{pl,Rk} = 168 * 10^2 * 275 + 325^2 * 0.85 * 25$$

$$N_{pl,Rk} = 6864.5 \text{ kN}$$

$$N_{cr,xx} = N_{cr,yy} = \frac{\pi^2 * EI_{xx}}{L^2} = \pi^2 * \frac{(7.806) * 10^{10}}{(2500)^2} = 123267.4kN$$

$$\bar{\lambda}_{xx} = \bar{\lambda}_{yy} = \sqrt{\frac{6864.5}{123267.4}} =, \qquad 0.236 < 2 \ \ ok$$

(3) Plastic axial load capacity of cross section

$$N_{pl,Rd} = \frac{Aa * fy}{\gamma_a} + A_c * \frac{0.85 * f_{ck}}{\gamma_c} + \frac{(A_s * f_{yk})}{\gamma_s}$$

$$N_{pl,Rd} = 16800 * \frac{275}{1.1} + 325^2 * 0.85 * \frac{25}{1.5}$$

$$N_{pl,Rd} = 5696.4kN$$

Steel contribution ratio: $\delta = \frac{\frac{A_a * f_y}{\gamma_a}}{N_{pl,Rd}} = \frac{4200}{5696} = 0.74 \rightarrow 0.2 < \delta < 0.9 \quad ok.$

Column designation	Width (mm)	Thickness (mm)	Area of steel tube (cm^2)	Moment of inertia (cm^4)
SFT-4	350 x350	12.5	168	31810
SFT-5	350 x350	12.5	168	31810
SFT-6	350 x350	12.5	168	31810
SFT-7	350 x350	12.5	168	31810
SFT-8	350 x350	12.5	168	31810

Column designation	Material data		Height (mm)	EI_{eff} (kNm^2) ($*10^{10}$)	Slenderness Ratio ($\bar{\lambda}$)	$N_{pl,Rd}$ (kN)	Steel contribution ratio
	concrete	steel					
SFT-4	C-30	S-275	3000	7.806	0.236	5696.4	0.74
SFT-5	C-30	S-275	3000	7.806	0.283	5696.4	0.74
SFT-6	C-30	S-275	3000	7.806	0.233	5696.4	0.74
SFT-7	C-30	S-275	3000	7.806	0.38	5696.4	0.74
SFT-8	C-30	S-275	3000	7.806	0.424	5696.4	0.74

Plastic resistance to axial compression capacity by considering steel yield strength

Material data:

Concrete: C-30, characteristic concrete compressive strength, fck = 25 MPa

Secant modulus for short term loading Ecm = 24.51 GPa

Steel: S-235, characteristics yield strength fy = 235 MPa ($t \leq 40\ mm$)

Modulus of Elasticity, Es = 210 GPa

Partial safety factor for ultimate limit state:

Concrete $\gamma_c = 1.5$

Structural steel, $\gamma_a = 1.1$

Column cross section data:

Specimen Designation: CFT-S-1

B =350 mm Aa = 168 cm^2

t = 12.5 mm $I_{xx} = I_{yy}$ = 31810 cm^4

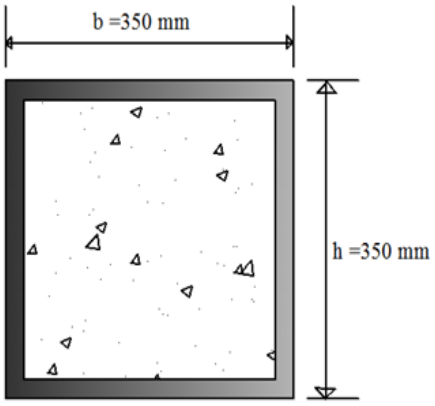

(1) Effective bending stiffness

$EI_e = E_a I_a + 0.6 * E_{cd} I_c + E_s I_s$

$$(EI)_e = 210 * 31810 * 10^4 + 0.6 * \frac{24.5}{1.35} * \frac{325^4}{12}$$

$$\boldsymbol{(EI)_e = 6.7645 * 10^{10} kN/mm^2}$$

(2) Related Slenderness ratios:

$$\bar{\lambda} = \sqrt{\frac{N_{pl,Rk}}{N_{cr}}}, \qquad N_{pl,Rk} = A_a * f_{yk} + A_c * (0.85 * f_{ck}) + A_s * f_{yk}$$

$$N_{pl,Rk} = 168 * 10^2 * 235 + 325^2 * 0.85 * 25$$

$$N_{pl,Rk} = 6192.5 \text{ kN}$$

$$N_{cr,xx} = N_{cr,yy} = \frac{\pi^2 * EI_{xx}}{L^2} = \pi^2 * \frac{6.7645 * 10^{10}}{(3000)^2} = 74181.04\ kN$$

$$\bar{\lambda}_{xx} = \bar{\lambda}_{yy} = \sqrt{\frac{6192.5}{74181.04}} = 0.29, \qquad 0.29 < 2\ \ ok$$

(3) Plastic axial load capacity of cross section

$$N_{pl,Rd} = \frac{Aa * fy}{\gamma_a} + A_c * \frac{0.85 * f_{ck}}{\gamma_c} + \frac{(A_s * f_{yk})}{\gamma_s}$$

$$N_{pl,Rd} = 16800 * \frac{235}{1.1} + 325^2 * 0.85 * \frac{25}{1.5}$$

$$N_{pl,Rd} = 5085.4\ kN$$

Steel contribution ratio:

$$\delta = \frac{\frac{A_a * f_y}{\gamma_a}}{N_{pl,Rd}} = \frac{3589.1}{5085.4} = 0.71 \rightarrow 0.2 < \delta < 0.9 \quad ok.$$

Column crosssection properties

Column designation	Width (mm)	Thickness (mm)	Area of steel Tube (cm^2)	Moment of inertia (cm^4)
SFT-1	350x350	12.5	168	31810
SFT-2	350x350	12.5	168	31810
SFT-3	350x350	12.5	168	31810

According to EN-EBCS-4, 2015, the values of plastic resistance to compression can be expressed in tabular form.

Column designation	Material data		Height (mm)	EI_{eff} (kNm^2) ($*10^{10}$)	Slenderness Ratio ($\bar{\lambda}$)	$N_{pl,Rd}$ (kN)	Steel contribution ratio
	concrete	steel					
SFT-1	C-30	S-235	3000	6.764	0.29	5085.4	0.71
SFT-2	C-30	S-275	3000	7.7	0.285	5696.35	0.737
SFT-3	C-30	S-355	3000	7.71	0.282	6918.2	0.784

Appendix B: Material properties of concrete core

Table A.1: Concrete damaged plasticity parameters with different diameter to thickness ratio

Compressive behavior				Compressive behavior			
Diameter to thickness ratio (D/t =36.8)				Diameter to thickness ratio (D/t =30.67)			
yield stress	inelastic strain	damage	inelastic strain	yield stress	inelastic strain	damage	inelastic strain
10.734	0	0	0	11.029	0.0000000	0	0
18.872	0.000780	0	0.000780	19.038	0.0007879	0	0.0007879
21.723	0.001172	0	0.001172	21.881	0.0011815	0	0.0011815
23.965	0.001586	0	0.001586	24.125	0.0015976	0	0.0015976
25.777	0.002017	0	0.002017	25.954	0.0020292	0	0.0020292
27.253	0.002461	0	0.002461	27.469	0.0024725	0	0.0024725
28.450	0.002915	0	0.002915	28.730	0.0029253	0	0.0029253
29.401	0.003379	0	0.003379	29.773	0.0033863	0	0.0033863
30.128	0.003851	0	0.003851	30.620	0.0038546	0	0.0038546
30.647	0.004331	0	0.004331	31.286	0.0043297	0	0.0043297
30.973	0.004819	0	0.004819	31.783	0.0048111	0	0.0048111
31.117	0.005313	0	0.005313	32.120	0.0052985	0	0.0052985
31.128	0.005490	0	0.005490	32.306	0.0057915	0	0.0057915
31.128	0.006313	0	0.006313	32.352	0.0062013	0	0.0062013
31.128	0.006813	0	0.006813	32.352	0.0062898	0	0.0062898
31.128	0.007313	0	0.007313	32.352	0.0072898	0	0.0072898
31.128	0.007813	0	0.007813	32.352	0.0077898	0	0.0077898
31.128	0.008313	0	0.008313	32.352	0.0082898	0	0.0082898
31.128	0.008813	0	0.008813	32.352	0.0087898	0	0.0087898
31.128	0.018813	0	0.018813	32.352	0.0187898	0	0.0187898
31.128	0.038813	0	0.038813	32.352	0.0387898	0	0.0387898
31.128	0.058813	0	0.058813	32.352	0.0587898	0	0.0587898
31.128	0.072256	0	0.072256	32.352	0.0803161	0	0.0803161

Tensile behavior				Tensile behavior			
Diameter to thickness ratio (D/t = 36.8)				Diameter to thickness ratio (D/t =30.67)			
yield stress	inelastic strain	damage	inelastic strain	yield stress	inelastic strain	damage	inelastic strain
1.880	0	0	0	1.880	0	0	0
0.511	0.0005745	0.7284	0.0005745	0.464	0.000583	0.753	0.000583
0.364	0.0006361	0.8065	0.0006361	0.451	0.000588	0.7603	0.000588
0.233	0.0006911	0.8762	0.0006911	0.197	0.000693	0.8952	0.000693
0.10168	0.0007461	0.94592	0.0007461	0.06337	0.000748	0.9663	0.000748

Compressive behavior				Compressive behavior			
Diameter to thickness ratio (D/t = 26.28)				Diameter to thickness ratio (D/t =23)			
Yield stress	inelastic strain	damage	inelastic strain	Yield stress	inelastic strain	damage	inelastic strain
11.33982	0.0000000	0	0.0000000	11.6608	0.0000000	0	0.0000000
19.25584	0.0007930	0	0.0007930	19.5102	0.0007964	0	0.0007964
22.10364	0.0011884	0	0.0011884	22.3719	0.0011932	0	0.0011932
24.35190	0.0016059	0	0.0016059	24.6298	0.0016117	0	0.0016117
26.19322	0.0020383	0	0.0020383	26.4831	0.0020449	0	0.0020449
27.73408	0.0024817	0	0.0024817	28.0427	0.0024886	0	0.0024886
29.03687	0.0029339	0	0.0029339	29.3743	0.0029406	0	0.0029406
30.13964	0.0033934	0	0.0033934	30.5181	0.0033994	0	0.0033994
31.06645	0.0038594	0	0.0038594	31.5000	0.0038640	0	0.0038640
31.83309	0.0043312	0	0.0043312	32.3367	0.0043338	0	0.0043338
32.45050	0.0048085	0	0.0048085	33.0395	0.0048084	0	0.0048084
32.92687	0.0052911	0	0.0052911	33.6165	0.0052876	0	0.0052876
33.26900	0.0057785	0	0.0057785	34.0738	0.0057711	0	0.0057711
33.48316	0.0062706	0	0.0062706	34.4163	0.0062588	0	0.0062588
33.57566	0.0067672	0	0.0067672	34.6487	0.0067504	0	0.0067504
33.58067	0.0069154	0	0.0069154	34.7756	0.0072458	0	0.0072458
33.58067	0.0072670	0	0.0072670	34.8043	0.0076274	0	0.0076274
33.58067	0.0077670	0	0.0077670	34.8043	0.0082448	0	0.0082448
33.58067	0.0082670	0	0.0082670	34.8043	0.0087448	0	0.0087448
33.58067	0.0087670	0	0.0087670	34.8043	0.0187448	0	0.0187448
33.58067	0.0187670	0	0.0187670	34.8043	0.0387448	0	0.0387448
33.58067	0.0387670	0	0.0387670	34.8043	0.0587448	0	0.0587448
33.58067	0.0883995	0	0.0883995	34.8043	0.0964535	0	0.0964535

Tensile behavior				Tensile behavior			
Diameter to thickness ratio (D/t =26.28)				Diameter to thickness ratio (D/t =23)			
Yield stress	inelastic strain	damage	inelastic strain	Yield stress	inelastic strain	damage	inelastic strain
1.8803	0	0.0000	0	1.8803	0	0	0
0.4342	0.000584	0.7691	0.000584	0.4047	0.0005854	0.78477	0.0005854
0.3893	0.000602	0.7929	0.000602	0.3281	0.0006158	0.82549	0.0006158
0.1618	0.000694	0.9139	0.000694	0.1274	0.0006954	0.9322	0.0006954
0.0257	0.000749	0.9864	0.000749	0.0165	0.0007394	0.9912	0.0007394

Table B. 1: Concrete damaged plasticity parameters with different concrete compressive strength

Compressive behavior				Compressive behavior			
Concrete compressive strength C-25				Concrete compressive strength C-30			
yield stress	inelastic strain	damage	inelastic strain	yield stress	inelastic strain	damage	inelastic strain
9.420	0	0	0.000000	11.340	0.000000	0	0
16.324	0.000850	0	0.000850	19.256	0.000793	0	0.000793
18.541	0.001262	0	0.001262	22.104	0.001188	0	0.001188
20.275	0.001693	0	0.001693	24.352	0.001606	0	0.001606
21.694	0.002137	0	0.002137	26.193	0.002038	0	0.002038
22.890	0.002589	0	0.002589	27.734	0.002482	0	0.002482
23.917	0.003048	0	0.003048	29.037	0.002934	0	0.002934
24.807	0.003513	0	0.003513	30.140	0.003393	0	0.003393
25.581	0.003982	0	0.003982	31.066	0.003859	0	0.003859
26.252	0.004455	0	0.004455	31.833	0.004331	0	0.004331
26.828	0.004932	0	0.004932	32.451	0.004809	0	0.004809
27.316	0.005413	0	0.005413	32.927	0.005291	0	0.005291
27.721	0.005897	0	0.005897	33.269	0.005778	0	0.005778
28.044	0.006384	0	0.006384	33.483	0.006271	0	0.006271
28.097	0.006478	0	0.006478	33.576	0.006767	0	0.006767
28.458	0.007367	0	0.007367	33.581	0.006915	0	0.006915
28.555	0.007864	0	0.007864	33.581	0.007767	0	0.007767
28.581	0.008298	0	0.008298	33.581	0.008267	0	0.008267
28.581	0.008863	0	0.008863	33.581	0.008767	0	0.008767
28.581	0.018863	0	0.018863	33.581	0.018767	0	0.018767
28.581	0.038863	0	0.038863	33.581	0.038767	0	0.038767
28.581	0.058863	0	0.058863	33.581	0.058767	0	0.058767
28.581	0.102653	0	0.102653	33.581	0.088399	0	0.088399

Tensile behavior				Tensile behavior			
Concrete compressive strength (C-25)				Concrete compressive strength (C-30)			
yield stress	inelastic strain	damage	inelastic strain	yield stress	inelastic strain	damage	inelastic strain
1.747	0	0	0	1.880	0	0	0
0.492	0.000549	0.7181	0.000549	0.451	0.0005775	0.7603	0.000577
0.414	0.000584	0.7630	0.000584	0.298	0.0006391	0.8415	0.000639
0.163	0.000694	0.9069	0.000694	0.162	0.0006941	0.9139	0.000694
0.037	0.000749	0.9788	0.000749	0.026	0.0007491	0.9864	0.000749

Concrete compressive strength C-37				Concrete compressive strength C-50			
yield stress	inelastic strain	damage	inelastic strain	yield stress	inelastic strain	damage	inelastic strain
13.34	0	0	0	17.577	0	0	0
22.205	0.00074	0	0.000739	28.134	0.00064	0	0.0006412
25.727	0.00112	0	0.001119	33.112	0.00099	0	0.0009892
28.524	0.00152	0	0.001523	37.086	0.00137	0	0.0013679
30.808	0.00194	0	0.001945	40.292	0.00177	0	0.00177
32.698	0.00238	0	0.00238	42.868	0.00219	0	0.0021914
34.264	0.00283	0	0.002826	44.899	0.00263	0	0.0026294
35.551	0.00328	0	0.003282	46.442	0.00308	0	0.0030823
36.586	0.00374	0	0.003747	47.541	0.00355	0	0.0035488
37.389	0.00421	0	0.004219	47.999	0.00383	0	0.0038327
37.976	0.00469	0	0.004699	48.549	0.00452	0	0.004518
38.036	0.00476	0	0.004761	48.580	0.00473	0	0.0047348
38.359	0.00519	0	0.005186	48.537	0.00552	0.0008986	0.0055184
38.552	0.00568	0	0.005679	48.509	0.00602	0.0014730	0.0060192
38.581	0.00596	0	0.005969	48.4812	0.00652	0.0020474	0.0065201
38.581	0.00669	0	0.006678	48.453	0.00702	0.0026218	0.0070209
38.581	0.00717	0	0.007178	48.425	0.00752	0.0031962	0.0075218
38.581	0.00767	0	0.007678	48.39	0.00802	0.0037706	0.0080226
38.581	0.00817	0	0.008178	48.369	0.00852	0.0043449	0.0085235
38.581	0.00867	0	0.008678	47.81	0.01854	0.0158328	0.0185405
38.581	0.01867	0	0.018678	46.695	0.03857	0.0388085	0.0385746
38.581	0.038678	0	0.038678	46.137	0.04859	0.0502963	0.0485916
38.581	0.078872	0	0.078872	45.110	0.06702	0.0714285	0.0670182

Tensile behavior				Tensile behavior			
Concrete compressive strength C-37				Concrete compressive strength C-50			
yield stress	inelastic strain	damage	inelastic strain	yield stress	inelastic strain	damage	inelastic strain
1.997	0	0	0	2.101	0	0	0
0.737	0.000475	0.6309	0.0004748	0.450	0.000586	0.7860	0.000586
0.445	0.000585	0.7771	0.0005848	0.294	0.000641	0.8598	0.000641
0.153	0.000695	0.9233	0.0006948	0.139	0.000696	0.9337	0.000696
0.066	0.000728	0.9672	0.0007278	0.015	0.000740	0.9927	0.000740

Square concrete filled steel tubular column

Table B. 2: Concrete damaged plasticity parameter's value with different width to thickness ratio for SCFST

Compressive behavior				Compressive behavior			
Width to thickness ratio (B/t =10)				Width to thickness ratio (B/t =12.5)			
yield stress	inelastic strain	damage	inelastic strain	yield stress	inelastic strain	damage	inelastic strain
9.924	0.000000	0	0	10.033	0	0	0
20.186	0.000641	0	0.00064	18.938	0.000732	0	0.000732
23.014	0.001021	0	0.00102	21.882	0.001113	0	0.001113
24.543	0.001456	0	0.00146	24.075	0.001524	0	0.001524
25.000	0.001936	0	0.00194	25.665	0.001960	0	0.001960
24.841	0.002443	0.006	0.00244	26.735	0.002416	0	0.002416
24.682	0.002950	0.013	0.00295	27.348	0.002892	0	0.002892
24.523	0.003456	0.019	0.00346	27.556	0.003383	0	0.003383
24.363	0.003963	0.025	0.00396	27.557	0.003417	0	0.003417
24.204	0.004470	0.032	0.00447	27.389	0.004390	0.0061	0.004390
24.045	0.004977	0.038	0.00498	27.302	0.004893	0.0092	0.004893
23.886	0.005484	0.045	0.00548	27.215	0.005397	0.0124	0.005397
23.727	0.005990	0.051	0.00599	27.129	0.005900	0.0155	0.005900
23.568	0.006497	0.057	0.00650	27.042	0.006404	0.0187	0.006404
23.409	0.007004	0.064	0.00700	26.955	0.006908	0.0218	0.006908
23.249	0.007511	0.070	0.00751	26.868	0.007411	0.0250	0.007411
23.090	0.008017	0.076	0.00802	26.781	0.007915	0.0281	0.007915
22.931	0.008524	0.083	0.00852	26.694	0.008418	0.0313	0.008418
22.772	0.009031	0.089	0.00903	26.607	0.008922	0.0345	0.008922
21.181	0.014099	0.153	0.01410	25.738	0.013957	0.0660	0.013957
19.589	0.019166	0.216	0.01917	24.869	0.018992	0.0975	0.018992
16.406	0.029302	0.344	0.02930	23.131	0.029062	0.1606	0.029062
15.451	0.032343	0.382	0.03234	19.676	0.049080	0.286	0.049080

Tensile behavior				Tensile behavior			
width to thickness ratio (B/t =10)				width to thickness ratio (B/t = 12.5)			
yield stress	inelastic strain	damage	inelastic strain	yield stress	inelastic strain	damage	inelastic strain
1.880	0	0	0	1.880	0	0	0
0.672	0.000565	0.642	0.000565	0.603	0.000570	0.679	0.000570
0.541	0.000627	0.712	0.000627	0.465	0.000631	0.753	0.000631
0.423	0.000682	0.775	0.000682	0.341	0.000686	0.819	0.000686
0.306	0.000737	0.837	0.000737	0.218	0.000741	0.884	0.000741

Table B. 3: Concrete damaged plasticity parameter's value with different concrete compressive strength for SCFST.

Compressive behavior				Compressive behavior			
Concrete compressive strength C-25				Concrete compressive strength C-30			
For B/t =12.5				For B/t =12.5			
yield stress	inelastic strain	damage	inelastic strain	yield stress	inelastic strain	damage	inelastic strain
7.951	0	0	0	10.033	0	0	0
15.433	0.000809	0	0.000809	18.938	0.000732	0	0.000732
17.662	0.001209	0	0.001209	21.882	0.001113	0	0.001113
19.348	0.001633	0	0.001633	24.075	0.001524	0	0.001524
20.617	0.002076	0	0.002076	25.665	0.001960	0	0.001960
21.536	0.002535	0	0.002535	26.735	0.002416	0	0.002416
22.145	0.003008	0	0.003008	27.348	0.002892	0	0.002892
22.475	0.003493	0	0.003493	27.556	0.003383	0	0.003383
22.557	0.003907	0	0.003907	27.557	0.003417	0	0.003417
22.481	0.004493	0.003	0.004493	27.389	0.004390	0.0061	0.004390
22.415	0.004996	0.006	0.004996	27.302	0.004893	0.0092	0.004893
22.350	0.005499	0.009	0.005499	27.215	0.005397	0.0124	0.005397
22.284	0.006002	0.012	0.006002	27.129	0.005900	0.0156	0.005900
22.218	0.006505	0.015	0.006505	27.042	0.006404	0.0187	0.006404
22.153	0.007008	0.018	0.007008	26.955	0.006908	0.0219	0.006908
22.087	0.007511	0.021	0.007511	26.868	0.007411	0.0250	0.007411
22.022	0.008013	0.024	0.008013	26.781	0.007915	0.0282	0.007915
21.956	0.008516	0.027	0.008516	26.694	0.008418	0.0313	0.008418
21.890	0.009019	0.030	0.009019	26.607	0.008922	0.0345	0.008922
21.235	0.014049	0.059	0.014049	25.738	0.013957	0.0660	0.013957
20.579	0.019078	0.088	0.019078	24.869	0.018992	0.0976	0.018992
19.267	0.029137	0.146	0.029137	23.131	0.029062	0.1606	0.029062
16.106	0.053375	0.286	0.053375	19.676	0.049080	0.2860	0.049080

Compressive behavior				Compressive behavior			
Concrete compressive strength C-25				Concrete compressive strength C-30			
For B/t =12.5				For D/t =12.5			
yield stress	inelastic strain	damage	inelastic strain	yield stress	inelastic strain	damage	inelastic strain
1.747	0	0	0	1.880	0	0	0
0.596	0.0005673	0.659	0.0005673	0.603	0.0005696	0.679	0.0005696
0.471	0.0006289	0.731	0.0006289	0.465	0.0006312	0.753	0.0006312
0.359	0.0006839	0.794	0.0006839	0.341	0.0006862	0.818	0.0006862
0.247	0.0007389	0.858	0.0007389	0.218	0.0007412	0.884	0.0007412

Compressive behavior				Compressive behavior			
Concrete compressive strength C-37				Concrete compressive strength C-50			
yield stress	inelastic strain	damage	inelastic strain	yield stress	inelastic strain	damage	inelastic strain
12.212	0	0	0	14.482	0	0	0
22.422	0.000664	0	0.00066	25.882	0.000601	0	0.000601
26.117	0.001026	0	0.00103	30.358	0.000946	0	0.000946
28.831	0.001425	0	0.00142	33.602	0.001333	0	0.001333
30.727	0.001854	0	0.00185	35.793	0.001757	0	0.001757
31.913	0.002310	0	0.00231	37.066	0.002213	0	0.002213
32.479	0.002789	0	0.00279	37.545	0.002697	0	0.002697
32.557	0.003065	0	0.00306	37.557	0.002792	0	0.002792
32.400	0.003792	0.005	0.00379	37.320	0.003704	0.006	0.003704
32.291	0.004296	0.008	0.00430	37.189	0.004209	0.009	0.004209
32.183	0.004800	0.012	0.00480	37.058	0.004713	0.013	0.004713
32.074	0.005304	0.015	0.00530	36.927	0.005218	0.017	0.005218
31.965	0.005808	0.018	0.00581	36.796	0.005723	0.020	0.005723
31.856	0.006312	0.021	0.00631	36.664	0.006227	0.024	0.006227
31.747	0.006816	0.025	0.00682	36.533	0.006732	0.027	0.006732
31.638	0.007320	0.028	0.00732	36.402	0.007236	0.031	0.007236
31.530	0.007824	0.032	0.00782	36.271	0.007741	0.034	0.007741
31.421	0.008328	0.035	0.00833	36.140	0.008245	0.038	0.008245
31.312	0.008832	0.038	0.00883	36.009	0.008750	0.041	0.008750
30.224	0.013873	0.072	0.01387	34.698	0.013795	0.076	0.013795
29.136	0.018914	0.105	0.01891	33.386	0.018841	0.111	0.018841
26.959	0.028995	0.172	0.02899	30.764	0.028932	0.181	0.028932
23.246	0.046198	0.286	0.04620	26.816	0.044124	0.286	0.044124

Compressive behavior				Compressive behavior			
Diameter to thickness ratio				Diameter to thickness ratio			
For D/t =26.28				For D/t =26.28			
yield stress	inelastic strain	damage	inelastic strain	yield stress	inelastic strain	damage	inelastic strain
1.997	0	0	0	2.101	0	0	0
0.604	0.000571	0.6977	0.000571	0.600	0.000573	0.714	0.000573
0.453	0.000633	0.7729	0.000633	0.439	0.000635	0.791	0.000635
0.319	0.000688	0.8401	0.000688	0.295	0.000690	0.860	0.000690
0.185	0.000743	0.9072	0.000743	0.151	0.000745	0.928	0.000745

Material Properties of Steel tube

Stress-strain diagram for structural steel was defined in ABAQUS software according to Tao,2013.

Items	Structural steel properties					
Steel grade	S-235		S-275		S-355	
Elastic parameters						
Modulus of elasticity	210000		210000		210000	
Poisson's ratio	0.3		0.3		0.3	
Plastic parameters	Yield stress	Plastic strain	Yield stress	Plastic strain	Yield stress	Plastic strain
	235.263	0.00000	275.360	0.00000	355.600	0.00000
	235.470	0.00088	275.550	0.00069	355.710	0.00031
	235.940	0.00287	276.100	0.00268	356.420	0.00230
	236.410	0.00486	276.650	0.00467	357.130	0.00429
	236.880	0.00685	277.200	0.00666	357.840	0.00628
	237.350	0.00883	277.750	0.00864	358.550	0.00826
	238.945	0.01553	280.402	0.01814	362.100	0.01811
	252.966	0.01868	282.025	0.01849	363.408	0.02172
	321.238	0.03810	359.541	0.03791	429.859	0.03753
	362.481	0.05715	413.554	0.05696	488.668	0.05658
	384.687	0.07584	448.545	0.07565	527.975	0.07527
	395.821	0.09419	469.409	0.09400	553.283	0.09362
	400.286	0.10496	486.310	0.12175	589.102	0.14250